# THE USE OF ELLIPSOMETRIC TECHNIQUE IN THE STUDY OF PHYSICAL ADSORPTION AND LOW ENERGY ION BOMBARDMENT

by

SAFAA MOHAMED MOHYEL-DIN ABDEL-HAMID, M.Sc.

Submitted in fulfilment of the Degree of

Doctor of Philosophy

of

Physics Department

The University of Aston in Birmingham



FEBRUARY 1976

## ABSTRACT

The optical and electrical effects of gas adsorption on polycrystalline and single crystal gold films have been observed simultaneously.

The bombardment of such films with low energy inert gas ions has been studied, in an attempt to relate ellipsometric parameters to the damaged layer.

Gold and inert gases were chosen to eliminate the possibility of changes in the optical constants due to oxidation or any chemical reactions between substrate and ambient.

Polycrystalline films were prepared on glass slides held at room temperature in an ultra-high vacuum system. Single crystals were prepared on sodium chloride crystals of <110> and <100> orientation held at 350-400$^{o}$C and 2-6 x $10^{-9}$ torr.

The optical constants of the polycrystalline gold films were determined in the wavelength range 0.39 - 1$\mu$ and compared with published results.

The sensitivity of the gas adsorption measurements was investigated over a wide range of wavelengths for two gases, argon and neon, and was found to be higher at wavelengths corresponding to an emission line for the gas used.

Gas adsorption was found to depend on the surface structure of the films, the smount of adsorption on polycrystalline films being approximately the average of those found for <110 > and <100 > orientations. Argon and neon were found to be optically absorbing at some wavelengths.

Low energy ion bombardment (surface held at room temperature) gave similar effects to gas adsorption for ion energies below a critical value corresponding to the onset of damage. These critical ion beam energies were 100 eV for argon ions on <100> gold, 110 eV for the <110> surface and 130 eV in the case of polycrystalline gold. The thickness of the damaged layer was calculated from the results and found to be in reasonable agreement with the range computed from the stopping power of the material in accordance with the theory of Lindhard et al. (1963). Changes in residual resistivity, measured at $4^{o}K$ confirmed the order of magnitude of damage layer thickness. The degree of damage was related to the surface structure, and ion type.

Annealing experiments showed that the damage produced was not only simple Frenkel pairs, but also dislocations resulting primarily from injected interstitial atoms or from substrate atoms displaced by energetic ions.

ACKNOWLEDGEMENT

My appreciation is due to the Egyptian Government for the financial support. Thanks are due to my supervisor Dr.R.W.Fane. I also wish to thank Dr.W.E.J.Neal for his invaluable advice and suggestions. The co-operation of the Physics Department workshop and the assistance of Mr.W. Cooper with some of the drawings is gratefully acknowledged.

INDEX



cont'd

CHAPTER 3 - continued Page



cont'd

# CHAPTER I

## INTRODUCTION

## 1.1 Introduction

The subject of studying surfaces and thin films covering them is becoming increasingly important in several fields. Among these are the physics and physical chemistry of adsorption, in metallurgy where care has to be taken with oxidation and corrosion processes, and in solid state electronics where surface phenomena are very important. A great many phenomena exist which can only be described in a satisfactory way by considering the details of the atomic and electronic structure in the surface region. Examples of such phenomena are electron emission, adsorption and oxidation, adhesion, friction, nucleation and epitaxial growth and heterogeneous catalysis.

The properties of solids may be modified to a shallow depth by ion implantation. The requirements of understanding the effects of radiation damage in materials has led to a considerable investigation of atomic collision processes and the bahaviour of defects introduced by radiation. Most of the early work concentrated on the application of ion bombardment to sputtering and ion-bombardment cleaning. Recently, however, injection of material into a target to change its physical properties has become of more interest.

The development of experimental techniques for the study of surfaces has been considerable during the last decade. Facilities are now quite commonly available for the production and maintenance of uncontaminated surfaces because of the availability of ultra high vacuum apparatus. Each of these many techniques tends to be limited by the type of information they provide. Ellipsometry proved to be a very sensitive and versatile optical method for analysis of the reflecting surfaces or of films deposited on them. It provides information concerning optical

constants and average film thickness, and may be used on surface areas as small as one square millimeter. In addition, it is not theoretically limited to any particular range of optical constants and it is non-destructive.

## 1.2 Physical adsorption: Background and Review

The phenomena now designated as adsorption and desorption of gases or vapours were first recorded by Scheele (1777), who found that a mixture of nitrogen and a little carbon dioxide was expelled from thoroughly dried wood charcoal when heated in a glass retort to a dull red heat. On cooling, the gases were re-adsorbed by the charcoal.. The first quantitative theory was proposed by Irving Langmuir in 1916, 1918 . Langmuir considered a dynamic equilibrium between the gas and the adsorbed film, and then, to bring this theoretical model to a convenient stage of development, made a number of simplifying assumptions about the mechanism of the process and nature of the solid surface. His assumptions were:

1. The surface contains a number of sites of low potential energy, each of which is capable of immobilizing a molecule of adsorbed gas.
2. All sites on the surface are equivalent.
3. No interaction occurs between the adsorbed molecules.
4. Adsorption is restricted to a single layer of molecules.

The first of these assumptions ignored certain experimental facts that indicate that adsorbed molecules are not always localized on specific sites but may be free to move about the substrate in two dimensions. In 1929 Langmuir himself investigating tungsten filaments in an atmosphere of oxygen, found a localized layer (a two-dimensional solid phase) of oxygen atoms is attached to the tungsten surface, and that a second layer of mobile oxygen molecules moves freely on top of it. An equally favourable approach was made by Polanyi (1916). Polanyi's theory,

essentially thermodynamic rather than kinetic, made fewer assumptions about the mechanism of the adsorption process. For more than fifty years the potential theory received no further development. It now offers too little in fundamental understanding to be an attractive approach, although its usefulness in allowing experimental data to be extended beyond a rather limited range of temperatures and gases other than oxygen has been exploited. Taylor (1950) was for a long time the most prominent of those opposed to this primary assumption of the Langmuir theory. He rejected any theoretical model of an adsorbent surface that postulated it as energetically uniform. However, with the introduction and subsequent success of the B.E.T. theory of multi-layer adsorption (Brunauer et al. (1938)), Langmuir's theory was given a new lease of life and usefulness. The B.E.T. theory accepted all the Langmuir assumptions, both explicit and implicit, excepting only the one that restricts adsorption to a monomolecular layer. The postulate that the substrate is energectically uniform was still retained. In spite of these faults, the usefulness of the B.E.T. method for determining the specific surface area of a powdered solid remains undisputed. More realistic models become too complex to be of use in the interpretation of experimental results. Most of this complexity arises from the attempt to take into account the actual heterogeneity of the substrate. An S-shaped isotherm is obtained, which cannot be described by the Langmuir equation. For more heterogeneous substrates, which are certainly by far the more common, the observed adsorption isotherm consists of a number of superimposed S-shaped isotherms, each one weighted by the relative frequency of its corresponding adsorptive energy compared with the whole distribution of energy levels of the substrates. The observed isotherm is the sum of all these individual isotherms. So complex a result obscures the S-shape of each term in the series, and

the Langmuir equation, because of its simplicity of form, reappears as an empirical description of the final summation. But while this may be useful as a first approximation, the basis of the theory is open to question. Opinions are sharply divided. Stebbins and Halsey (1964) wrote: "The Langmuir equation occupies a central position in the theoretical discussion of monolayer adsorption because of its simplicity of form and directness of derivation." At about the same time Polanyi (1963) wrote: "That the Langmuir isotherm is theoretically false still seems to be insufficiently appreciated today.....To present (it) as a proper approximation to the adsorption equilibrium is therefore misleading. The formula should be dropped altogether."

The properties of solid-gas interface regions depend on the ambient atmosphere. Such properties, which are of considerable technological importance, may differ physically and chemically from the bulk phases which they separate. Different techniques have been applied to study physical adsorption of several gases on different materials, e.g. LEED (Lander et al. (1967) , Steiger et al. (1969), Bootsma et al. (1969)), field emission and field ion microscope (Gomer (1959), Ehrlich (1960), Ehrlich (1964)), surface conductivity (Bootsma et al. (1969)), gas volumetric measurements (Bootsma(1969) ), ellipsometry (Bootsma et al. (1969 a,b,c), Steiger et al. (1969), Morgan (1974 ) ) and others.

Several recent studies of physical and chemical adsorption using ellipsometry have been reported.

Claussen (1964) on studying vapour adsorption of water and some lower monohydric alchohols, acetone, benzene and hexane on single crystal silicon found a marked difference in the amount of water adsorbed after various surface treatments. He attributed the difference to change in both structure and composition of the adsorbent surface after etching. He assumed that the values of the indices of refraction of adsorbed layers were constant and equal to those of the bulk liquid phase.

Archer (1964) studied physical adsorption of water, carbon tetrachloride and acetone on variously treated silicon surfaces. He calculated monolayer thicknesses from ellipsometric measurements using the refractive indices of the bulk liquid phase. He found that the adlayers were comparable with the diameter of the adsorbed molecules. He (1965) claimed a precision of $\pm$ 0.02 monolayers of oxygen adsorbed on freshly cleaved (111) faces of silicon. The degree of submonolayer coverage was obtained from a two dimensional theory.

Bootsma et al.(1969) reported changes in the ellipsometric parameter $\psi$ much larger and of opposite sign to theoretical prediction upon chemisorption of various gases on silicon and germanium. This was ascribed to a transition layer of different refractive index to that of the bulk.

Similar results are observed by Corroll (1969) for oxygen on tungsten (110).

Steiger et al.(1969) found good agreement between ellipsometric information and LEED when studying physical adsorption of several gases on single crystal silver surfaces. LEED measurements show the degree of ordering of the adsorbed phase on the silver single crystal surface used and the appearance of surface structure as a function of coverage.

They used ellipsometry to study optical properties of clean silver surface and their variation as a function of time. Isotherms, in the pressure range $10^{-10}$ to $10^{-6}$ Torr and temperature range $0^{\circ}C$ to $-195^{\circ}C$, measured by ellipsometry yielded information about heat of adsorption, the cross sectional areas and coverage ratio of the adsorbed gases.

Smith (1972) studied chlorine adsorption on aluminium and titanium with combined ellipsometry, Auger electron spectroscopy and surface potential measurements. Monolayer thicknesses of $10^{\circ}A$ and $4.5^{\circ}A$ on aluminium and titanium respectively were calculated using a refractive index n of 2.4 for chlorine.

Disagreement between the interpretation of the ellipsometric measurements in the submonolayer range is found in the literature. Linear dependence of the relationship between the ellipsometric signal and the degree of coverage is reported by Bootsma et al.(1969), Steiger et al. (1969) in agreement with the measurements of adsorption of long polar organic molecules [Bartell et al. (1960), Miller (1966)] or tritium on metal substrates [Stromberg (1964)], studied simultaneously using ellipsometry and radio tracer methods. Hayfield and White (1964) found that the change in ellipticity is proportional to the average thickness of the film. They used controlled vacuum evaporations of calcium fluoride on aluminium and metal oxide surfaces to obtain partially covered surfaces. Jackson et al.(1949) also found a linear relationship when studying helium creeping on stainless steel mirrors. On the other hand Hall (1966) concluded that the ellipticity of the reflected light from covered surfaces varies as the square root of fractional coverage.

## 1.3 Low energy ion bombardment: Background and Review

The bombarding ions may be captured for a certain length of time in the target lattice (Almen et al.(1961) ) to arrive later at the surface via diffusion or "burst" processes and there once again produce impurity (contamination) layers and either desorb or result in chemical heterogeneities on the surface. Brown and Leck (1955), Varnerin and Carmichael (1957) and Carmichael and Trendelenburg (1958) have made a detailed investigation of the re-emission of such ions shot into a target. Carmichael and Trendelenburg were able to observe the re-emission of noble gas atoms which were originally shot into a nickel target as ions and then were driven out of the lattice as a result of bombardment with another type of noble gas ion. Their results lead to the conclusion that, at the ion energy employed (about 100eV), a nickel target can absorb up to the equivalent of 15 atomic layers of helium before saturation begins, whereas the absorption of other noble gases is equivalent to only about one layer of atoms. Their explanation is that the helium ions are more easily incorporated in the interstitial spaces than are the other noble gas atoms.

Another effect that can occur during the ion bombardment of the target is the development of physical heterogeneities on the surface. Thus, for example Trillat (1956) showed that bombarding a gold single crystal layer with 12 keV ions converted it into a polycrystalline layer. Ogilvie et al.(1959) found a similar disturbing effect in the bombardment of silver single crystal layers with argon ions in the energy range from 12 to 4000eV. The original single crystal layer is split up after the ion bombardment into a number of small crystallites (around 100 Å in length), the crystallites being oriented with respect to the original single crystal layer as if a rotation had occurred around the (112) axis.

Farnsworth et al.(1955) found that bombarding titanium, nickel and platinum surfaces with argon ions likewise produced disturbances of the crystal lattice at the surface. Guntherschulze and Tollmien (1942) observed that bombardment of metals such as platinum, aluminium, bismuth and magnesium with ions induced the development of submicroscopic cones on the surface (but gold, platinum, iron and nickel did not show the effect). The development of physical heterogeneities as a result of ion bombardment of surfaces can be regarded as well established for many systems. Some macroscopic results of bombardment may be observed even in the case of non-crystalline materials, since the implanted ions can cluster to create precipitates. Naturally, the effects of damage are most evident when the target possesses an initially ordered structure.

The removal or reduction of radiation damage is a most important aspect of ion implantation, since otherwise the properties of the material are likely to be dominated by the many defects that each ion will produce in coming to rest. Only when the damage is minimized do the properties of the embedded ions themselves become observable and usable. Occasionally the properties of the defects themselves may be beneficial, for example in the production of high-resistivity silicon by irradiation (Messier et al.(1964)) or the generation of colour centres. However, in such cases a more uniform distribution of damage is required than would result from ion bombardment.

In recent years, the injection of material into a target specimen in the form of an accelerated ion beam has been utilised as a most valuable tool for altering its physical properties in a controllable manner. This is particularly the case for semiconductors, in which the electrical behaviour is determined by extremely small concentrations

of certain impurities. It is feasible that magnetic properties, mechanical hardness and optical transmission may be usefully modified by ion implantation. In 1955 Cussins, bombarded germanium with twelve types of ion and in each case observed an increase in the acceptor concentration.

Interest grew rapidly at a number of laboratories after 1963. At about that time the phenomena of ion chanelling became recognised. The study of this subject formed a basis for the development of the ion implantation techniques and also gave rise to new ways of locating the positions of ions implanted into a lattice.

Comparison of conventional techniques of introducing doping material by diffusing at high temperatures with ion implantation revealed that the depth of diffusion and the degree to which the impurities diffuse laterally are not very controllable in practice, while the possible concentration profiles are limited by the nature of the diffusion process. By contrast, ions entering the solid as a directed beam come to rest with very little lateral spreading. The range distribution is highly reproducible and may be controlled by variation of the ion energy, the ion species, and dose as well as by the crystal orientation and temperature. Although thermal annealing is necessary in most cases after implantation, in order to reduce the effects of radiation damage, the annealing temperatures are substantially lower than those required for diffusion. The relatively low temperature involved in ion implantations removes the tendency, present in diffusion technology, for impurities to migrate during successive stages, but they do require that, if both techniques are employed in the fabrication of a device, the diffusion

must be carried out prior to implantation. At other times, implantation may be a convenient method of introducing material as a source for diffusion (Roughan et al.(1968) ).

Several different investigators using different techniques studied radiation effects on different materials. All studies lead to the same qualitative conclusion which is in agreement with the present ellipsometric measurements. Using LEED, Jacobson et al.(1965), Farnsworth et al.(1967) and Henzler (1970) showed deterioration of the LEED pattern as a function of ion dosage and energy. MacDonald et al.(1966) estimated the depth of damage induced in germanium by low energy ion bombardment by monitoring the changes of the sputtering yield. Optical techniques have been used by Mayer (1970) and Hart et al.(1969) to detect surface change induced by high energy ions. Bowden et al.(1963) studied radiation damage in gold, copper and nickel by bombardment with 100 eV argon ions using transmission electron microscope. They found a high concentration of damage close to the surface in a short time. They estimated the depth of damage to be 100 Å below the surface. Kelly et al.(1970) using transmission microscopy gave evidence for a type of structural evolution following ion impact. Bombardment of amorphous $ZrO_2$ leads to complete crystallization. Also Merkle (1970) demonstrated, by bombarding single crystal gold films with protons and xenon, that the damage rate does depend strongly on the orientation of the beam relative to the crystallographic directions by measuring the change in resistance on bombarding the film at low temperature. Venables (1970) discussed a selection of phenomena associated with low energy ion bombardment of solids, with particular emphasis on information obtained with the transmission electron microscope and on techniques which give specific information about the processes which take place in the surface layers of the solids.

Ibrahim et al. (1972) reported lattice damage in silicon induced by 400 eV argon ions. They interpreted their ellipsometric results in two ways. In one the model consisted of residual surface contamination and the partially damaged substrate. In the other case, the damage was analysed by a three layer model consisting of residual surface contaminant, the damage layer and the underlying substrate.

Nomura et al.(1974) studied the change of electrical resistance of metal films bombarded with helium ions of energy 4-10 keV. They found an increase of resistance with ion dose without saturation. 80% of the resistivity changes induced in copper and 60% in gold were recovered after annealing to $453^{o}$ K.

## 1.4 Ellipsometry

### 1.4.1 Background and Review

Ellipsometry is the name applied to measurement and analysis of elliptically polarized light in the broadest sense irrespective of the cause of elliptical polarization. Elliptical polarization may be caused by reflection from a metal or dielectric surface with or without a surface film. In ellipsometry two angles are measured the ratio of amplitude vectors, and the phase differences. Methods of analysing elliptical polarization are credited to Senarmont in the middle of the nineteenth century. Ellipsometry is based on the Fresnel formulae which indicate that when light is reflected at any two interfaces, the two components vibrating in and perpendicular to the plane of incidence, generally called $r^{p}$ and $r^{s}$, respectively, undergo a phase shift of $180^{o}$ or $0^{o}$, and furthermore, that $r^{p}$ vanishes at a certain angle called the Brewster angle. Fresnel, postulating transverse vibration, was able to account for the existence of polarization by reflection.

In the early 19$^{th}$ century, there was a great deal of interest fundamentally concerned with the analysis of reflected polarised light. Since ellipsometry is essentially based on the analysis of reflected polarized light, it can be said that its history began in 1808 with the detection of polarization by reflection by Malus.

In 1815 Brewster published a paper in which he formulated the analytical relationship between refractive index and polarizing angle (the angle of incidence at which the reflected light is plane polarized).

Airy in 1833 studying Newton's rings formed between a convex lens and flat surfaces of diamond and of metal, observed and analyzed tne nature of the non-vanishing p-component reflected at the Brewster angle. He arrived at expressions similar to those which are now called fundamental equations of ellipsometry by applying Fresnel's coefficients to the multiple reflections in the gap between glass surfaces and introducing the phase difference due to passage through the air layer.

In 1840 although the nature of elliptically polarized light was well characterised, it had not been clearly established at that time what was the origin of elliptical polarization by reflection

In 1850 Jamin, in his extensive experimental studies on reflection of light from many solids and liquids, examined the relative phase change with angle of incidence. He found, that for angles near the Brewster angle, the reflection of light deviates sensibly from Fresnel's law and he found an appreciable amount of ellipticity was present. He distinguished between two types of ellipticity, and coined the expressions

positive and negative ellipticity. The presence of a thin film at the solid or liquid-air interface was responsible for the failure of Fresnel's law as explained later by Drude (1890) and Rayleigh (1892). Also Jamin(1851)was unable to suggest the quantitative relationship between ellipticity and refractive index and indeed consider them as independent constants.

The earliest statement connecting optical and surface phenomena was achieved by Lorenz (1860), he concluded that the calculations of reflection and refraction of light on the assumption of an abrupt transition from one medium to the other, and then the sudden change in refractive index at the boundary cannot exist in nature. He suggested that the calculations would be more accurate and more valid if a gradual transition was assumed over a certain region, which may be made arbitrarily small. He was also able to show that Jamin's results could be accounted for by the existence of a film of thickness between a hundreth or a tenth of a wavelength. Lorenz explained the tendency of surfaces of low and high refractive index to exhibit negative and positive ellipticity.

Van Ryn Alkemade (1883) attacked the Lorenz problem using the new electromagnetic theory. He treated the longitudinal vibration and transition zone equally, and came out in favour of the latter. Van Ryn showed that the ellipticity observed at the polarizing angle might be caused by a film of molecular dimensions.

In 1886 Maxwell showed that the Fresnel formulae for the reflection coefficients could be simply derived from the electromagnetic theory of light.

Before the end of the last century, Lord Rayleigh in England (1892) and Paul Drude in Germany (1890) found a correct explanation for the failure of Fresnel's law. Rayleigh found that light reflected from water at the Brewster angle had a small negative ellipticity which was contrary to the Fresnel equation. He concluded that the effect was due to a contaminating film of grease on the water surface which he estimated to be less than one micrometer in thickness. Between 1890 and 1908 he studied reflection from many liquids and solids and showed Jamin's data on water to be affected by surface films, and confirmed Drude's confidence in Fresnel's equations as a limiting case. At the same time as Rayleigh was investigating the optical properties of the light reflected from the surface of liquid, Drude was testing the optical properties of the light reflected from solids. He was able to correlate quantitatively the optical thickness of a film and the optical constants of the material upon which the film was deposited. In two fundamental articles published in 1889 and 1890, Drude derived the fundamental equations of ellipsometry from Maxwell's equations with suitable boundary conditions. He was able to correlate quantitatively the optical thickness of a film and the optical constants of the material upon which the film is deposited with two parameters characterizing the ellipse representing the reflected light. The two parameters were the ratio:

$$\tan \psi = \rho^p / \rho^s$$

and

$$\Delta = \delta^p - \delta^s$$

where $\rho^p$ and $\rho^s$ are the reflection coefficientsof the components in and perpendicular to the plane of incidence after reflection respectively.

$\delta^p$ and $\delta^s$ the absolute phase shifts of the same two components brought about by the reflection.

Drude obtained a most general equation, valid for films of any thickness deposited on metallic surfaces.

Voigt (1888) derived nearly the same fundamental formulae as Drude's formulae, but for dielectric systems.

Parallel to the development of the theory of ellipsometry the actual apparatus used for ellipsometric measurements slowly evolved to the present instrument. Hauschild in 1920 and Skinner 1925 were the first to describe instruments very similar in principle to those of the present day.

From late 1920 onward, ellipsometric studies of film formation in both liquid and gaseous environments have been made mostly with visual instruments.

In 1927 Ives and Johnsrud were able to determine the thickness of spontaneously deposited photoelectrically active rubidium film deposited in vacua on glass and platinum surfaces making use of calculations of Fry (1927) of the relationship between thickness of alkali metal upon the underlying glass base and the resulting changes in optical behaviour.

In 1934 Blodgett was the first to develop a technique for depositing thin films of known thickness. With her apparatus a film 10 Å to 20 Å in thickness could be deposited with a precision of about 3 Å. The thickness of the film was measured by means of the interference of monochromatic light reflected by the film.

In 1934 Tronstad and Feashem investigated the optical constants of a mercury surface which they used as a standard surface for the calibration and adjustment of the ellipsometer since it was found to give more reproducible results than any surface produced by mechanical polishing.

In 1935 Tronstad, by using the technique of deposition of thin films of known thickness, was able to verify Drude's formula and its modification. He used a monomolecular film of fatty acids deposited on a mercury surface. He found close agreement between calculated values and length of fatty acid chains.

In 1933 and 1936 Murmann suggested that the optical constants could be determined by measuring the intensity of the light transmitted and reflected from both sides of the film, although this requires a separate determination of the thickness.

In 1945 Rothen was the first to determine the thickness of films deposited on metal slides by an apparatus which was modified from that of Hauschild and coined the name ellipsometer. In 1948 Rothen and Hanson gave practical information concerning the calibration of an ellipsometer. The instrument was provided with a half shadow device to facilitate setting the crossed polaroids. Fig. (1.4.1.a) shows a schematic diagram of the basic components of an ellipsometer.

Additional developments in ellipsometric instruments and methods have been achieved by the addition of many auxillary services, but the principle of operation remains unchanged. Such additional developments lead to more sophisticated instruments. The following are examples of these auxillary services:

a) More sensitive photoelectric methods replace the classical visual procedures.

b) The modulation and compensation of the instrument to use the Faraday effect.

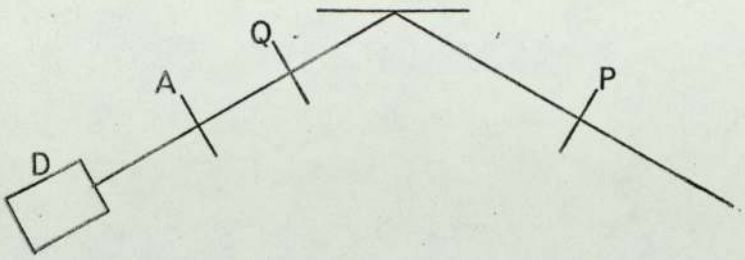


Fig. (1.4.1a) Basic components of an ellipsometer

P = polarizer Q = compensator A = analyser D = detector

Two different methods can be used to measure the ellipsometric parameters $\psi$ and $\Delta$.

(i) Beattie method

(ii) Compensator method

The Beattie method was used in the present work and is explained in section (2.6). In the compensator method, plane polarized light, produced by the polarizer P, is incident on the specimen with its plane of polarization inclined at an angle $\psi$ to the plane of incidence. Generally, the reflected light is elliptically polarized. Then elliptically polarized light passes through the compensator which consists of a bi-refringent material. The thickness of the compensator is such as to produce a 90 degrees phase difference between the ordinary and extra-ordinary ray for the particular wavelength of light used. If the fast axis of the compensator is arranged to be parallel to the major axis of the reflected ellipse, the vibrations along the major and minor axes of the ellipse are brought again into phase and plane polarized light results. Finally the light passes through the analyzer to the photomultiplier.

Two geometrical arrangements of the ellipsometer may be used. One with the retardation plate Q following the sample and the other with it preceding the sample.

1.4.2 Computational techniques

The use of Drude's exact equations for the calculations of optical constants was very tedious until the advent of the modern high speed computers in the last two decades. The use of the exact equations is necessary to correctly interpret the results of ellipsometric measurements for the optical parameters of the systems of interest. When polarized light is reflected from a surface, the state of polarization of the light is changed. This change of polarization may be represented by the ratio of the reflection coefficients $r^p$ and $r^s$ for light polarized with its electric vector parallel and perpendicular to the plane of incidence respectively. In general, these reflection coefficients are complex numbers, so they determine the change in both amplitude and phase of the light and they are given by Fresnel coefficients:

$$r_{12}^p = (n_2 \cos\phi_1 - n_1 \cos\phi_2)/(n_1 \cos\phi_1 + n_2 \cos\phi_2) \qquad 1.4.2a$$

$$r_{12}^s = (n_1 \cos\phi_1 - n_2 \cos\phi_2)/(n_1 \cos\phi_1 + n_2 \cos\phi_2) \qquad 1.4.2b$$

$n_1$ and $n_2$ are the refractive indices of the medium above the surface and the surface itself respectively. For absorbing materials the refractive index N is complex. $\phi_1$ and $\phi_2$ are the angles of incidence and refraction. $\phi_2$ is complex in an absorbing medium.

The parameters measured by an ellipsometer are related to the ratio of t reflection coefficients ($\rho$) by

$$\rho = r^p/r^s = \tan\psi\, e^{i\Delta} \qquad 1.4.2c$$

which represents the relative attenuation, $\tan\psi$, and the phase shift, $\Delta$, for the components of the electric vector in and normal to the plane of incidence. If a film is placed on the surface, these reflection coefficients of the composite surface are changed. For a very thin film,

appreciable changes in the reflection coefficients result, making the ellipsometer a sensitive instrument, since these changes can be detected.

For a film covered surface, the exact Drude equations for the reflection coefficients are:

$$R^p = (r_{12}^p + r_{23}^p \exp D)/(1 + r_{12}^p r_{23}^p \exp D) \qquad 1.4.2d$$

$$R^s = (r_{12}^s + r_{23}^s \exp D)/(1 + r_{12}^s r_{23}^s \exp D) \qquad 1.4.2e$$

Where

$$D = -4\pi i n_2 \cos\phi_2 d_2/\lambda$$

Where $d_2$ is the film thickness, $\lambda$ the wavelength of light and the subscripts 1, 2 and 3 are used for the medium, film and substrate respectively. The Fresnel coefficients $r_{12}^p$, $r_{12}^s$ and $r_{23}^p$, $r_{23}^s$ refer to reflection between medium and film, and film and substrate respectively and the ratio of the reflection coefficients is:

$$\rho = R^p/R^s = \tan\psi\, e^{i\Delta}$$

For a particular angle of incidence, film thickness and refractive indices of surrounding medium, film and substrate, the ellipsometric values $\psi$ and $\Delta$ may be computed. The film thickness of known refractive index may be determined from these calculations by comparison with the experimentally measured values of $\psi$ and $\Delta$. If the refractive index is not known, both the film thickness and refractive index may be determined from ellipsometric readings. Values of the refractive index and different film thicknesses are assumed. The correct values are those for which nearly zero error in $\delta\Delta$ and $\delta\psi$ are found (smallest error). In the case of absorbing material (complex refractive index), if either the real or imaginary parts or the film thickness is known, the other two parameters can be determined as previously explained by searching for

the values which give the least error in the calculated values of $\delta\Delta$ and $\delta\psi$. However, the complex index of refraction and film thickness are very difficult to determine from a single set of ellipsometric readings since a set consists of only two values, $\psi$ and $\Delta$. By increasing the number of ellipsometric measurements, all three values can be determined. The following are possible ways of increasing the ellipsometric information.

1. A series of ellipsometric measurements for films of the same refractive index for different but unknown thicknesses or of thicknesses in known ratios.
2. Different ellipsometric measurements on a single film for different surrounding media of known refractive index.
3. Different readings for the same film on different substrates.
4. Changing the angle of incidence, different readings for the same film being taken.

Because of the complexity of the exact equation, the application of ellipsometry was limited to materials covered with films very thin relative to the wavelength of light.

The fundamental equation of ellipsometry is:

$$\frac{(R^p/R^s)_{refl}}{(R^p/R^s)_{inc}} = \frac{\tan\psi_{refl}}{\tan\psi_{inc}} \exp(i(\Delta_{refl} - \Delta_{inc})) \equiv e^{i\Delta} \tan\psi \qquad 1.4.2f$$

where

$$\tan\psi_{refl} = (R^p/R^s)_{refl}$$

$$\Delta_{refl} = (\delta^p - \delta^s)_{refl}$$

Similar definitions hold for the incident wave.

In general, the incident light is plane polarized with the plane of vibration of the electric vector inclined at $\pm\pi/4$ with respect to the plane of incidence, so that

$$\tan\psi_{inc} = (R^p/R^s)_{inc} = 1$$

$$\Delta_{inc} = 0$$

and

$$e^{i\Delta}\tan\psi = (R^p/R^s)_{refl}$$

and since generally

$$R^p \neq R^s$$

and

$$\delta^p \neq \delta^s$$

the reflected wave is elliptically polarized. The ellipsometer measures experimentally quantities that allow $\psi$ and $\Delta$ to be determined. The Fresnel coefficients R can be expressed in terms of the optical constants of the media bounding the reflecting interfaces and the angle of incidence as in equations (1.4.2a,b). If all the Fresnel coefficients are substituted in equation (1.4.2f) and the real and imaginary parts of the resulting equation are separated, there results one equation for $\psi$ and one for $\Delta$ .

For very thin films $d<<\lambda$ Drude expanded the exponential term in equation (1.4.2f) in a power series of $d/\lambda$ and, neglecting terms of higher order than the first, obtained:

$$\Delta = \bar{\Delta} - \alpha d \qquad 1.4.2g$$

$$\psi = \bar{\psi} + \beta d \qquad 1.4.2h$$

where:

$$\alpha = (4\pi/\lambda_o)\ \frac{\cos\phi_o \sin^2\phi_o (\cos^2\phi_2 - a)(\frac{1}{n_1} - \frac{1}{1})}{(\cos^2\phi_o - a)^2 + a_1}$$

$$\beta = (2\Pi/\lambda_o) \frac{\cos\phi_o \sin 2\bar{\psi} \sin^2\phi_o a_1 (1-n_1^2 \cos^2\phi_o)(\frac{1}{n_1^2} - 1)}{(\cos^2\phi_o - a)^2 + a_1^2}$$

$$a = \frac{n_2^2 - k_2^2}{(n_2^2 + k_2^2)^2}$$

$$a_1 = \frac{2n_2 k_2}{(n_2^2 + k_2^2)^2}$$

For filmsof thickness large compared with $\lambda$ the exact theory must be used. More details can be found in the books by Vasicek (1960) and Heavens (1955).

These linear approximations (equations 1.4.2.g,h) are commonly known as Drude approximations. Tronstad (1935) modified the Drude approximations to include more terms, and such equations are known as Drude-Tronstad formulae. On the other hand Archer (1957) modified the Drude-Tronstad equations by including first order terms and found them to be significant in many cases. Burge and Bennett (1964) comparing these approximations with the exact theory, concluded that Drude's approximations could cause errors for films as thin as 10 Å, and the difference might be as high as 10 - 30% in some cases. Saxena (1965) derived a new generalized equation for $\psi$ and $\Delta$ which is valid in the thin film region ($<$100 Å) and also in certain ranges of the thick region, and showed that Archer's equation for $\psi$ is not valid in the thin film region.

In 1962 Archer was the first to develop a computational programme to calculate the thickness and optical constants of silicon surfaces using the exact theoretical equation without the limitation of the approximate theory.

McCrackin et al in 1963 gave a critical survey of the potentialities and limitations of ellipsometry for the determination of the optical properties of solids. They developed a numerical method which allowed the calculation of the variation of ellipsometric parameters as a function of the optical parameters of the system of interest. They also discussed the variations in ellipsometric readings with different film thicknesses, different surrounding media, various substrates and variation of angle of incidence. McCrackin's programme has a numerical computational method for determining only the optical constants of an absorbing film and its thickness provided the optical constants of the absorbing substrate are known.

Burge and Bennett (1964) and Archer (1964) have shown that optical constants of substrates can be determined only if the values of n, d of the film are known even though the thickness of the film is as thin as 10 - 50 $\mathring{A}$. They demonstrated this in detail for a special case using silicon. Burge and Bennett (1964) concluded that the variation in ellipsometric parameters $\psi$ and $\Delta$ with angle of incidence cannot be used to determine the presence of a thin surface film, since calculations show that the variation of these parameters with angle of incidence for a partially covered surface is practically identical with that for a fictitious surface with appropriate optical constants.

Vedam et al (1969) have developed an ellipsometric method for the determination of all the optical parameters of a transparent film on an absorbing substrate system from a series of measurements on different film thicknesses or with different incident media. The method is based on the constancy of the normal reflectance, R, at small film thickness.

Ellipsometric measurements of $\Delta$ and $\psi$ are performed on the sample with two or more different film thicknesses or in two different ambients. The final results are obtained by a computer search which finds those values of $n_1$ and $n_2$ which yield, on computation, values of $\Delta$ and $\psi$ in exact agreement with the experimentally measured values. Then since $n_2$ is now known, $k_2$ is automatically specified from the value of R. Film thicknesses are also obtained in the process. This method is applicable to materials with a large ratio of $n_2$ to $k_2$ such as silicon or gallium arsenide.

The range of surface film thickness over which the normal reflectance is constant is very small. In other cases different experimental techniques have to be used for the precision measurement of the normal reflectance before the method is applicable.

1.5 Aim of the present work

The production and maintenance of atomically clean surfaces in ultra high vacuum is a necessary first step in the investigation of many surface phenomena. However, there is not general agreement concerning the most acceptable method to be used in individual cases. This situation may be due to several factors.

1. A lack of sufficient experimental data to completely characterise the required conditions.
2. To insufficient understanding of many determining factors which must be controlled or taken into account.
3. To the variation of requirements for different surfaces.
4. To a lack of a suitable method of testing the surface in question.

Ellipsometry proved to be a sensitive, non-destructive method for examining surfaces, in addition to there being no restriction on the size of sample to be investigated.

The purpose of the present work was to continue the study of the relationship between optical constants and structure already initiated in this laboratory by Fane and Neal (1970), and Neal et al. (1970). The aim was the improvement of the detection system to increase the sensitivity of the ellipsometer to facilitate the detection of fractional monolayer of adsorbed gas.

Measurements were also made on ion bombarded surfaces in an attempt to correlate ellipsometric parameters with the damage produced. Such a correlation is important in the interpretation of optical constants, known to depend on preparation of the material and structure. Possible methods of calculating the thickness of the damaged layer from $\psi$ and $\Delta$ measurements was investigated to assess the usefulness of the instrument as a monitor of damage produced in the first few hundred Angstroms of a metal or semi-conductor surface.

# CHAPTER 2

## EXPERIMENTAL ARRANGEMENTS AND PROCEDURES

## 2.1 Experimental chamber and vacuum system:

A conventional vacuum system similar to that described by Fane and Neal (1970) was used. The experimental chamber (stainless steel) was pumped by a four-stage diffusion pump, filled with D.C.705 oil, which was backed through a liquid nitrogen trap by a rotary pump. A water cooled baffle and liquid nitrogen trap separated the pump system from the chamber. The flange between the chamber and the cold trap was sealed with aluminium wire (0.625 mm diam.) and that between the trap and the diffusion pump with indium wire, all other flanges used copper gasket seals. Fig.(2.1a) shows a schematic diagram of the vacuum system and the experimental chamber. Fig.(2.1b) shows the optical arrangement.

The substrates (glass to produce polycrystalline gold film and sodium chloride single crystal to produce single crystal gold film) were supported on a stainless steel block, welded to the stainless steel central tube inside which was a second tube with the heater welded at the end. The substrates could be heated to 500°C using a nichrome heater tape insulated by mica sheets and fixed in position with a glass tube.

The experimental chamber was connected to the gas admission system through a bakeable leak valve, type MD6 (Vacuum Generators Ltd.) which allowed the total pressure to be varied and accurately controlled during the experiment. A quartz crystal thickness monitor was mounted beside the substrate holder so that the distances between the evaporation filament and both the substrate and the quartz crystal were the same. Two quartz windows permitted the use of light to a wavelength of 1800 Å.

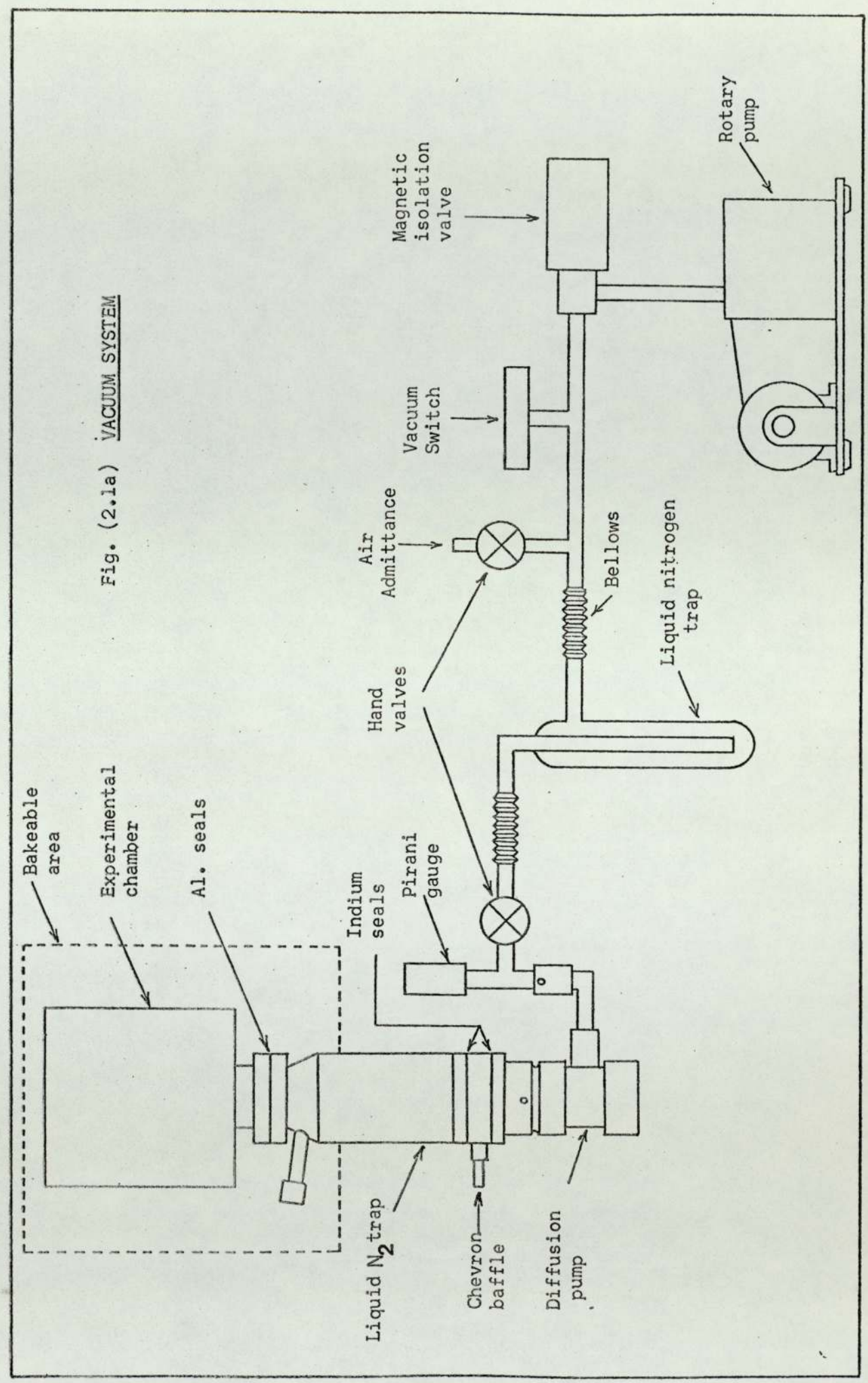


Fig. (2.1a) VACUUM SYSTEM

Fig.(2.1.b) Optical arrangement used in the present experiment.

A = monochromator B = light chopper

C = polarizer D = Quartz window

E = Analyser F = Photomultiplier

G = Experimental chamber

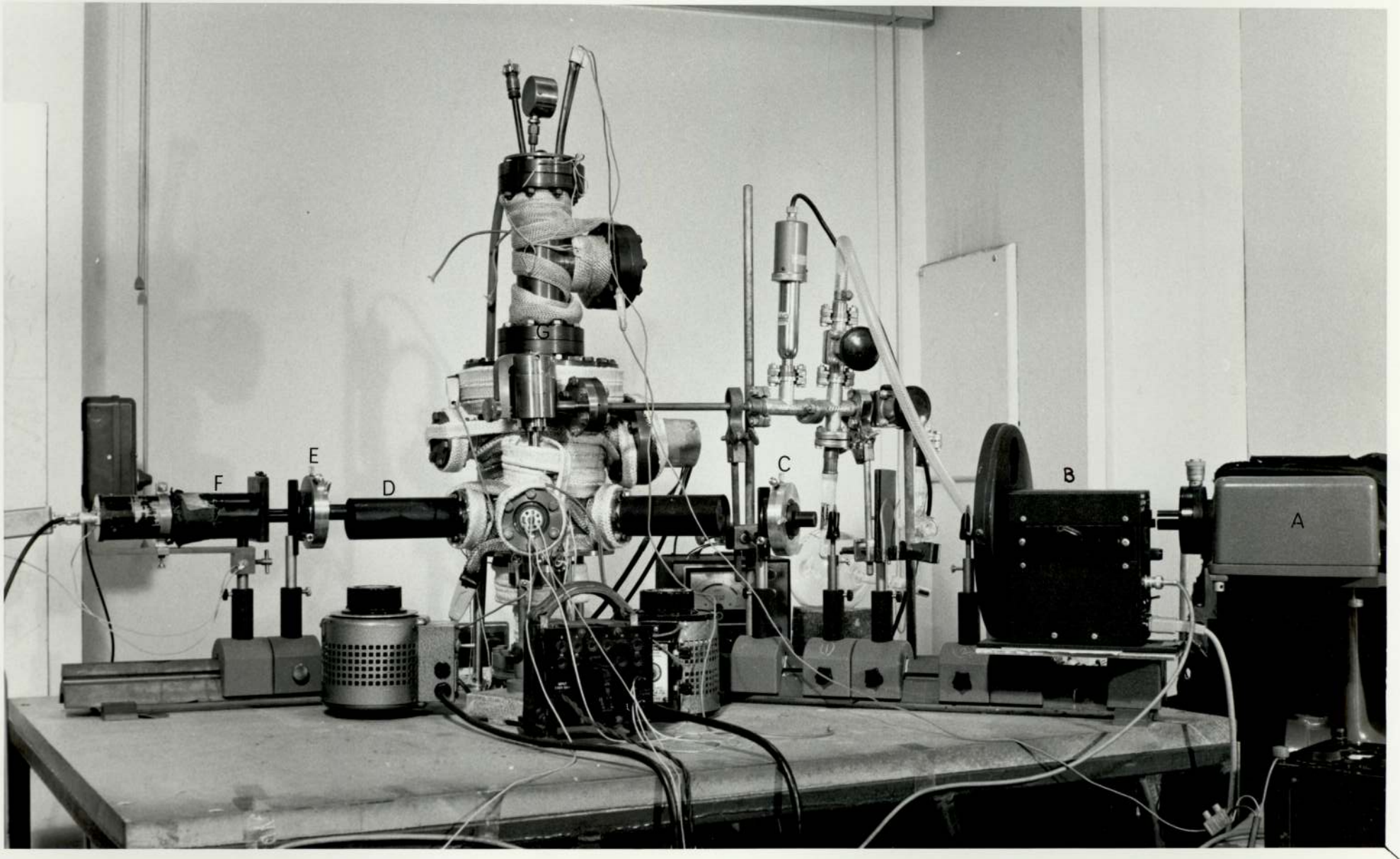
A
B
C
D
E
F
G

The electrical contact areas were evaporated onto the substrate before the films were prepared and the size of the sample films were defined by evaporation masks. For most of the optical and electrical measurements, the shape of the film was as shown in Fig.(2.1c) while for electrical measurements at liquid helium temperature, the arrangement for preparing two pairs of films each of the same thickness is shown in Fig.(2.5.2a). After deposition, all four films were transferred to the holder as shown in Fig.(2.5.2b) for annealing. Electrical connections to the specimens were made through an eight-way ultra-high lead-out and nickel wires insulated with ceramic beads and pyrex glass tubes. The final connections to the specimens were made with pressure contacts using thin copper strips.

## 2.2 Gas admission system

The arrangement for the gas admission system is shown in Figs. (2.2a,b). All gases used were stated to be spectroscopically pure (British Oxygen Company). The system was pumped to a pressure of $10^{-2}$ torr with a rotary pump through liquid nitrogen traps before the gas bulb seal was broken. The gas admission system was connected to the experimental chamber through a bakeable leak valve and a stainless steel cross tube as shown schematically in Fig.(2.3b).

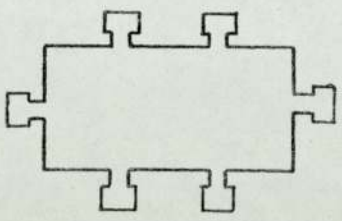

Fig. (2.1c) Shape of the films used for optical and electrical measurements

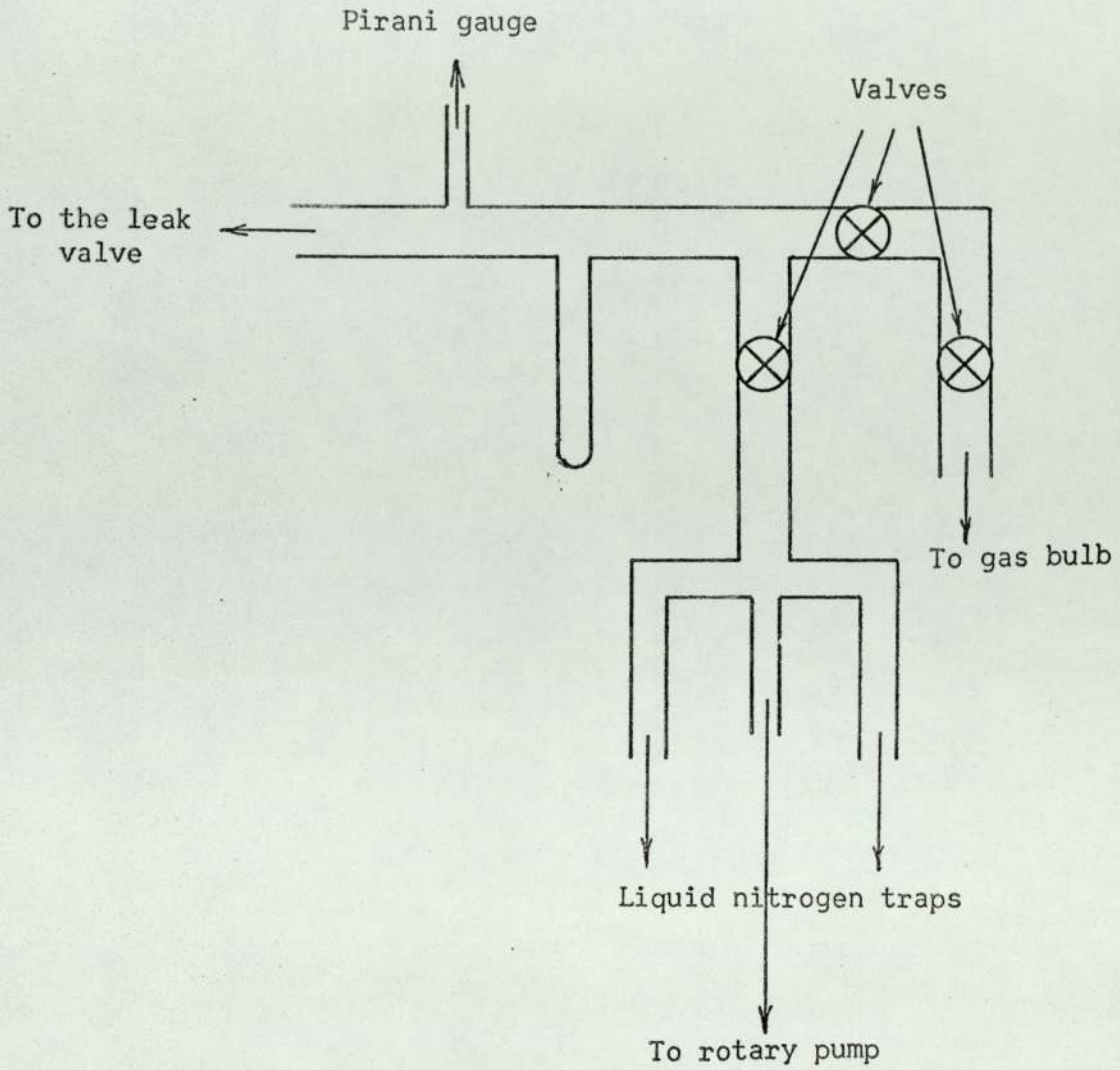


Fig.(2.2a) Schematic Diagram showing the gas side.

## 2.3 Ion gun

The ion gun was a type AG1, (Vacuum Generators) similar in construction to the hot cathode ion gauge with additional electrodes to extract and accelerate the ions in the form of a beam. In this type of gun any contamination effect due to electrons is minimized, as the filament is enclosed in the outer electrodes which are only

Fig. (2.2.b) Gas admission system

A = Gas bulb B = Pirani gauge head

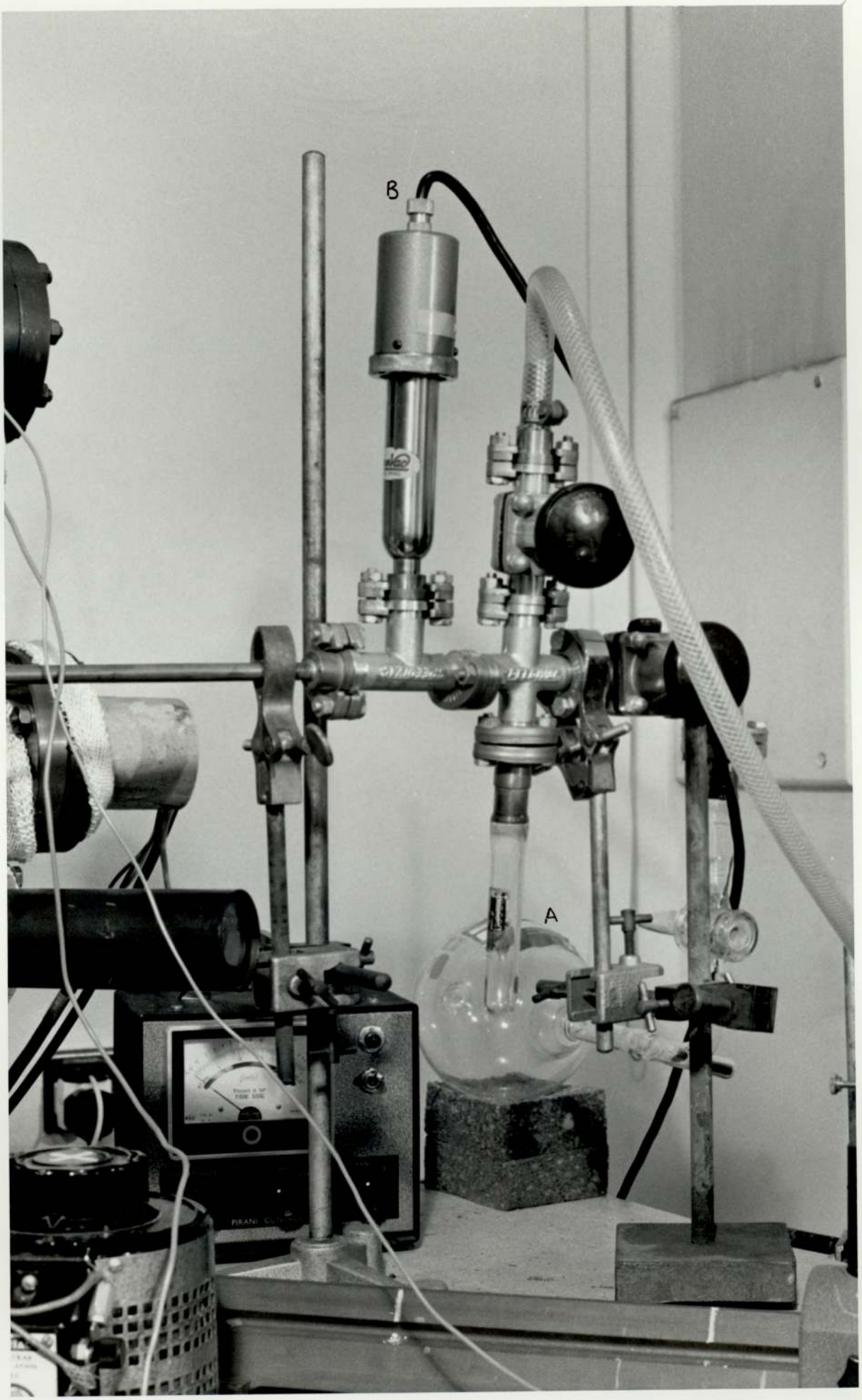
B
A
PIRANI

perforated from one side to permit the ions to emerge. The structure of the gun is shown schematically in Fig. (2.3a).

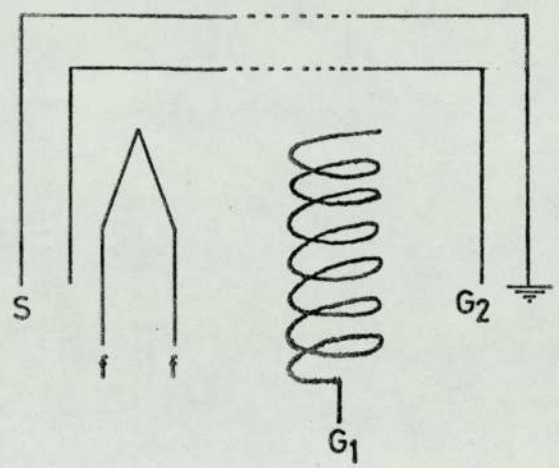


Fig.(2.3a) Construction of ion gun

The principle of operation of the gun is similar to that of the ionization gauge. Electrons make several traverses before being collected. During these multiple traverses, the residual gas is ionized. $G_2$ which is slightly negative, attracts the positive ions outwards and suppresses the electrons. The meshed apertures in $G_2$ and the earthed screen S allow a beam of ions to emerge into the field free region. Ions of energies from 200 to 500 electron volts can be produced.

The ion gun is connected to the system with a bakeable valve type MD6, (Vacuum Generators) through a cross tube as shown in Fig. (2.3b).

A tungsten filament is connected as shown in Fig.(2.3b), for evaporation of the gold film.

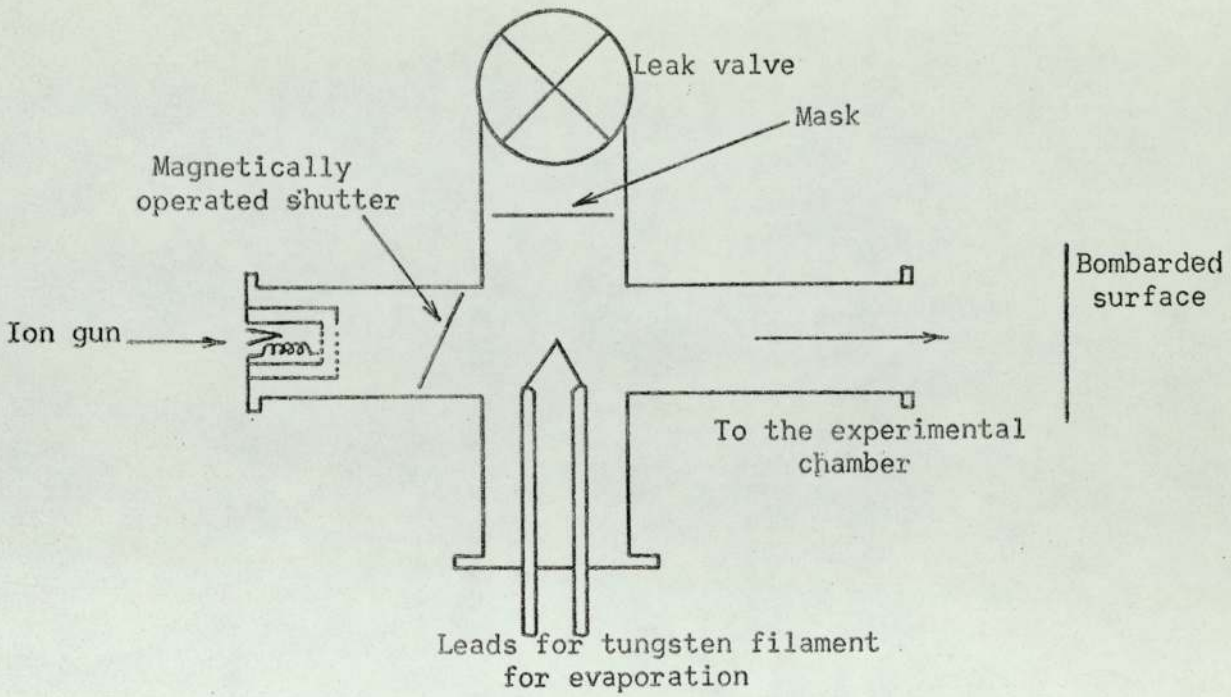


Fig.(2.3b) Construction of the ion gun and the gas side

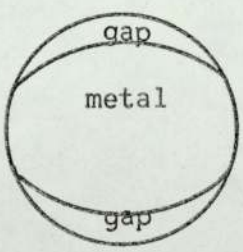


Fig.(2.3c) Mask to protect the leak valve from evaporated metal

Two shutters are positioned in the tubes carrying the ion gun and the leak valve. The upper one protects the leak valve from the metal evaporated. Its shape is shown in Fig.(2.3c) with two side gaps to allow the gas to enter the system with a metal sheet in the middle to stop the evaporated metal from closing up the valve. The other shutter is magnetically operated to stop the ions from reaching the substrate surface.

## 2.4 Optical arrangements

The ellipsometer used in this study is schematically illustrated in Fig. (2.4a) and consisted of the following parts:

### 2.4.1 Light source and monochromator

Two types of lamp were used. A 150 watt ordinary projector lamp and 75 watt Wotan high pressure xenon arc type XBO (AEG-Telefunken (U.K.)) which produces a continuous spectrum and is water cooled. The xenon lamp was supplied from a 60 volt battery.

The selection of the wavelength at which measurements were to be taken was made by means of the monochromator,(H & W D323). The width of the spectral lines produced could be defined by the width of the monochromator input slit which was varied by means of a micrometer screw from zero to a few millimeters. Similarly the radiation leaving the monochromator by the exit slit could be varied in width. The light was focused onto the monochromator entrance slit by means of a condenser lens which can transmit light to 2500 $\mathring{A}$. All the lens systems used were the same.

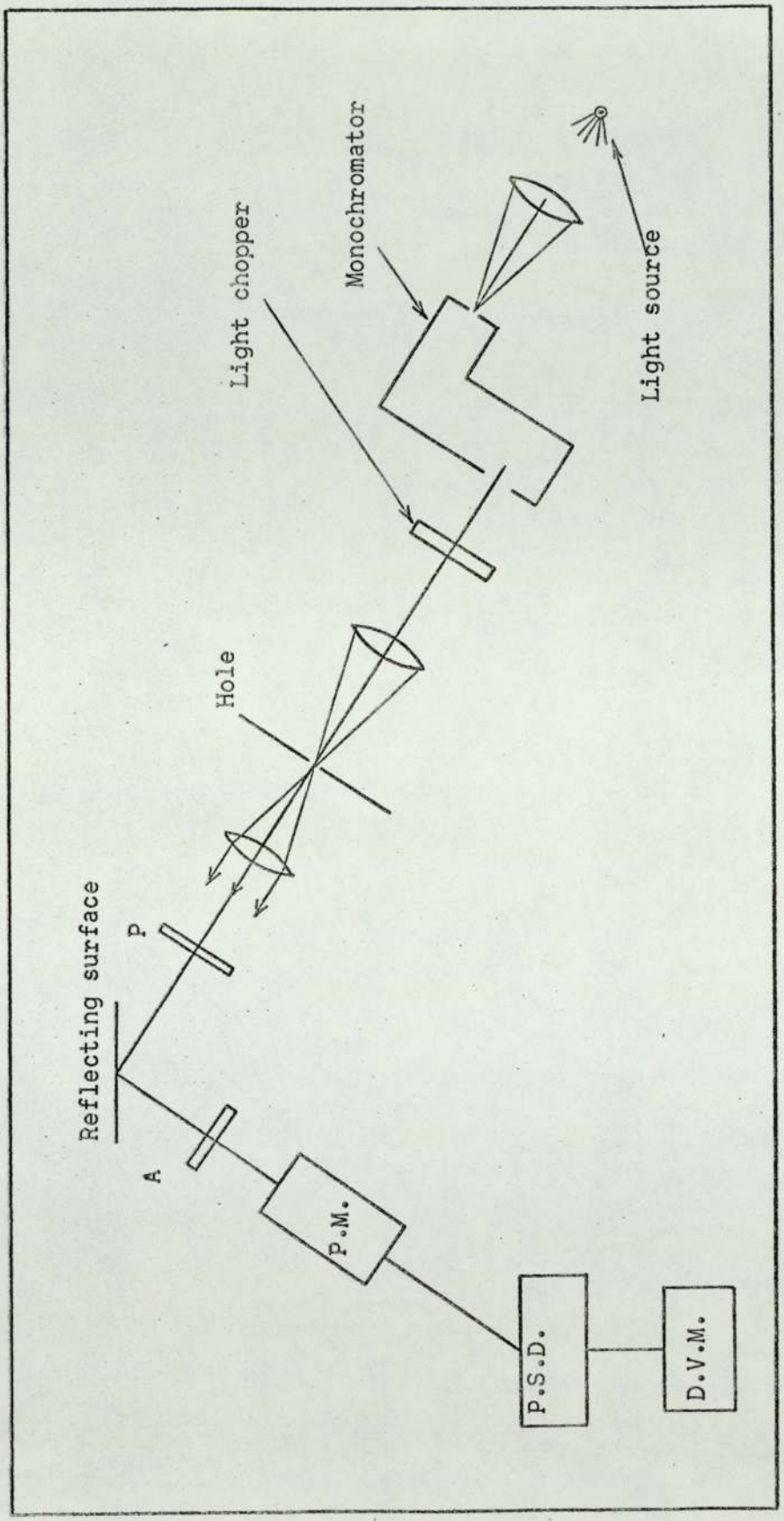


Fig.(2.4.a) Schematic diagram of the construction of the ellipsometer used.

P = Polarizer, A = Analyzer, P.M. = photomultiplier, P.S.D. = Phase sensitive detector

D.V.M. = Digital voltmeter

2.4.2 Polarizer and analyser

Again two types of polarizer and analyser were used:

a) HN22 polaroid, for which the minimum intensity of the light was extended over an angle of 0.5 degree and which increases the error in determining the ellipsometric parameters $\psi$ and $\Delta$. Also, the range at which it is transparent is limited.

b) Two calcite nicol prisms (Bellingham & Stanley) were mounted onto graduated circular vernier scales. The minimum for these prisms was quite sharp (about $0.05^{o}$) which allowed accurate determination of $\psi$ and $\Delta$.

The vernier scale was modified in the departmental workshop to read to 0.02 of a degree.

2.4.3 Detection system

The monochromatic radiation passed through the variable speed light chopper (Type 9479 Brookdeal Electronics Ltd.). The radiation could be chopped at different selected frequencies from 0.5 hz to 3 khz. The light chopper also provides a synchronous square wave signal to drive the reference channel of a lock-in-amplifier. The chopped light emerged from the polarizer, falling onto the sample and then after transmission through the analyzer, was detected by a photomultiplier tube (EMI 9526 B). The response of this photomultiplier tube to incident radiation is at maximum at the blue end of the spectrum as may be seen from the response curve shown in Fig.(2.4.3a). The tube was used in conjunction with a stabilized power supply (Type 532D Isotope Development Ltd). The control circuit of the tube is shown in Fig.(2.4.3b). The signal from the photomultiplier is then fed into an amplifier and phase sensitive detector, the output being indicated by a digital voltmeter. Fig.(2.4.3c) shows the detection system used in these studies.

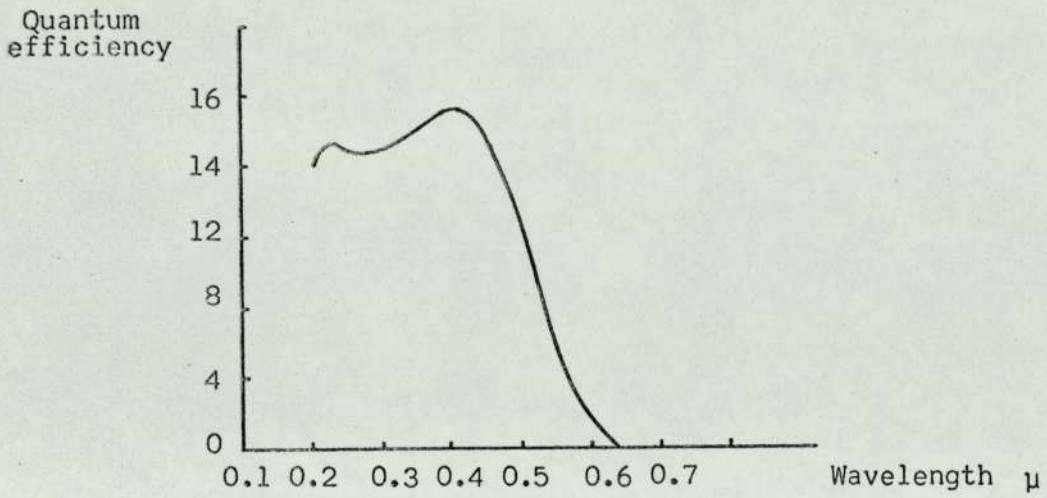


Fig. (2.4.3a) Spectral response of the tube 9526B

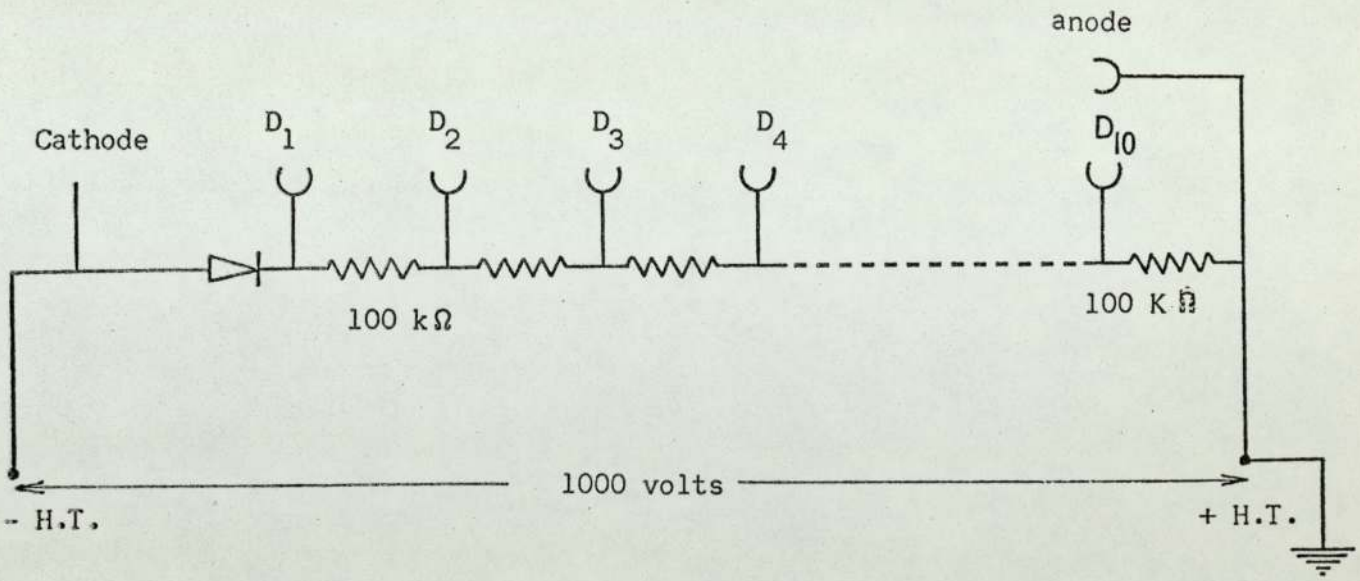


Fig. (2.4.3b) Control circuit of the tube 9526B

Fig. (2.4.3c) Detection system

A = Photomultiplier

B = Phase sensitive detector

C = Power supply to photomultiplier

D = Digital voltmeter

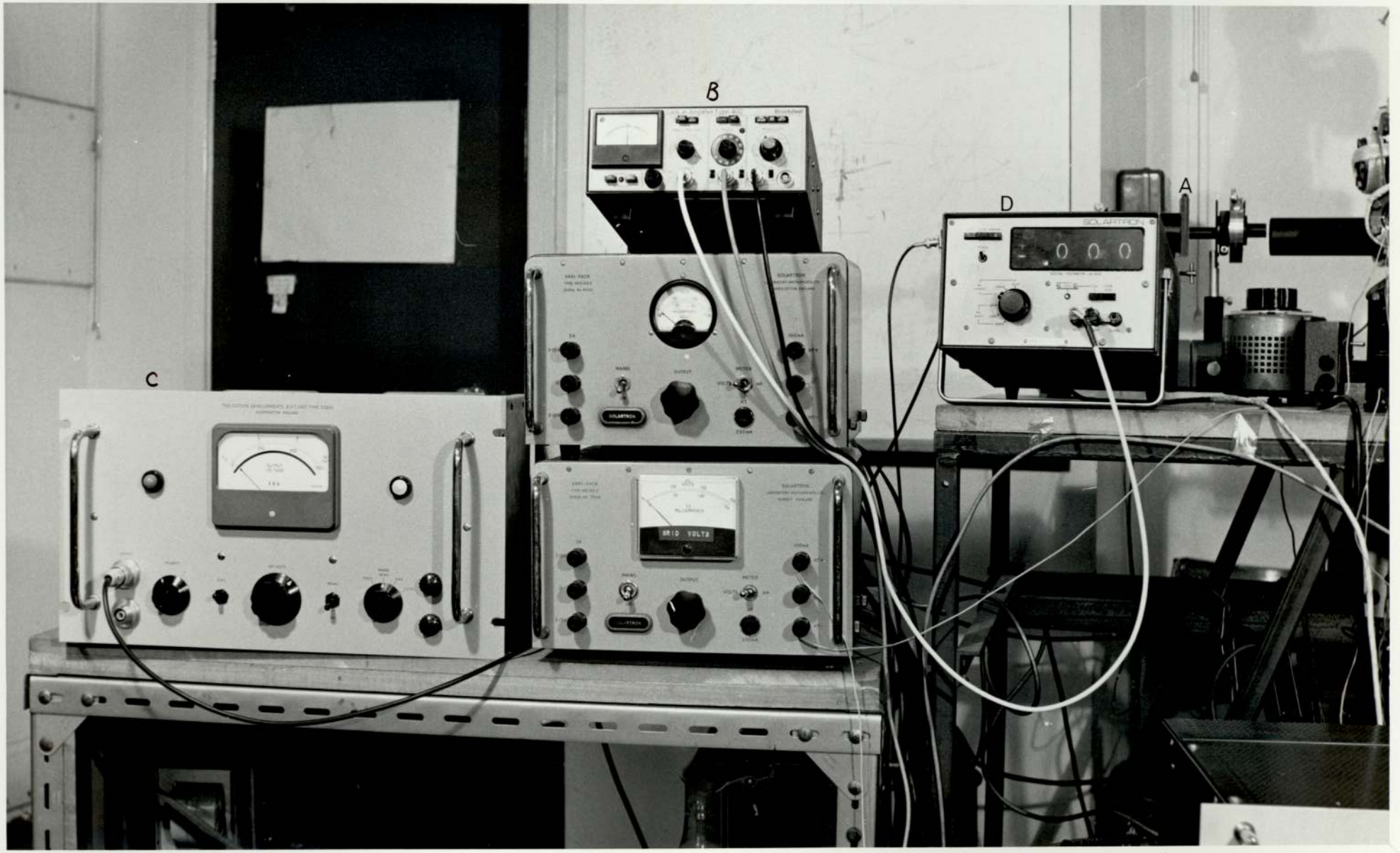
B
A
D
C
GRID VOLTS

## 2.5 Experimental procedure

The experimental chamber was baked with heater tapes to 250°C. The trap adjacent to the chamber also was baked and allowed to cool earlier than the system. While the system was still hot, the trap was filled with liquid nitrogen and after the system was cooled down the pressure reached 2-6 x $10^{-9}$ torr. A polycrystalline and single crystal gold film were prepared and measured in situ. During evaporation, the substrate was held at room temperature (for polycrystalline film) and the pressure in the system rose to 2 x $10^{-7}$ torr. The glass substrates were cleaned, by boiling them for several minutes in dilute detergent (5%) and washing with hot water. They were washed again in distilled water and the substrates were then cleaned in isopropyl alcohol in an ultrasonic vibrator for 15 minutes and finally boiled in isopropyl alcohol and withdrawn through the vapour.

On the gas side, to maintain the purity of the gas which entered the chamber, the following precaution was taken. The tube connecting the experimental chamber and the gas bulb was evacuated to $10^{-2}$ torr through a liquid nitrogen trap, to remove water vapour. Then it was flushed with the gas and again pumped down. The procedure was repeated several times before introducing the gas to the chamber.

After preparing the film, it was annealed to 300°C for five hours and left in vacuum to settle down. After that the film was stable and reproducible results, within the experimental error, were achieved.

2.5.1 Single crystal preparation

Epitaxy is the phenomenon of the oriented growth of one substance on the crystal surface of a foreign substance. The epitaxial growth stongly depends on the deposition conditions. In the present work, single crystal gold films of orientations (110) and (100) were prepared. Sodium chloride single crystals (Cock Light Company) were used as substrates. Two different orientations of (110, 100) enabled single crystal gold films of similar orientation to be prepared. Films prepared in poor vacuum ($5 \times 10^{-5}$ torr) required the substrate to be heated to over $500^{\circ}C$ and contained impurities of other orientations and gold chloride as shown from X-ray diffraction patterns, while for films deposited in $2\text{-}6 \times 10^{-9}$ torr the substrate needed heating to only $350\text{-}400^{\circ}C$.

2.5.2 Preparation of several films in the same run

Two pairs of polycrystalline gold films could be prepared in the same run. Each pair of these films were of the same thickness. The sample holder is shown in Fig. (2.5.2a) in which films 1, 2 were of the same thickness and films 3,4 were also of the same thickness but different from the other two. After preparation all four films were transferred to another sample holder shown in Fig.(2.5.2b) to be annealed. After annealing, one film from each pair was exposed to ion bombardment. The others were used as monitors.

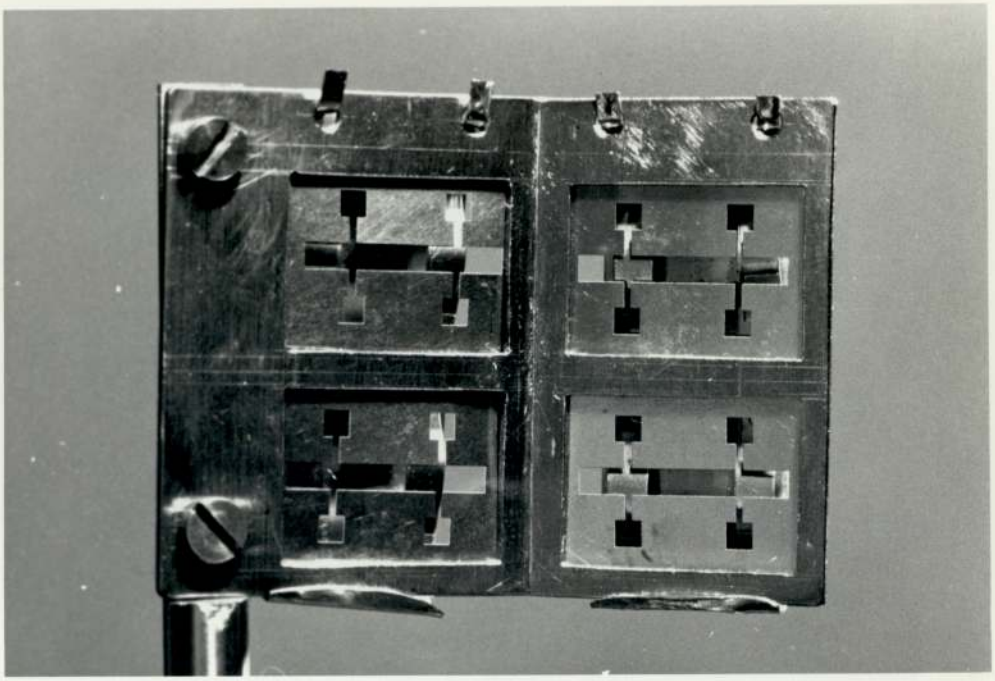

Fig.(2.5.2a) Sample holder for preparation of two pairs of different film thickness.

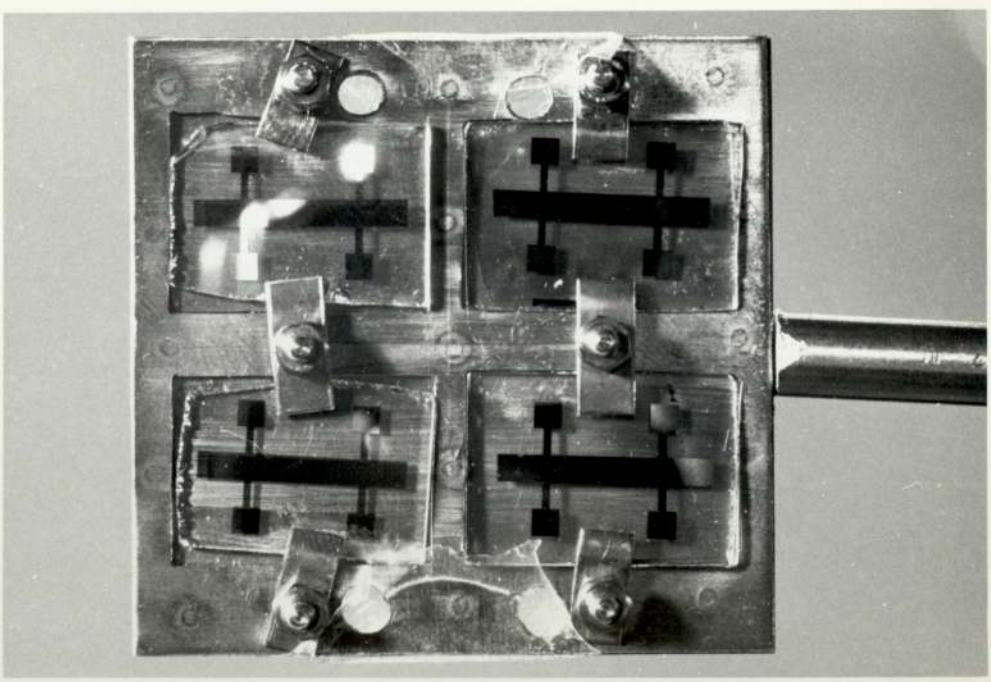

Fig.(2.5.2b) Sample holder for annealing the four films.

## 2.6 Experimental details

Attempts were made to correlate ellipsometric measurements and electrical resistance measurements made on films after low energy ion bombardment with argon and neon ions, or after adsorption of the same gases. Gas adsorption measurements were made at both room temperature and liquid nitrogen temperature. With the system held at a pressure of 2-6 x $10^{-9}$ torr neon or argon gases were introduced in steps up to a pressure of 5 x $10^{-5}$ torr. Each time after introducing the gas a period of ten to fifteen minutes was allowed for equilibrium to be reached and then measurements were carried out. Measurements were taken over the wavelength range 0.39 to 1μ. In measuring $\psi$ and $\Delta$ values, the Beattie method (Beattie 1955) was used to overcome the difficulty of changing the quarter wave plate and to eliminate errors arising from using only one quarter wave plate over a wide range of wavelengths. In this method $\psi$ and $\Delta$ can be determined in two ways:

1. Either by fixing the analyser at 45 degrees from an azimuthal position ($\psi_A$) and measuring the intensity of light at four polarizer settings, or
2. Fixing the polarizer at 45 degrees from an azimuth position ($\psi_P$) and measuring the light intensity at four analyzer settings.

Method 2 was adopted in this work and the light intensities $I_1$, $I_2$, $I_3$ and $I_4$ were measured at analyzer settings of $90^\circ$, $0^\circ$, $+45^\circ$ and $-45^\circ$ with respect to an azimuth. Thus $I_1$ ($+\pi/4$, $+\pi/2$) indicates the light intensity with the polarizer at $\pi/4$ ($\psi_P$) and the analyser at $\pi/2$ with respect to an azimuth. A similar notation is adopted for the other intensity values.

The intensity measured may be expressed as:

$$I(\psi_p,\psi_A) = I_o(\sin^2\psi_p \sin^2\psi_A + \rho^2\cos^2\psi_p \cos^2\psi_A + \tfrac{1}{2}\rho \sin 2\psi_p \sin 2\psi_A \cos\Delta) \qquad (2.6a)$$

where $\rho = r^p/r^s = \tan\psi$

For metals of high conductivity, $(r^s)^2$ differs little from unity so that it can be incorporated into an intensity $I_o$, such that

$$I_o = \tfrac{1}{2}E^2(r^s)^2$$

where E is the electric vector.

From equation (2.6a) the four intensities are:

$$I_1(+\pi/4, +\pi/2) = \tfrac{1}{2} I_o$$

$$I_2(+\pi/4, 0) = \tfrac{1}{2} I_o \rho^2$$

$$I_3(+\pi/4, +\pi/4) = \tfrac{1}{4} I_o(1 + \rho^2 + 2\rho\cos\Delta)$$

$$I_4(+\pi/4, -\pi/4) = \tfrac{1}{4} I_o(1 + \rho^2 - 2\rho\cos\Delta)$$

Values of $\psi$ and $\Delta$ can then be evaluated using

$$\rho = \tan\psi = (I_2/I_1)^{\frac{1}{2}}$$

and

$$\cos\Delta = \tfrac{1}{2}(\frac{1}{\rho} + \rho)\,(\frac{I_3 - I_4}{I_3 + I_4})$$

A simple check which is found to be true to within 0.5 to 1.0% is that:

$$I_1 + I_2 = I_3 + I_4$$

and errors due to incorrect reference azimuths can be reduced by measuring the four corresponding intensities on the opposite sides of the reference azimuth and averaging.

Ideally at all wavelengths, all eight values should be measured, but this procedure would double the time of measurement. Therefore intensities $I_5$ to $I_8$ were measured occasionally to test the reliability of the technique, and also check that:

$$I_5 + I_6 = I_7 + I_8$$

is valid to within the same error limits.

A computer programme to calculate the values of $\Psi$ and $\Delta$ from ellipsometric measurements is described in Appendix I a.

# CHAPTER 3

## INTRODUCTION TO EXPERIMENTAL WORK AND POSSIBLE THEORETICAL MODELS

## 3.1 Physical Adsorption

A gas molecule in the neighbourhood of a solid surface experiences forces which will generally result in a greater concentration of gas molecules near the surface than in the gas phase, i.e. in the phenomenon of adsorption. It is apparent that a complete understanding of the solid gas interface depends uponaknowledge of the mechanism of surface forces. Fundamentally they originate from the electromagnetic interactions of the nuclei and electrons comprising the system. The distribution of these entities is determined by their mutual interactions and by the principles of quantum mechanics. The quantum-mechanical state of the solid and the molecule should be determined for varying positions and orientations of the molecule relative to the surface, and the energy of each of these states could then be compared with the energy of the system when the molecule is at a great distance from the surface. The difference in the energies would be the energy of interaction, and its various space derivatives would yield the forces and torques on the molecule. Such a problem is very difficult to treat in anything approaching real situations, and it is necessary to introduce a variety of simplifications and approximations.

The first of these simplifications is partially suggested by experiments and is associated with the terms physical adsorption and chemisorption. Physical adsorption is usually considered to arise from the presence of Van der Waals forces. These forces appear when the equilibrium distribution of electrons in the molecule and the solid are such that there is no sharing or transfer of electrons between molecule and the solid, and the electrons in the interacting species maintain their respective associations as the molecule approaches the surface.

As the electron clouds interpenetrate, only antibonding or repulsive effects are introduced. The physical and chemical properties of the molecule and the surface are modified but not drastically altered. In chemisorption, the perturbation of the electronic configuration of the crystal due to the creation of a surface is taken into account to deduce the surface states and the distribution of electrons on the surface of metals.

### 3.1.1 Van Der Waals Forces

Van der Waals forces between a molecule and a solid surface may result from several different effects. In any case, the largest contribution to such forces is due to London dispersion forces, which arise from mutually induced in-phase components in the oscillations of the electron clouds. In addition, the gas molecule may possess a permanent dipole and/or higher multipole moments which can (a) induce attractive charge distributions in the solid and/or (b) interact with any permanent external field of the solid. If the solid does possess such an external field, this field can induce electric moments in the molecule which can also result in attractive forces.

For heterogeneous surfaces, the Van der Waals forces are relatively weak at edges, peaks and corners on the surface. The maximum binding forces occur in positions where the adatoms are surrounded by the maximum number of the lattice atoms.

For homogeneous surfaces, a distinction usually is made between three types of Van der Waals forces namely, those that depend on orientating electric dipoles (the directional effect), on electrostatic induction, and on interaction between transient dipoles (the dispersion effect).

The forces that depend on the directional effect arise from the fact that molecules with permanent electric dipole moments $\mu$ exert directional forces on one another as soon as their distance of separation, r, is sufficiently small. According to Debye (1920) and Keesom (1921 a,b and 1922), the exchange energy is given by:

$$E_w = -\frac{2}{3}\frac{\mu_1^2 \mu_2^2}{r^6}\frac{1}{kT} \qquad 3.1.1a$$

If a molecule that has a permanent moment $\mu$ is approached by one that has none, an electric moment proportional to the polarizability $\alpha$ of the latter is induced. Then at a distance of separation r the energy of interaction between these dipoles is

$$E_1 = \frac{2\alpha\mu^2}{r^6} \qquad 3.1.1b$$

The dispersion effect, which was first introduced by London (1930 a,b) takes account of the fact that two atoms can exert dipole forces on one another by virtue of their transient dipole moments. Such a moment develops between the positive nuclear charge of the centre of gravity of the electric charge, so its magnitude and direction will vary periodically. However, since all directions are equally probable, the time average of the dipole moment will be equal to zero. If now such an atom with an instantaneous dipole enters the field of another atom with an instantaneous dipole moment, there results an additional induced dipole whose periodic variation follows the variations of the inducing dipole. These short-term perturbations of the electron vibrations may be treated in analogy to a dispersion effect. According to London, the interaction energy which results from these instantaneous dispersion forces is inversely proportional to the sixth power of the distance of separation r of the atoms,

$$E_i = C/r^6 \text{ with } C = -(3/2)\alpha_1\alpha_2 (I_1 I_2/(I_1 + I_2)) \qquad 3.1.1c$$

where $I_1$, $I_2$ are the ionization energies for atoms 1 and 2, and $\alpha_1$ and $\alpha_2$ are their polarizabilities respectively. Slater and Kirkwood (1931), on the basis of a different assumption, found

$$C = -(3/4\pi)\,(eh/\sqrt{m_e})(\alpha_1\alpha_2/((\alpha_1/n_1)^{\frac{1}{2}} + (\alpha_2/n_2)^{\frac{1}{2}})) \qquad 3.1.1d$$

where $n_1$ and $n_2$ are the numbers of electrons in the outermost shells of atoms 1 and 2, and $m_e$ and e are the mass and charge of an electron respectively. In treating Van der Waals forces operative in the interactions of atoms with metal surfaces, it is not clear how the incident atom (or molecule) interacts with a metal atom. The difficulty arises from the fact that the metal atom is not actually "free", but rather is coupled with its neighbours in the atomic lattice.

Lennard-Jones (1932) used a highly simplified model. He regarded the metal as a completely polarizable body and treated the interaction between the metal surface and the fluctuating dipole of the impinging molecule by means of the classical method of electrical image forces. The molecule itself was treated as a quantum mechanical system on which the image potential acts as a perturbation. For the interaction energy he found

$$E_1 = -(m_e c^2 \chi/2N_A r^3) \qquad 3.1.1e$$

where $\chi$ is the magnetic susceptibility of the gas, c is the speed of light, $N_A$ is Avogadro's number, and $m_e$ is the mass of the electron.

Bardeen (1940), who treated the adatom-metal system completely quantum mechanically, obtained

$$E_1 = \frac{-M_e C^2 \chi}{2N_A r^3} \quad \frac{C_B e^2/(2r_s h\nu_o)}{1+[C_B e^2/(2r_s h\nu_o)]} \qquad 3.1.1f$$

where $C_B$ is a numerical constant, $r_s$ is the radius of a sphere which on the average contains one electron, and $h\nu_o$ is a characteristic energy approximately equal to the ionization energy of the gas.

If the values of the individual quantities are substituted, the term $(C_B e^2/2r_s h\nu_o)$ is found to be approximately equal to one. This means that values given by equation 3.1.1f are only about half as large as those given by equation 3.1.1e.

## 3.2 Interaction of radiation with matter

The phenomena of interaction between energetic radiation and matter is a complex one. The direct effects consist of:

a) The displacement of electrons (ionization)

b) The displacement of atoms from lattice sites

c) Excitation of both atoms and electrons without displacement

d) The transmutation of nuclei.

Primary ionizations are produced by irradiation with energetic charged particles, and, depending on the conditions, primary atomic displacements may be produced. While neutron irradiation produces ionization only as a secondary process, the primary effect being atomic displacement. The important primary effects, caused by irradiation with gamma rays, is ionization but atomic displacements sometimes result as a secondary effect. At high energy (up to 10 MeV) nuclear transmutation can be produced by any of these forms of radiation. At extremely high energy (100 MeV), other special nuclear effects may be observed. Further excitation and disruption of the structure are secondary effects

of the interaction of radiation with matter. The basic laws governing the secondary stages are in all cases the same as those governing the primary stage of charged particle bombardment, so the stopping of charged particles in matter must be considered.

When a, supposedly perfect, crystal is exposed to energetic radiation, defects and imperfections are created. The term radiation damage is given to the spatial arrangement of defects which remain after the irradiation has ceased, and any physical property change which may result from the irradiation of the damage is termed a radiation effect. At the lower end of the range of energies, several features of the experimental and theoretical problem differ significantly from those at higher energies.

In the last twenty years, many solid state physicists have directed their attention to establishing fundamental principles which predict the behaviour of different defects in structuresin different circumstances. The properties of crystals are dominated by the presence of certain defects and many interesting effects in solid state science may be traced to these defects. As an example, the electrical conductivity and other electrical properties of a semiconducting crystal depend on the content and nature of the impurity defects it contains. The careful control of such defects and the resulting semiconductivity enable these crystals to be used as devices. The dislocations and defects which are present, influence the deformation of both metallic and non-metallic solids under an applied force. Even the growth of the crystal is governed by the nature of defects emerging at the surface.

The study of radiation effects in solids has been the subject of many investigations in recent years. In 1942 Wigner predicted that energetic neutrons and fission fragments have the ability to displace atoms from their equilibrium positions. He expected that energetic massive particles and heavy bombardment of solids will lead to serious and important technological effects. Since then many programmes of theoretical and experimental studies on the nature and magnitude of the effects have been conducted.

During the last decade it has been realised that the study of radiation effects may lead to a new and valuable insight into the properties of imperfections in solids. The change in the physical and electrical properties as a result of defects has become an increasingly important part of solid state research. Large numbers of defects can be introduced in a crystal in a well controlled way.

3.2.1 Moving charged particles

An energetic charged particle is slowed down in moving through matter by successive collisions. The collisions which the moving atom undergoes may be divided into two classes, elastic and inelastic collision. In an elastic collision the moving atom interacts with an atom of the target material, imparting some energy to the target atom and losing a like amount of energy (the collision is elastic in the sense that the total kinetic energy of incident and struck atoms is conserved not that the incident atom is scattered without loss of energy). In an inelastic collision, there is loss of energy because of electronic excitation. In all collisions, the interaction force is the Coulomb force between nuclear and electronic charges. In elastic collisions

it is sufficient to consider that the electrons partially screen the nuclear charges but play no other role, while inelastic collisions require that electrons interact directly with the incident particle, being left in excited states after its passage. In general, the collision is inelastic when the atoms have high energy, while elastic collisions become more important after the atom has slowed down. The transition from inelastic to elastic behaviour is not abrupt but if the moving atom has a velocity much less than that of an electron in the target, that electron will be left without excitation. If the moving atom has a velocity equal to or greater than that of the electron, electronic excitation becomes probable. The most important primary process in irradiation is the displacement of atoms. The displaced atoms are produced by the moving charged particles by elastic collision interacting essentially one at a time with the stationary atoms. In such collisions, it is convenient to assume that the moving and stationary atoms interact with a screened Coulomb potential energy of the form:

$$V(r) = (Z_1 Z_2 e^2/r)e^{-r/a} \qquad 3.2.1a$$

where r is the separation of the two atoms and

a is the screening radius which is constant for a given pair of atoms.

The screening radius may be given by:

$$a = a_o/(Z_1^{2/3} + Z_2^{2/3})^{1/2} \qquad 3.2.1b$$

where $a_o$ is the Bohr radius of Hydrogen ($a_o = \hbar^2/me^2 = 5.29 \times 10^{-9}$ Cm).

The collisions can be calculated from classical mechanics with good accuracy in most cases. At close approach, equation 3.2.1a describes the Coulomb repulsion of the two nuclei of charges $Z_1 e$ & $Z_2 e$, respectively.

At separations of the order of a, the repulsion is lessened by the partial screening of the nuclei by the two electron clouds.

A moving atom colliding with a stationary atom will be deflected from its path by an amount which depends on its energy and on its distance of approach, the deflection being greater for smaller energies and for closer approach. Also the momentum and hence the energy transferred to the stationary atom increases as the angle of deflection increases. Whenever the nuclei of the two atoms approach to a distance much less than the screening radius a, the nuclear Coulomb repulsion produces most of the deflection and the collision can be calculated by ignoring the screening, as given by Rutherford scattering laws. More distant collisions are partly screened, and no single expression for the cross sections has been deduced.

3.2.2 Hard Sphere Approximation

For very distant collisions the colliding bodies may be assumed as hard elastic spheres. This assumption has been much used in displacement calculations, although it is not very accurate in the range in which it is applied. Numerical calculations of screened Coulomb scattering, which cover the intermediate range between the Rutherford and hard sphere limits, have been made by Everhart, Stone and Carbone (1955). The scattering is governed by a parameter 'b' given by:

$$b = 2Z_1Z_2e^2/\ v^2\mu \qquad 3.2.2a$$

$$\mu = M_1M_2/(M_1 + M_2)$$

where $\mu$ is the reduced mass and v is the velocity of the incident particle, b, the distance to which the two nuclei would approach in a head-on collision in the absence of screening and is called the collision diameter.

For collisions to be approximately of the hard sphere type, it is necessary that $b/a \gg 1$. An idea of whether the Rutherford or hard-sphere approximation is appropriate can be obtained by comparing the energy of the moving atom to a critical energy $E_A$ so defined that

$$\frac{b}{a} = 1 \quad \text{at} \quad E = E_A$$

The elastic collisions are of Rutherford type when $E \gg E_A$ and approximately of hard sphere type when $E \ll E_A$ then:

$$E_A = E_R(2(M_1+M_2)/M_2)Z_1Z_2(Z_1^{2/3}+Z_2^{2/3})^{1/2} \qquad 3.2.2b$$

Where $E_R$ = Rydberg energy = 13.6 eV.

The most important characteristic of a collision is the energy transferred to the struck atom. This may range from zero in glancing collisions to a maximum, $T_m$, which is transferred in a head-on collision. From energy and momentum conservation, we can get

$$T_m = (4M_1M_2/(M_1+M_2)^2)E \qquad 3.2.2c$$

Small energy transfers are more probable than large in Rutherford collisions. The differential cross section for energy transfer T to T + dT being:

$$d\sigma = C(dT/T^2) \qquad 3.2.2d$$

Where the coefficient C is given by:

$$C = 4Ta_o^2(M_1/M_2)Z_1^2 Z_2^2(E_R^2/E) \qquad 3.2.2e$$

Equation 3.2.2d is valid for T ranging from $T_m$ to some small but finite lower limit at which electronic screening can no longer be neglected. The total cross section for production of a displacement can be found to be

$$\sigma_d = \int_{t=t_d}^{t=t_m} d\sigma = C(1/E_d - 1/T_m) \qquad 3.2.2f$$

Where $E_d$ is the threshold energy for displacement. Substituting for $T_m$ and C we get:

$$\sigma_d = 16\pi a_o^2 Z_1^2 Z_2^2 \frac{M_1^2}{(M_1 + M_2)^2} \frac{E_R^2}{T_m^2} \left(\frac{T_m}{E_d} - 1\right) \qquad 3.2.2g$$

In Rutherford collisions, the average energy transferred which displaces atoms, $\bar{T}$, may be calculated as:

$$\bar{T} = \int_{T=E_d}^{T=T_m} T\, d\sigma \Big/ \int_{T=E_d}^{T=T_m} d\sigma$$

$$\bar{T} = (E_d T_m/(T_m - E_d)) \ln(T_m/E_d) \qquad 3.2.2h$$

In typical cases $\bar{T}$ is much less than $T_m$ which emphasizes the strong preference for low-energy transfers in Rutherford collisions. On the other hand, in hard-sphere collisions, all energy transfers from zero to $T_m$ are equally probable, and the differential cross section for energy transfer T to T+dT can be given by:

$$d\sigma = c'dT \qquad 3.2.2i$$

where $c' = \pi a_1^2/T_m$

and $a_1$ is the diameter of the effective hard sphere, approximately the screening radius as given by equation 3.2.1b. For screened Coulomb collisions at energies in a rather broad range in the neighbourhood of $E_A$, the differential cross section is neither of the Rutherford nor for the hard sphere type and may be represented by:

$$d\sigma \;\alpha\; T^{-m}\, dT \qquad 3.2.2j$$

where the exponent m ranges between 1 and 2.

3.2.3 The displacement threshold.

The energy which would be required to move an atom from its site and force it into the surrounding lattice to form a Frenkel defect can be estimated. In a solid, the energy of sublimation $E_c$ of a typical atom or ion is in the range of 5 or 6 eV, so that the energy required to move an atom from an internal site, might be expected to be of the order of double the value since twice as many bonds are involved. However, atoms on neighbouring sites will oppose this removal and so the energy required to carry the process through will be at least $4E_c$. On the basis of this kind of reasoning, it can be shown that some 25 eV of energy will be needed to be transferred in a collision if the struck atom is to be displaced from its normal lattice position to an interstitial site. In the most simple treatments of radiation damage problems, this displacement energy $E_d$ is given a value of 25 eV. If the atom receives an energy less than this value, the probability that it will be displaced is zero and the atom remains bound to its lattice position and dissipates, through vibrational motion, the energy it has accepted. On the other hand, if the energy communicated to the lattice atom by the colliding particle is greater than $E_d$, the probability of displacement is unity. The atom is ejected and becomes a knock-on atom. Primary knock-ons of sufficient energy leave their lattice sites and, by further collision, initiate a whole cascade of vacancies and interstitials. It must be anticipated that the effect of temperature of the irradiated crystal will have to be taken into account. The effect of atomic vibrations would be expected to lower the value of $E_d$ or to introduce a natural width of the order of $kT$, where $k$ is Boltzmann's constant and $T$ is the temperature. In a real crystal an atom ejected towards a position in the lattice between two adjacent neighbours must experience less resistance than if it was directed towards an atom. An idealized displacement curve is

shown in Fig. .3.2.3a where the crystallinity of the sample and blurring-out effects of increasing the crystal temperature are accounted for.

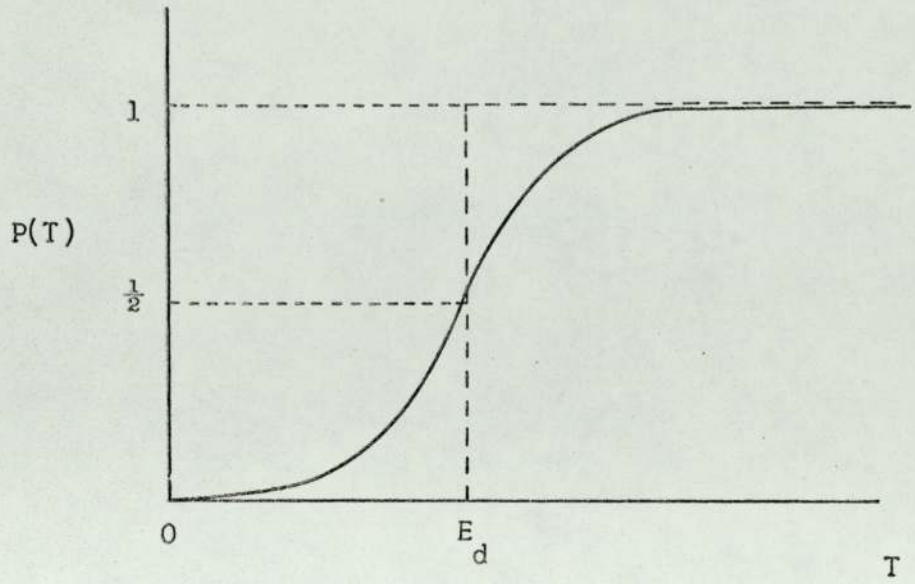


Fig. 3.2.3.a. An idealized displacement probability curve taking account of crystallinity of the sample and of anisotropy. The probability of displacement in any direction at a given temperature at a transferred energy of $T = E_d$ is 1/2.

## 3.3 Influence of the ordered lattice structure

No one potential model properly describes atomic interaction over the complete range of impact parameters. A large variety of potential models are available in studying radiation damage of which some relations have been formulated with a particular problem in mind. For example, the screened Coulomb relation might be useful for high energy collisions, and the energy dependent hard sphere model for near-threshold events. Similarly the Born-Mayer potential, which takes the form:

$$V(r) = A \exp(-r/B) \qquad 3.3.1a$$

where A and B are assumed to be determinable constants, can be used with success either as the explicit form in the energy dependent hard-sphere model, or alone in describing low-energy impact. For intermediate separations the problem remains. Brinkman's potential equation describes generally the interaction between two identical atoms, each atom is represented by a model consisting of a nucleus surrounded by a rigid charge distribution and it is assumed that both atoms supply a screened Coulomb field of the same type. The potential of interaction is given by:

$$V(r) = (Z^2e^2/r) \exp(-r/a) (1-(r/2a)) \qquad 3.3.1b$$

Where r is now the separation of the two nuclei. The fact that this first potential could be criticized on the grounds of predicting too strong an interaction energy at large distances led Brinkman to formulate a new empirical relation which he considered to be valid generally for radiation damage calculations covering a wide class of interacting atoms. This potential energy function, known as Brinkman potential II is

$$V(r) = (AZ_1Z_2e^2 \exp(-Br)) / (1-\exp(-Ar)) \qquad 3.3.1c$$

The Brinkman potential II is particularly useful since it joins the screened Coulomb and Born-Mayer relations at the two extremes. This is shown in Fig. 3.3.a.

Another type of approximation, which takes into account the change in electron energy connected with the mutual approach of the nuclei, has been formulated by Firsov. Since the Thomas-Fermi statistical model of the atom is the basis for this formulation the resulting potential is often referred to as the Thomas-Fermi (Firsov) TF two-centre potential. The Firsov potential is also shown in Fig. 3.3.a so that the extent of its deviation from the Born-Mayer and screened Coulomb relations is obvious for large separations.

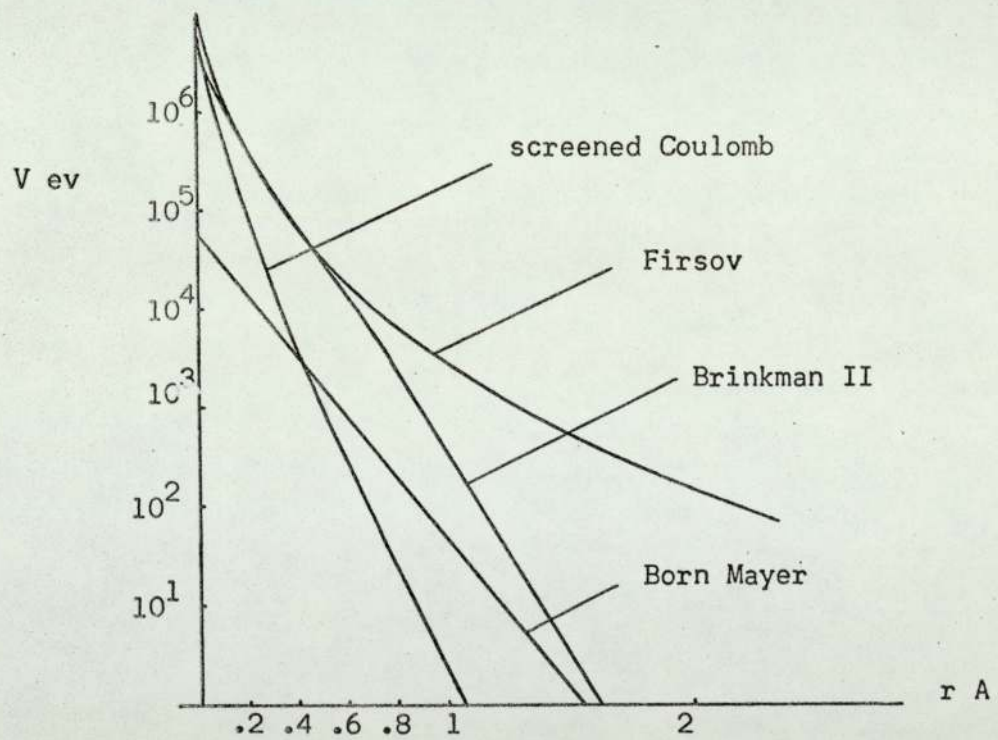


Fig. 3.3.a. Deviation of potential for different models at some values of r. The Brinkman II potential is particularly useful since it joins to the screened Coulomb and Born-Mayer relations at values of r where they are valid and may be applied over intermediate distances.

The Brinkman potential II was derived particularly for copper silver and gold, whilst for certain other values of Z an error was introduced into V(r). The spatial density of lattice atoms could be the same for a single crystal, a polycrystalline specimen and an amorphous substance but account would have to be taken of the spatial arrangements of atoms. This is an important parameter in single crystals and in most cases, crystals exhibit a marked anisotropy in their properties. In the most simple model of a crystal lattice, atoms are represented by hard spheres with their centres at lattice sites. A primary knock-on then becomes a similar hard-sphere which is moving in the lattice and which makes collisionsrather like a billiard ball collision in three dimensions. On the basis of this simple picture, it is clear that there are some directions in which the knock-on can move with comparative ease, while in other directions the primary moves towards a seemingly impenetrable wall of atoms. Holmes (1963) and Leibfried (1959) have made an improvement on the hard-sphere potential. Since the interaction actually decreases monotonically with increasing distance, two atoms in a head-on collision will penetrate closer to each other at higher energies than at lower energies. Consequently the effective radius of strong interaction must increase with decreasing energy. Moreover, since during the slowing-down process a primary passes through a range of energies below its initial energy, it is necessary to allow for this effect. One way of doing this is to let the sphere radius depend upon energy, then for the equal mass case, it may be shown by conserving energy and momentum that:

$$V(2R) = E/2 \qquad 3.3.1d$$

Where V(2R) is the potential at the distance of closest approach 2R, and E is the kinetic energy of the primary. It can be seen how R

depends on the energy if we choose a particular equation, say the Bohr relation, for the interaction potential V(r), equation 3.3.1d may then be written as follows:

$$(Z^2e^2/2R(E))\exp(-2R(E)/a) = E/2 \qquad 3.3.1e$$

The atoms are treated as hard spheres, but that the radius of each sphere, as "seen" by the primary during its motion, depends upon the latter. This dependence of hard sphere radius on energy leads us to a similar dependence for the mean free path ($\lambda$) which can be written:

$$\lambda(E,T) = 1/n_o.\pi p^2 \qquad 3.3.1f$$

where p is the impact parameter, $n_o$ is roughly $10^{23} cm^{-3}$. In the hard sphere model the impact parameter becomes twice the radius of the sphere R(E) so that:

$$\lambda(E) = 1/n_o 4\pi R^2(E) \qquad 3.3.1g$$

according to Leibfried Fig. 3.3b -1 shows how a primary of energy E "sees" the copper lattice in the hard-sphere approximation. The primary is drawn as a point at the origin, and the stationary atoms circles with radius 2R(E) are drawn to demonstrate the space into which the primary cannot penetrate. At higher energies the circles are small and the mean free path between collisions is long Fig. (3.3b-2). The mean free path becomes of the order of one lattice distance ($a_o$) at energies of the order of $E_d$, the displacement energy.

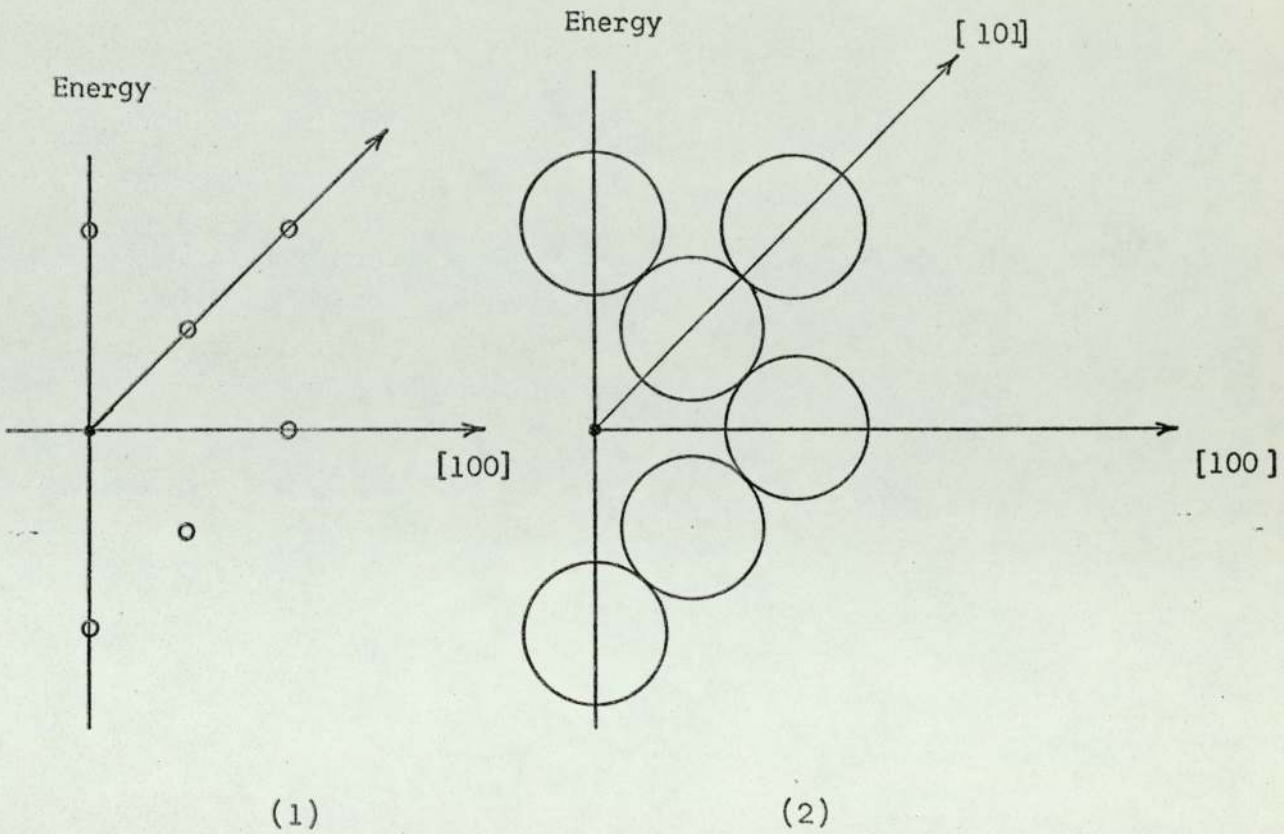


Fig. 3.3.b. The lattice of copper crystal as "seen" by a primary knock-on of energy E in the energy dependent hard-sphere approximation.

1 ) Radius $2R(E) = a_o/7$ energy $E \sim 10^4$ eV, mean free path for collision $\lambda \sim 10a_o$

2 ) Radius $2R(E) = a_o/2$ energy $E \sim 60$ eV, mean free path for collision $\lambda \sim a_o$

$a_o$ is the lattice distance (After G. Leibfried)

### 3.3.1 Focusing collision

From the energy dependent hard-sphere model, we can see that when the energy of a primary becomes small enough the lattice is able to impose rigid conditions upon the possible modes of momentum transfer. When a struck atom cannot penetrate the surrounding lattice it can only transfer energy and momentum to one of its immediate neighbours, and so the possibility of collision correlation becomes apparent. More particularly where close packed rows of atoms exist in the crystal, one may expect an energy pulse or a sequence of collisions, to be propagated along them. This is the phenomena of focusing as it was first suggested by Silsbee (1957), though more recently it has been demonstrated through a series of experiments performed by M.W.Thompson and his co-workers.

Consider the hard sphere collision which is represented schematically in Fig. 3.3.1a. Each sphere is given a radius of R, and the initial separation is denoted by D. If the first atom receives a momentum vector which lies in the direction of AP and makes an angle $\theta_1$, with the line of centres AB, then a hard sphere collision occurs when the centre of atom(1) reaches the point P. Atom(2) then possesses a momentum vector which lies along PB and makes an angle of $\theta_2$ with the line AB. If $\theta_1$ and $\theta_2$ are sufficiently small then:

$$AP = D - 2R \qquad 3.3.1a$$

and by a simple geometrical consideration we can write

$$\theta_1(D-2R) = -2R\theta_2 \qquad 3.3.1b$$

If we define a focusing parameter f as follows:

$$-f = \theta_2/\theta_1$$

$$f = (D/2R) - 1 \qquad 3.3.1c$$

and then we can see that:

$$D > 4R \quad \text{for} \quad f > 1 \quad \text{and} \quad |\theta_1| < |\theta_2| \qquad 3.3.1d$$

$$D < 4R \quad \text{for} \quad f < 1 \quad \text{and} \quad |\theta_1| > |\theta_2| \qquad 3.3.1e$$

now the possibility of further hard sphere collisions are considered along the same row of atoms and that a sequence of collision representing the energy pulse, passes down the row after irradiation at atom( 1). By the time the pulse reaches atom n, the relation between the angles involved is still given by:

$$\theta_n = (-f)\theta_{n-1}$$
$$= (-f)^2\, \theta_{n-2} \qquad 3.3.1f$$

and it can be finally written:

$$\theta_n = (-f)^n \theta_1$$
$$= (1-(D/2R))^n \theta_1 \qquad 3.3.1g$$

There will be in general two distinct physical possibilities.

a) If the separation D is greater than 4R, the focusing parameter f is greater than unity, so that the angles $\theta_n$ will increase at successive collisions, and momentum and energy will be transferred to neighbouring close-packed rows.

b) If D is less than 4R, f is less than unity, and the angles $\theta_n$ converge to zero through the factor $(-f)^n$ until all collisions are of the head-on kind.

At this stage of the proceedings, the momentum transfer is perfectly efficient for every collision, and some component of the initial momentum is focused into the line AB. The bundle of energy which passes-down the row is called a focuson.

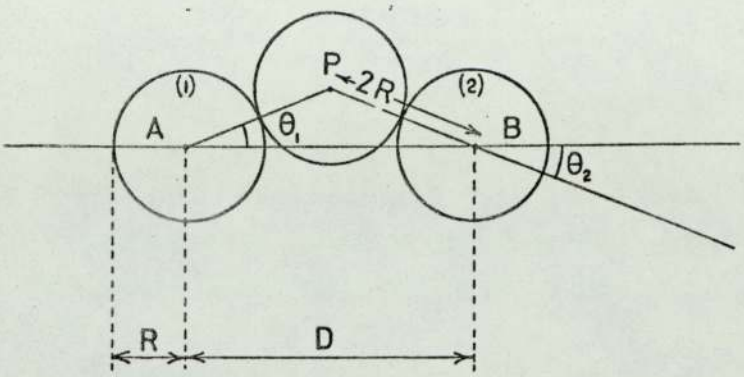


Fig. 3.3.1a. The simple focusing effects, hard sphere collision (After M.W.Thompson)

3.3.2 Critical focusing

Critical focusing occurs when a particular angle $\theta_c$ is maintained for successive collisions, this is shown in Fig. 3.3.2a. The value of the critical angle depends upon the ratio of atom size to separation. The smallest value of f is obtained for the closest packed rows of atoms. Focusing of momentum will be favoured along rows of atoms (in the $<hkl>$ direction) for which the interatomic separation $d_{hkl}$ is minimal. A critical focusing energy $E_f^{hkl}$ can therefore be defined below which $f < 1$, $R < D/4$ and focusing is possible. At the critical energy, f is unity, by definition and R is exactly equal to D/4.

The expression for $E_f^{hkl}$ can be found by describing the interaction of atoms by a potential of the Born-Mayer kind:

$$V(r) = A \exp(-r/B) \qquad 3.3.2a$$

where A and B are assumed to be determinable constants, when

$$E = E_f^{hkl} \qquad (R = D/4) \qquad 3.3.2b$$

It follows that:

$$E_f^{hkl} = 2A \exp(-D^{hkl}/2B) \qquad 3.3.2c$$

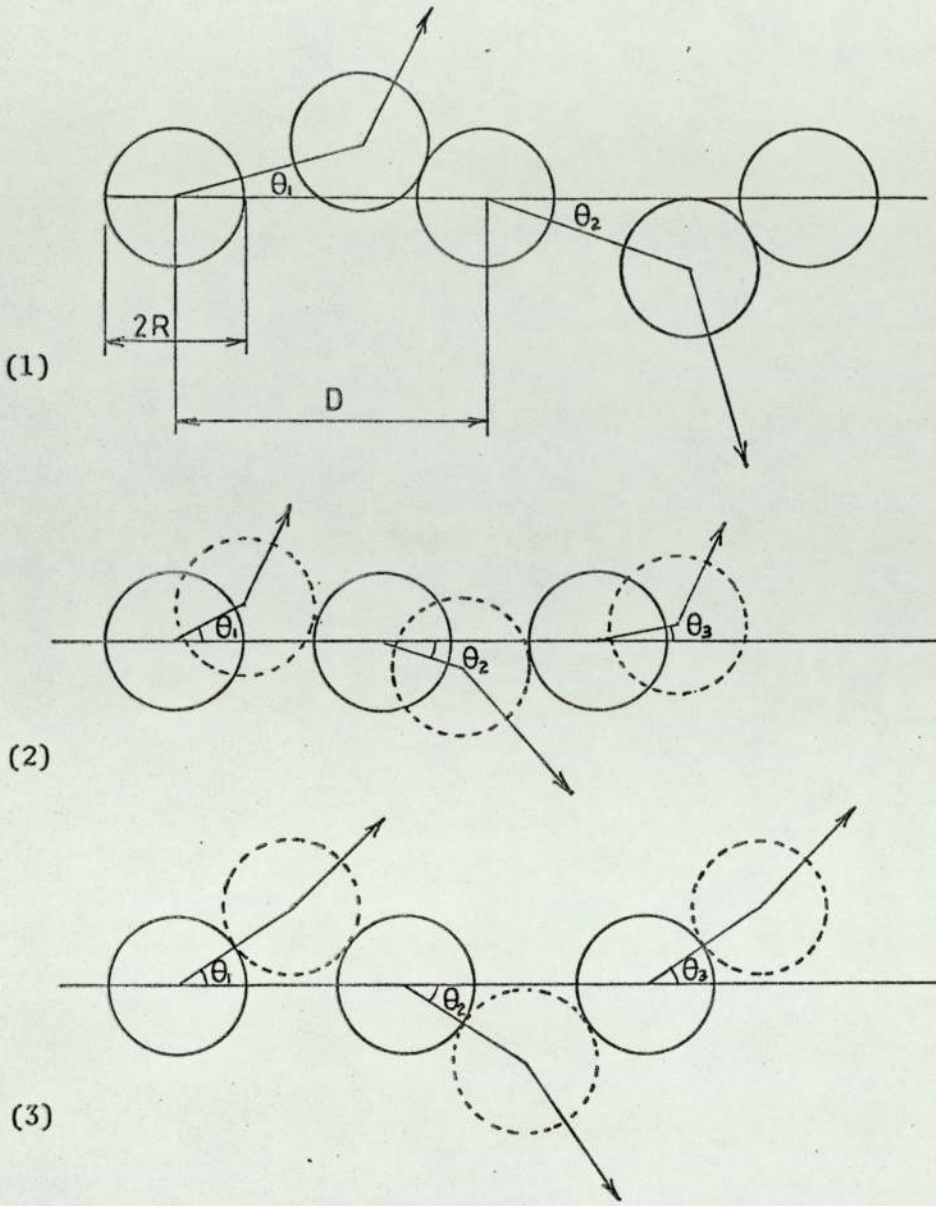


Complete Defocusing

$\theta_c > \theta_1 > \theta_2 > \theta_3$

Focusing

$\theta_1 = \theta_2 = \theta_3$

Critical Focusing

Fig. 3.3.2a. Focusing.

1 - The distance D between atoms is too large to allow focusing.

2,3 - Focusing is determined by the initial angle of projection $\theta_1$. If $\theta_1 < \theta_c$, focusing occurs. If $\theta_1 > \theta_c$ no focusing occurs. The critical angle $\theta_c$ is determined by the ratio of atom size to separation R/D.

3.3.3 Assisted focusing

The influence of neighbouring rows of atoms on the focusing process is not so severe for circumstances where the neighbouring rows lie at some distance from the line in question, in other cases it is very important. To illustrate this point, the propagation along the < 100 > direction of a face-centred cubic crystal is considered. Fig. 3.3.3a.1 shows one collision in this sequence. An atom $A_1$ passes through a ring of four B atoms and makes a head-on collision with another atom $A_2$. Fig. 3.3.3a-2 shows a less ideal collision, in which a small deviation $\theta_1$ of the initial trajectory of $A_1$ from the axis results in a final deflection $\phi$. $A_1$ suffers from glancing collision with the B atom, but more momentum is transferred to one side of the ring than the other, and focusing occurs.

The critical nature of the assisted focusing process can be most easily visualized by noting that if focusing is to occur ($\theta_2 < \theta_1$) then the extended trajectory of $A_1$ must cut the axis to the left of $A_2$. An analytical expression for the focusing parameter itself, $f^{100}$ ($\theta_2 = \theta_1$), may be obtained from consideration of the geometry of Fig. .3.3.3a-3

$$f^{100} = (D^{100}/2\sqrt{2R}) - 1 - ((D^{100}/4\sqrt{2R}) - 1)(2A(D^{100})^2/3EB^2)\exp(-3D^{100}/4B) \qquad 3.3.3a.$$

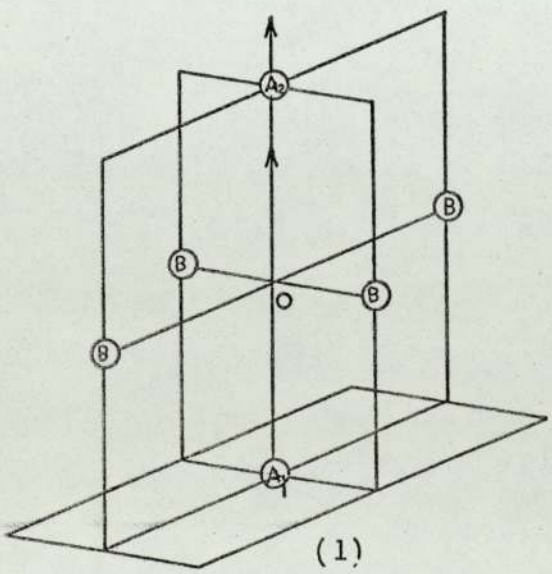


(1)

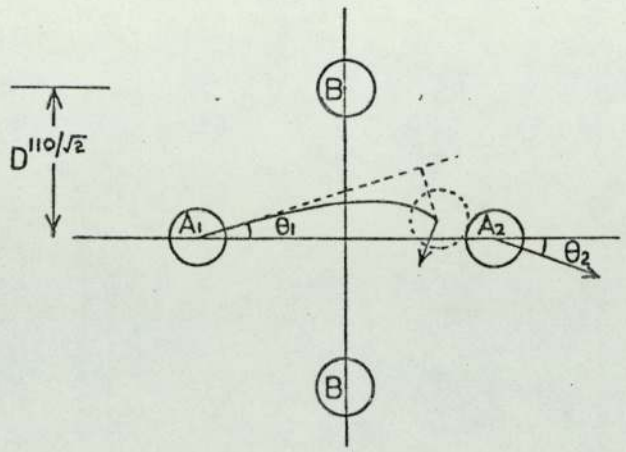


(2)

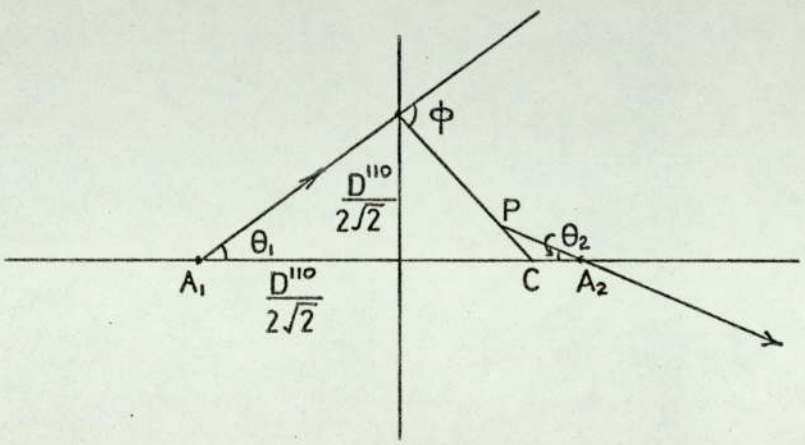


(3)

Fig.3.3.3a-1 - Propagation of an idealized collision sequence in the <100> direction of a face-centred cubic crystal begins when an atom $A_1$ passes axially through a ring of four B atoms and makes a head-on collision with atom $A_2$.

2 - Propagation of a less idealized collision sequence begins with a small deviation $\theta_1$ of the initial trajectory of $A_1$ from the axis.

3 - Geometry of the collision in (B) (After M.W.Thompson).

For assisted focusing $D^{hkl} \rightarrow 4R$, so that replacements and therefore the transfer of mass inevitably occur. The basic limitations of the treatment are the impulse approximation, which overestimates $\phi$ since the trajectory is not straight and the hard sphere potential, which underestimates $\theta_2$ since the atoms are not perfectly elastic. A principal attraction of the method is that it can be applied with success to different directions in different crystals and so a comparison with experimental results is thereby facilitated. In addition the assisted focusing process is very similar to the action which a simple thin converging lens exerts upon a beam of light. If the atoms B lie close to the optic axis, then the atomic lens is strong, focusing is enhanced, and the effective focal length is small.

### 3.3.4 Channeling

Another possible mode of energy and mass transfer has been suggested by experimental investigations of the ranges of particles along different crystallographic directions. In the previous section, the motion of an atom $A_1$ through a ring of B atoms Fig. 3.3.3a-2 is considered, and its subsequent collision with another atom $A_2$. Suppose that the primary atom $A_1$ is alone on the axis, any motion of $A_1$ down the axis is now a much easier proposition since collision of small impact parameter with atoms in the row are completely eliminated, and only glancing collisions with B atoms can lead to energy loss. The energy of a primary may be propagated down a close-packed chain as a dynamic crowdion or focuson, and in this manner be distributed over a relatively large volume of the crystal. However, there do exist open channels which are bordered by close-packed chains, and which run parallel with them. If the primary enters and moves down such a channel, its interaction with the lattice

will be small. It will travel long distances in an almost force-free space, and although relatively few primaries are expected to execute this type of motion, a small, far-travelling component will weight the average primary range to larger values than would be obtained if the lattice order were neglected. By analogy with the focuson, a primary of this kind is called a channelon, in some original papers the word stenon is used. A channelon always transfers mass.

To illustrate the chanelling phenomena, we consider< 110> channel of a face centred cubic lattice. This channel is bordered by four atomic < 110 > chains as shown in Fig. 3.3.4a-1 and possesses central axis of symmetry. Because of this symmetry the net force acting on the primary in the axis has only a component along the axis. Consequently once a primary is moving along axis it stays there and loses interactions with the bordering lattice atoms. The surrounding atoms are regarded as fixed, and this means that the primary is moving in a static potential V(xyz) which is periodic in x, the axis of symmetry. Leibfried and Lehmann show that a primary atom can follow a trajectory which bounces back and forth between the adjoining rows, and that active chanelling for which the amplitude of transverse motion tends to decrease with the distance along which channel can occur. Figs.3.3.4a-2 show a schematic representation of a typical channelon. It is not clear how an atom can get into a channel, because the mechanism of displacement much more favours the initiation of focusons and dynamic crowdions. The focuson and channelon present different energy effects, the former occurring predominantly at low energies and the latter at high energies. Nevertheless both these methods of energy transport are susceptible to changes in lattice temperature, and are similarly affected by defects

introduced into the lattice. The channelon, because of the non-displacement nature of its energy loss, leads to the further possibility of a reduction in the expected radiation damage.

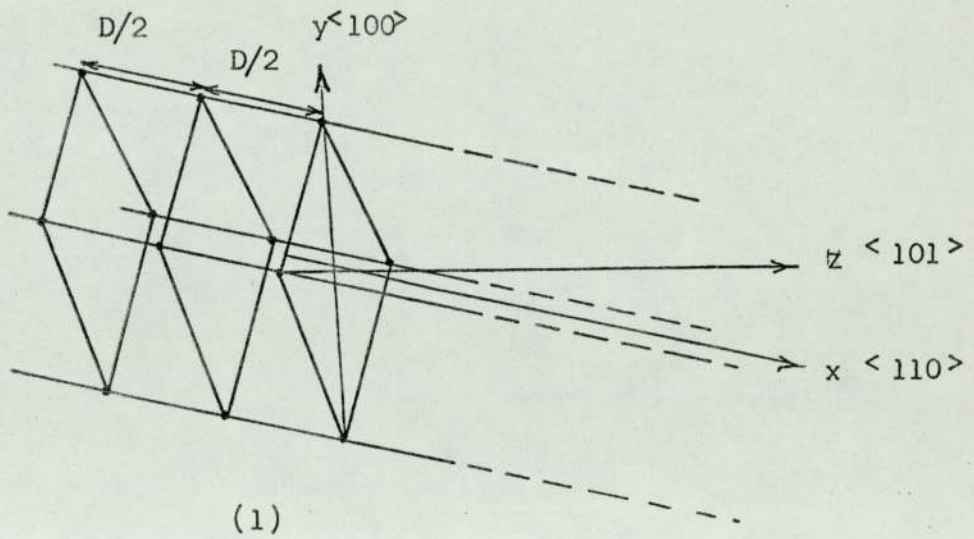


(1)

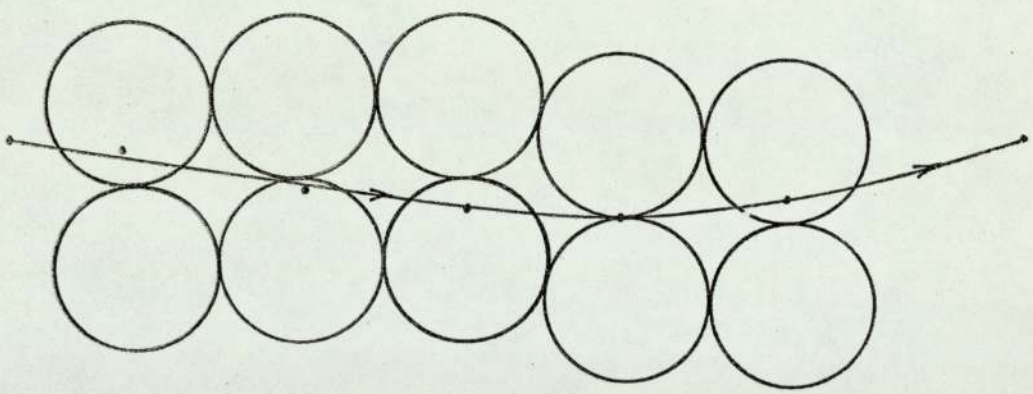

(2)

Fig..3.3.4a. 1 - The<110> channel of a face-centred cubic crystal is bordered by four atomic <110> chains.(After G.Leibfried).
2 - Schematic representation of a chanelling event. The moving atom follows the trajectory shown, oscillation between close-packed rows of lattice atoms. Dots represent collision points, circles represent atomic volume in which the interatomic potential is effective (After Holmes)

3.3.5 Long range transport of matter

In a previous section we have seen that focusons carry energy down close packed rows and away from the immediate environment of the primary event in a region of a displacement cascade. By an extension of the same argument, it can be shown that it is also possible to transport mass in a like manner. The hard sphere approximation was found useful, but this can hardly be sufficient since our knowledge of the atom insists that any interaction potential must demonstrate a basic "softness", so that in an interatomic collision the scattering angle for a given impact parameter will be less than that which would be predicted on the hard sphere model. The problem of establishing a proper interaction potential which gives the atoms their correct amount of "softness" is basic to the entire problem of radiation damage itself. The use of a "soft" potential modifies our idea of the focusing mechanism in a number of ways:

a) Since the hard sphere model overestimates the angle of scattering for a particular impact parameter, the amount of focusing must also be overestimated.

b) In the process of irradiation of a focused collision sequence any atom in the row feels the influence of the oncoming disturbance long before it actually arrives at the atom in question, so that the atoms in the line are already moving. This is because the soft potential does not cut off the interaction between two atoms at a particular value of r, say $r_o$. The effect of this early atomic motion is that there is a reduction in $D^{hkl}$, and focusing is enhanced.

c) These two effects oppose each other and it is not easy to say which will dominate, though Leibfried has investigated the case of copper and has shown that $E_f^{100}$ is reduced to a value somewhere between 17eV and 35eV.

The most important result of this examination of the focusing problem is the proof of the existence of a range of energy over which not only energy, but also mass can be transported.

In a hard sphere collision Fig. (3.3.1a) it is only possible to replace the struck atom if $D>4R$ and $PB<D/2$. From focusing criteria we can deduce that it is never possible for a collision sequence to sustain both focusing and replacement simultaneously. In soft collisions the situation is quite different, because atom(n+1) begins to move forward before atom(n) is at rest. The situation which then prevails is represented schematically in Fig.(3.3.5a), the centre of mass coordinates is used and a head-on collision is assumed to take place. A focused replacement will only occur if atom(n) comes to rest at a position which is beyond the mid-point between the $n^{th}$ and $(n+1)^{th}$ lattice sites. The replacement energy $E_r^{hkl}$ is given by

$$E_r^{hkl} = (A/2)\exp(-D^{hkl}/2B)$$

and it may be concluded that there is a definite range of energy

$$E_f^{hkl} > E > E_r^{hkl}$$

over which both focusing and replacement can occur, within this energy interval, matter is propagated down the line of atoms as a dynamic crowdion, and a vacancy is left behind at one end of the line. When the energy falls below $E_r^{hkl}$ the extra atom of the crowdion is deposited as a permanent interstitial, and for the remainder of the sequence only energy is transferred. For binary materials the existence of focused replacements is again of extreme importance since in addition to the formation of Frenkel defects, it leads to the introduction of line disorder.

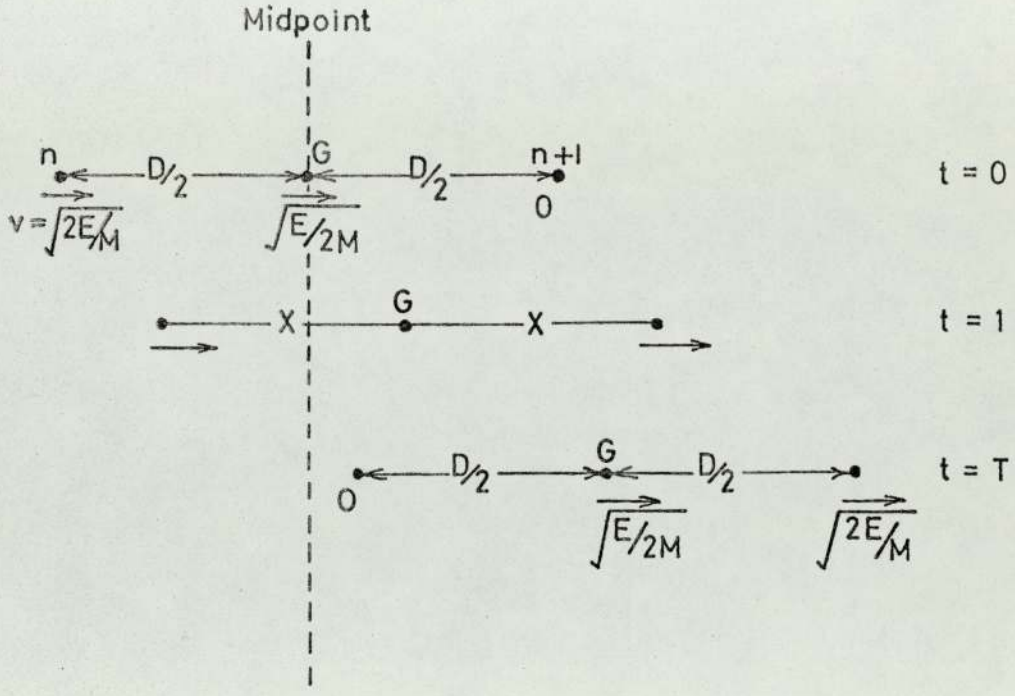


Fig. (3.3.5a). Diagram showing the dynamic stages in a soft collision when atom (n) collides in a head-on fashion with atom (n+1). In a centre of mass co-ordinates, and at time t=0, 1, T a focused replacement only occurs if atom n, after the collision comes to rest at a position which is beyond the mid point between (n) and (n+1) (After Thompson)

## 3.4 Temperature dependence of the diffusion coefficient

The interesting information concerning the migration of any atomic species is summarised in the diffusion coefficient D. If the numerical value of D is known, the flow and distribution of matter can be computed from Fick's laws. Also D is directly related to the atomic properties that control the diffusion mechanisms (jump frequency, vacancy mechanism). It is therefore understandable that a great deal of experimental research in diffusion is concerned with measuring D, while a great deal of theoretical research is concerned with relating D to fundamental solid state theory.

The most important single fact that can be known about the diffusion coefficient is its variation with temperature. The diffusion coefficient equations are all different in detail, but they all consist of two factors: a constant that is independent of temperature and an exponential function of temperature containing an energy term. All of the equations for D can then be written in the form:

$$D = D_o \exp(-Q/KT) \qquad 3.4a$$

where $D_o$ is temperature independent,

Q is an energy

In the case of an interstitial impurity

$$D_o = \alpha \lambda^2 \nu \quad \text{and}$$

$$Q = E^*$$

$E^*$ is the activation energy for the process.

For simple vacancy mechanisms

$$D_o = \alpha \lambda^2 \nu \, e^{S_v^f/K}$$

$$Q = E^* + E_v^f$$

where $\nu$ is the atomic vibration frequency,

$\lambda$ is the jumping distance.

$S_v^f$ and $E_v^f$ are entropy and energy of formation of vacancy respectively. Q is called the energy of activation for diffusion and $D_o$ is called the diffusion pre-exponential factor. Equation (3.4a) is referred to as the Arrhenius equation for the diffusion coefficient. Referring to equation (3.4a), the form of this dependence has been verified experimentally in a large number of diffusion systems in a wide variety of materials. It is found that equation (3.4a) is so firmly established in solid state diffusion, that in those rare cases when it is not fulfilled, anomalous factors are always sought to explain the discrepancy, these anomalies are generally found to be such that they modify the assumption made in the theoretical substructure leading to equation (3.4a).

Converting equation (3.4a) to logarithmic form gives:

$$\ln D = (-Q/KT) + \ln D_o$$

and plot of ln D against 1/T for experimentally measured D values at various temperatures gives a straight line that allows:

a) The heat of activation Q to be calculated from the slope.

b) $D_o$ to be calculated from the interception.

Experimental results are usually summarized by giving D and Q values.

3.5 Thermal vibration and the activation energy:

Atoms in a crystal are not stationary, but are executing small, rapid oscillations about their average positions. The vibrational amplitude of a particular atom remains small most of the time but occasionally the atom acquires enough energy for its amplitude to become quite large. A fluctuation of this type might arise when all the atoms on one side of a particular atom move simultaneously towards

it. If all the atoms on the other side are moving away from that atom, it is clear that the atom can be displaced from its normal position by an amount considerably greater than the average. An occurrence of this kind is relatively rare, since it can only take place if a number of its surrounding atoms are moving in concert. These thermal fluctuations, although rare on the time scale appropriate to vibrations in crystals, are very important in diffusion. The simplest way to show the importance of thermal fluctuations is to consider the special case of an impurity atom in an otherwise pure monatomic crystal. The impurity atom sits in a cage formed by the surrounding atoms of the host crystal, and most of the time it just vibrates in the small space allotted to it in the cage. The energy of the atom as it approaches the atoms forming its cell rises rapidly as shown in Fig.(3.5a). If the impurity atom is moved from the centre of its cell, through the cell wall, and to the centre of an adjacent cell, the energy as a function of position has the form shown in Fig. (3.5a). The energy is minimum when the atom is in the centre of the group of atoms in the plane midway between the two normal positions.

The impurity atom can reach the central position B only if it has enough energy to overcome the repulsive forces of the atoms surrounding B. The maximum energy in the diagram forms a barrier that the atom must climb if it is to jump into the next cell. It can climb this barrier only if it is sufficiently activated by a thermal fluctuation. The height of this barrier is known as the activation energy $E^*$ which can be given by the difference between the energy at B and the energy at a normal position. B is called the activated position, and the crystal is in an activated state when the impurity atom is at B.

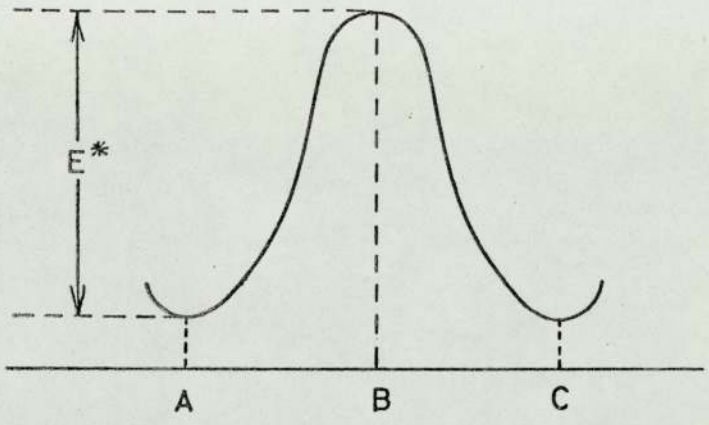


Fig.(3.5a) Energy of an impurity atom as it moves from an initial position A in one cage to a final position C in an adjacent cage in a simple cubic structure.

# CHAPTER 4

## EXPERIMENTAL RESULTS AND DISCUSSIONS : PHYSICAL ADSORPTION

## 4.1 Introduction

The presence of an absorbed gas layer (arising from an inadequate vacuum) affect surface measurements at low temperatures and particularly ellipsometric measurements as will be illustrated later. For this reason it is necessary to carry out such investigations under ultra high vacuum conditions.

The adsorption of inert gases on different gold surfaces prepared in ultra high vacuum ($10^{-9}$ torr) are investigated. The dependence of the sensitivity of measurements on the wavelength of light used and the subsequent desorption are also studied.

## 4.2 Optical constant of freshly evaporated gold film

Gold films were evaporated inside the ellipsometer at a pressure of $10^{-9}$ torr. After annealing to 300°C in vacuum for five hours, ellipsometric measurements were taken at room temperature. Typical experimental errors are $\pm 0.002^{o}$ for $\psi$ and $\pm 0.01^{o}$ for $\Delta$

In Figs.(4.2a),(4.2b) the values of n and k for polycrystalline film calculated from experimental values of $\psi$ and $\Delta$ are plotted as a function of wavelength of the light used to test the system. Good agreement was found between the present measurements and measurements of Schulz (1957) and Johnson and Christy (1972) as shown in Figs.(4.2a) and (4.2b).

Fig. (4.2c) compares the present results with measurements of Abeles (1969) for the variation of 2nk with wavelength. According to Abeles these measurements correspond to a good film, i.e. a film having properties similar to those of bulk material.

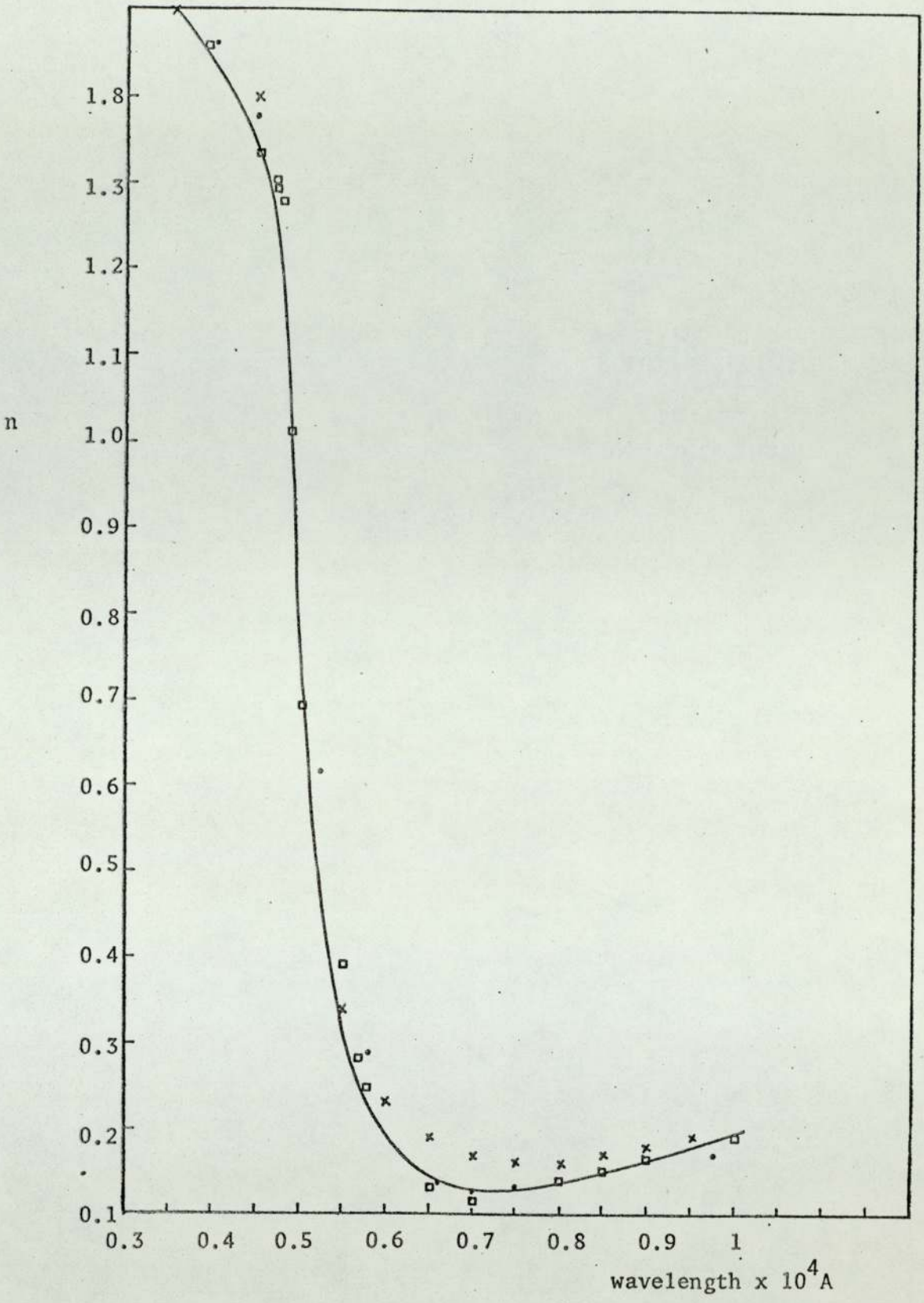


Fig.(4.2a). Values of n as a function of wavelength for freshly evaporated polycrystalline gold film.

□ present x Schulz • Johnson & Christy

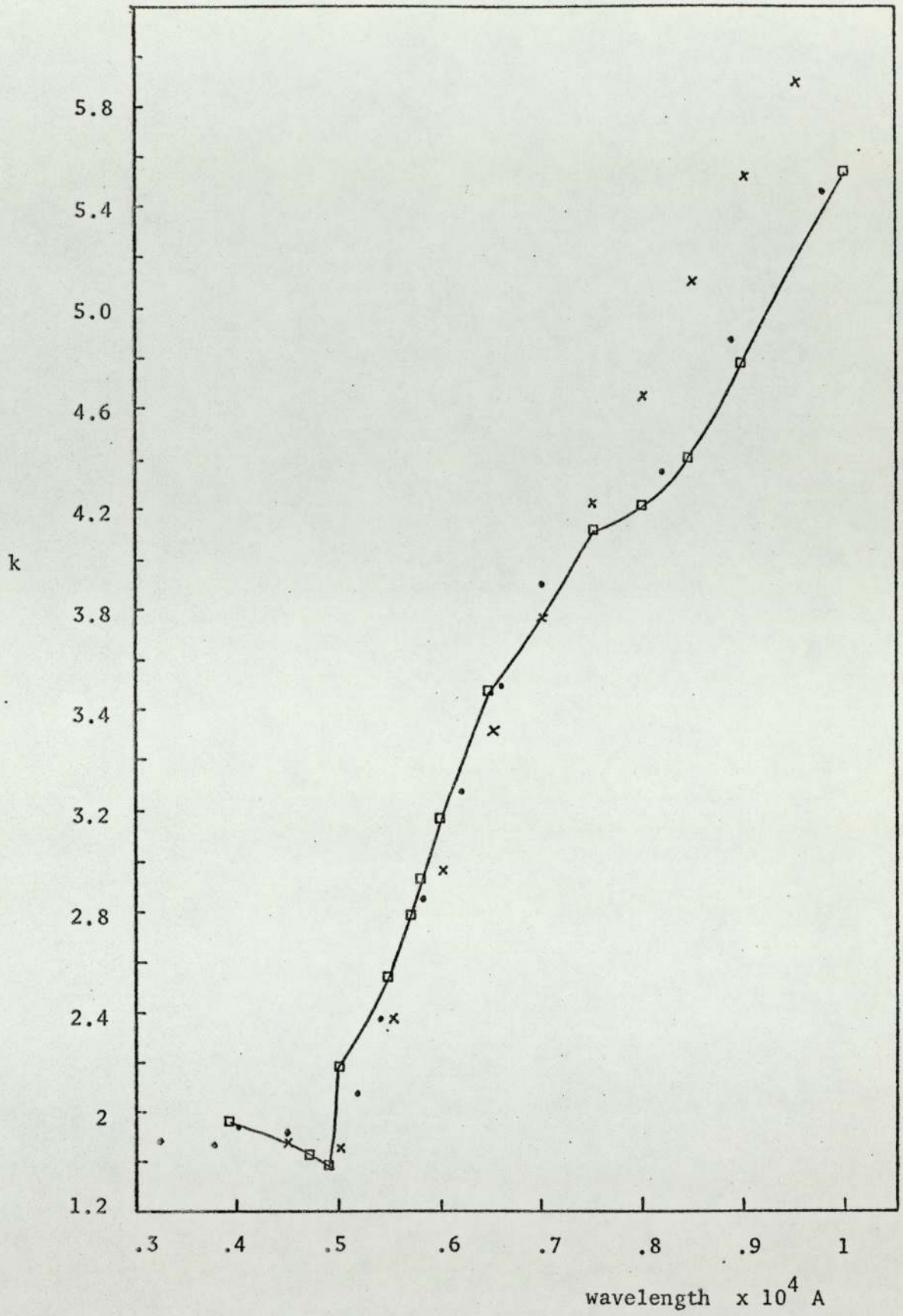


Fig.(4.2b) Values of k as a function of wavelengths for freshly evaporated polycrystalline gold film.

□ present work  x Schulz  • Johnson & Christy

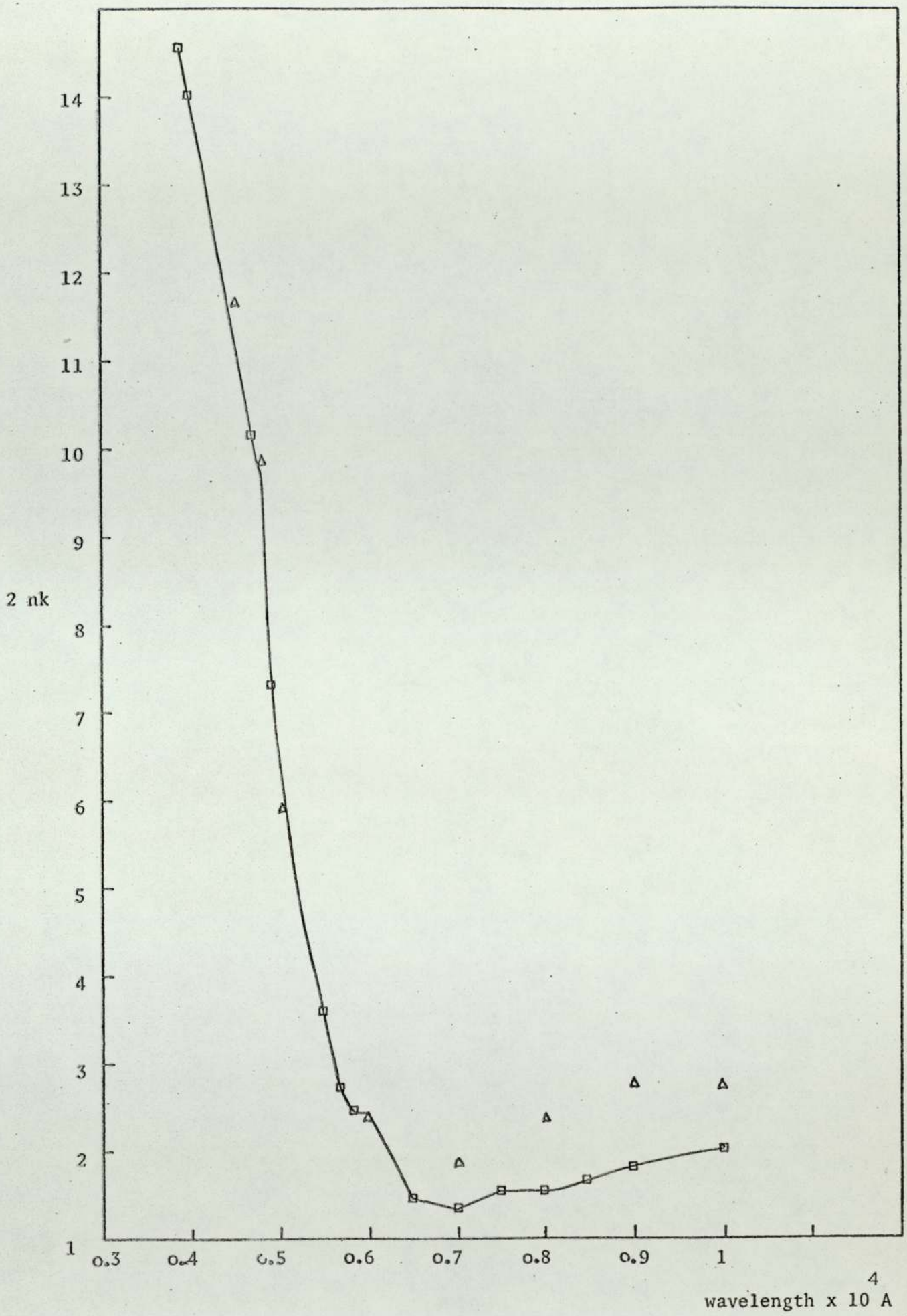


Fig. (4.2c) Values of 2nk as a function of wavelength for freshly evaporated polycrystalline gold film.

□ present work  Δ Abeles

4.3.1 Sensitivity of measurements: Wavelength dependence

Measurements of the change of the ellipsometric parameters $\psi$ and $\Delta$ on adsorption of gas on a clean polycrystalline gold film yielded different values at different wavelengths. The change of the value of $\Delta(\delta\Delta)$ and $\psi(\delta\psi)$ as a function of wavelength of light used is studied for neon and argon gases, where:

$$\delta\Delta = \bar{\Delta} - \Delta$$

and

$$\delta\psi = \bar{\psi} - \psi$$

where $\bar{\Delta}$ , $\bar{\psi}$ refers to the value of the clean surface at the lowest pressure obtainable

and $\Delta$ , $\psi$ are the values after introducing the gas.

In Fig.(4.3.1a) is shown the change of the value of $\delta\psi$ with wavelength. Measurements were made at a pressure of $10^{-6}$ torr of neon gas, the surface was held at liquid nitrogen temperature. The points a,b,c correspond to the strongest emission for neon gas while d is a medium line. Points e and f correspond to weak lines of the gas. It was difficult to select the exact wavelength corresponding to the emission line of the gas because these lines are very sharp and close. Near the strongest emission line, the sensitivity of the measurements is found to be one order of magnitude higher than that at any random wavelength as is also shown in the figure. On the otherhand, the value of $\delta\Delta$ was found to be twice as much for the same lines than at any other wavelength as illustrated in Fig. (4.3.1b).

Similar results were found to be true using argon gas under the same experimental conditions. The measurements were found more sensitive at some other wavelength corresponding to argon atoms, as illustrated in Figs.(4.3.1c) and (4.3.1d).

In all cases the values of $\delta\Delta$ were found to be positive at all wavelengths but by differing amounts. The values of $\delta\psi$ were only positive at wavelengths corresponding to the emission line of the gas used and negative at any other wavelengths as shown in Fig.(4.3.1e).

From the calculations of the refractive index of the surface film, for an absorbing film on an absorbing substrate, the calculated values of $\psi$ were found to decrease with film thickness, i.e. $\delta\psi$ is positive while for non-absorbing film on an absorbing substrate, the value of $\delta\psi$ is negative which confirms that adsorbed neon and argon gases are slightly absorbing at wavelengths near the emission lines for the corresponding gas.

Table (4.3.1a) shows the computed values of both $\psi$ and $\Delta$. Drude's exact equations (see Section 4.6), were used for a surface film of optical constant (1.08 - 0.25i) and substrate optical constant (0.175 - 3.05i) at a wavelength of 6150 Å and at an angle of incidence of 64 degrees.

| Film Thickness in Å | Delta Deg. | Psi Deg. |
|---|---|---|
| 0 | 119.910 | 43.690 |
| 1 | 119.870 | 43.663 |
| 2 | 119.831 | 43.636 |
| 3 | 119.792 | 43.609 |
| 4 | 119.752 | 43.582 |
| 5 | 119.713 | 43.555 |
| 6 | 119.674 | 43.528 |
| 7 | 119.635 | 43.501 |
| 8 | 119.595 | 43.474 |
| 9 | 119.556 | 43.447 |

Table 4.3.1a. Computed values of $\psi$ and $\Delta$ as the film thickness increases (as explained in Section 4.6).

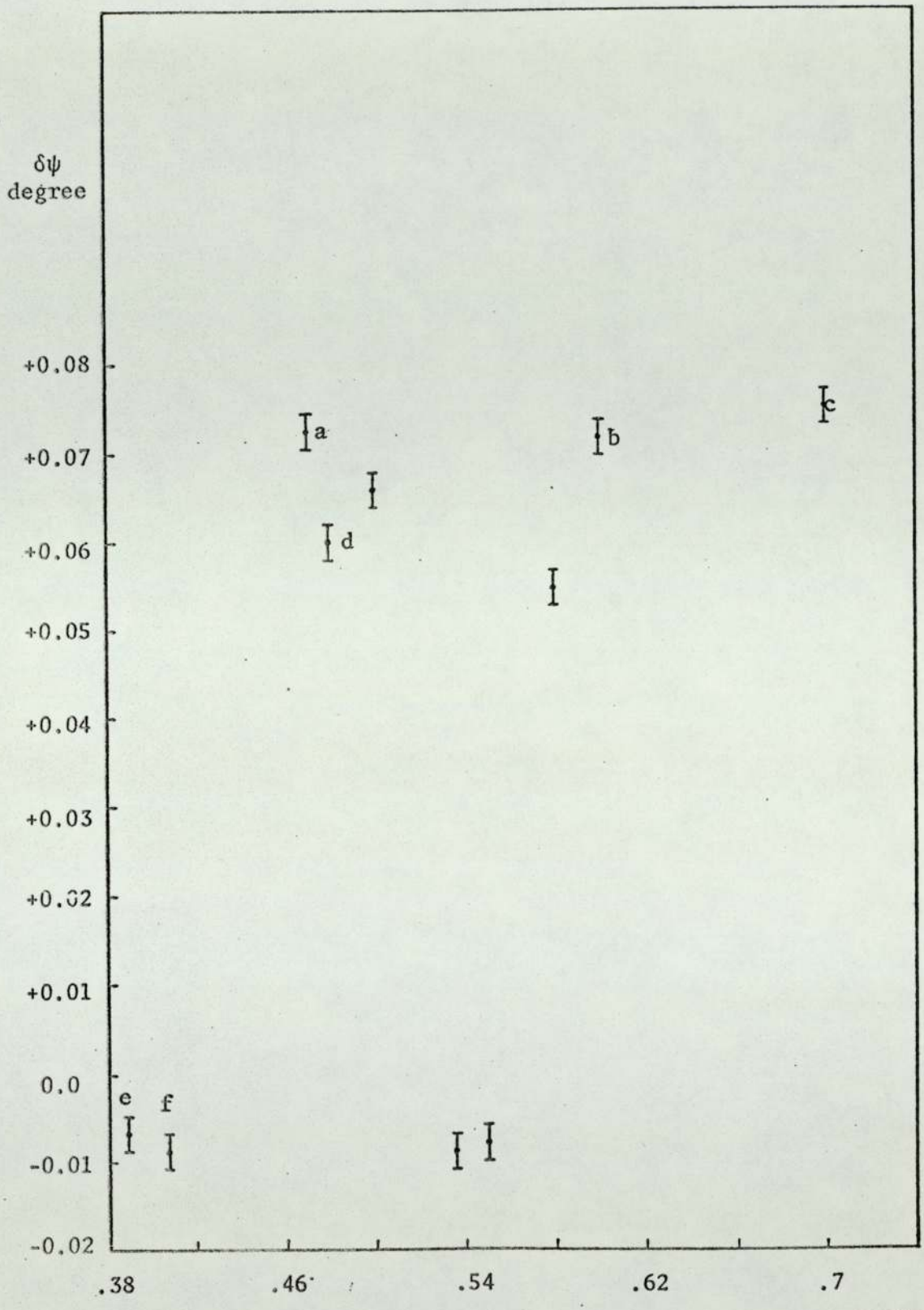


Fig. (4.3.1a) Change of $\delta\psi$ as a function of wavelength for adsorbed neon gas on polycrystalline gold film held at liquid nitrogen temperature at gas pressure of $10^{-6}$ torr.

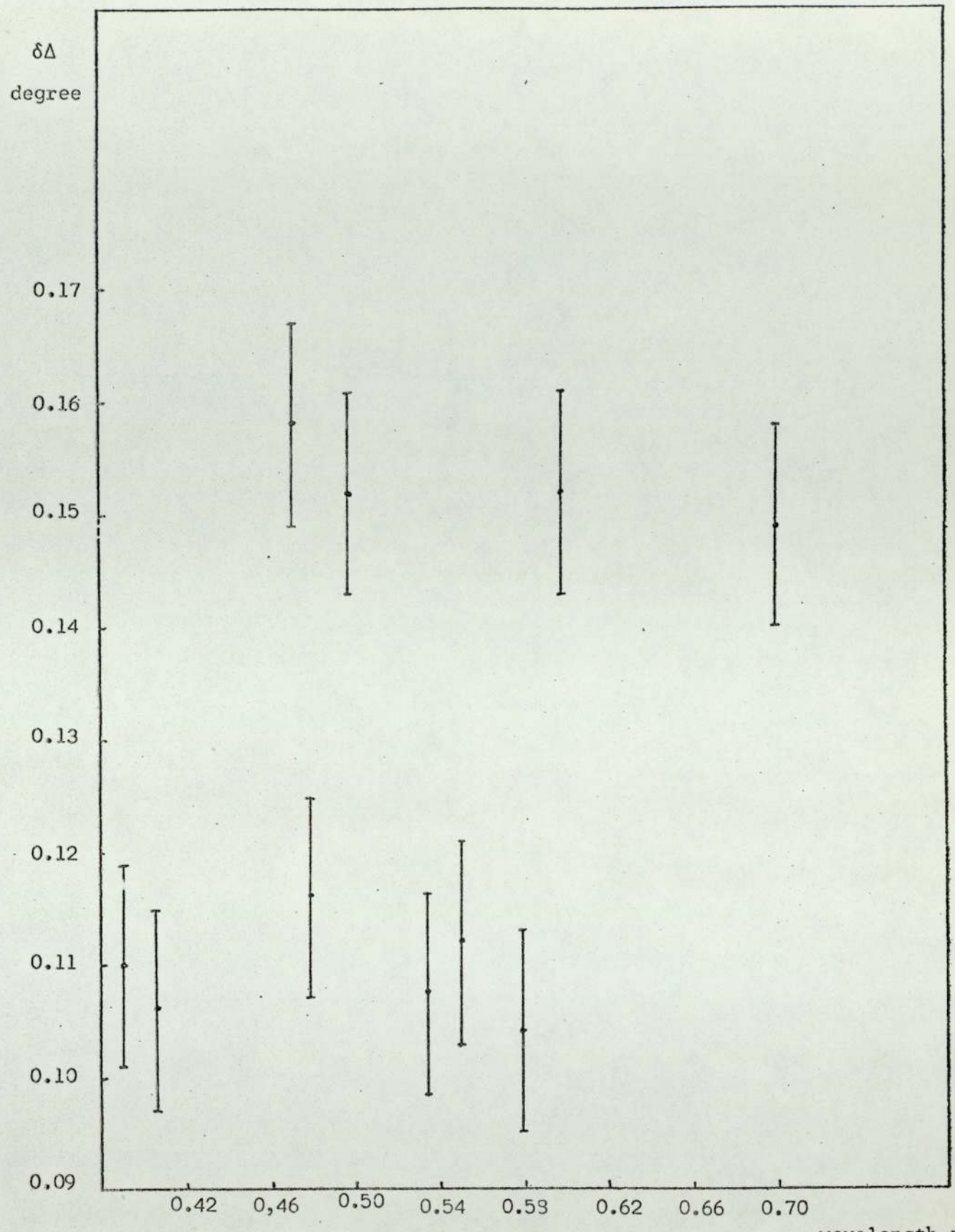


Fig. (4.3.1b) Change of $\delta\Delta$ as a function of wavelength for adsorbed neon gas on polycrystalline gold film held at liquid nitrogen temperature at gas pressure of $10^{-6}$ torr.

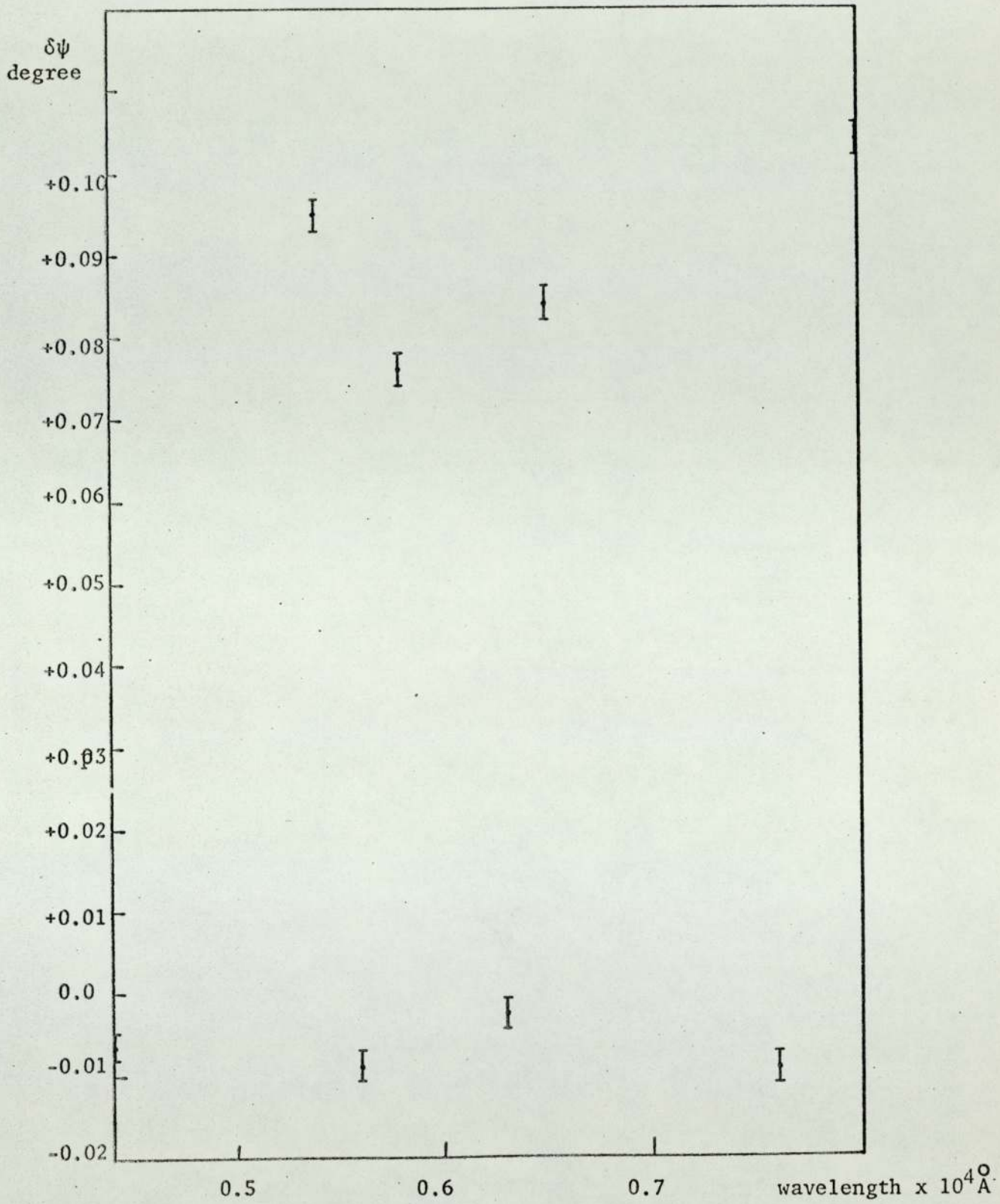


Fig. (4.3.1c) Change of $\delta\psi$ as a function of wavelength for adsorbed argon gas on polycrystalline gold film held at liquid nitrogen temperature at gas pressure of $10^{-6}$ torr.

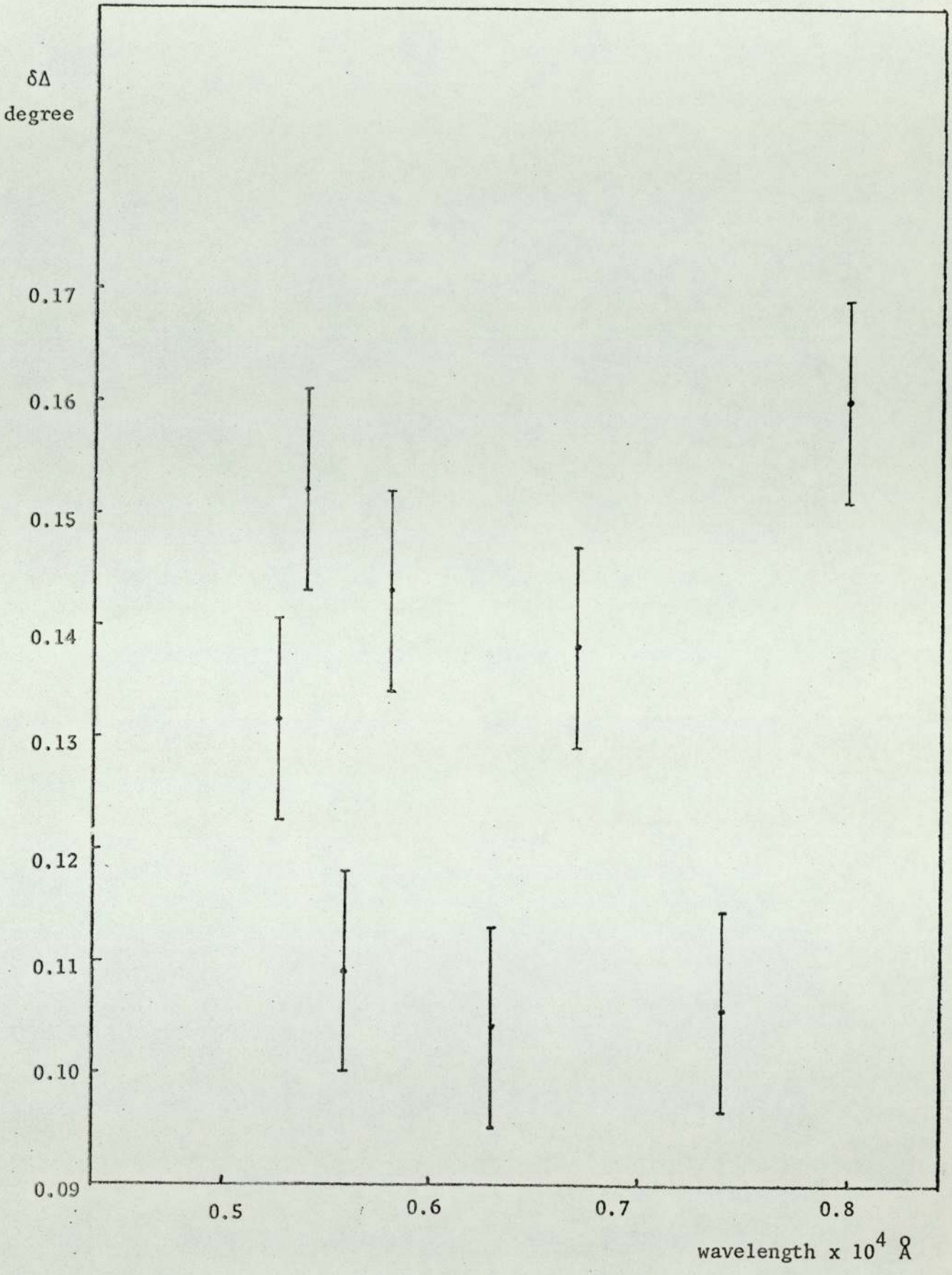


Fig. (4.3.1d) Change of δΔ as a function of wavelength for adsorbed argon gas on polycrystalline gold film held at liquid nitrogen temperature at gas pressure of $10^{-6}$ torr.

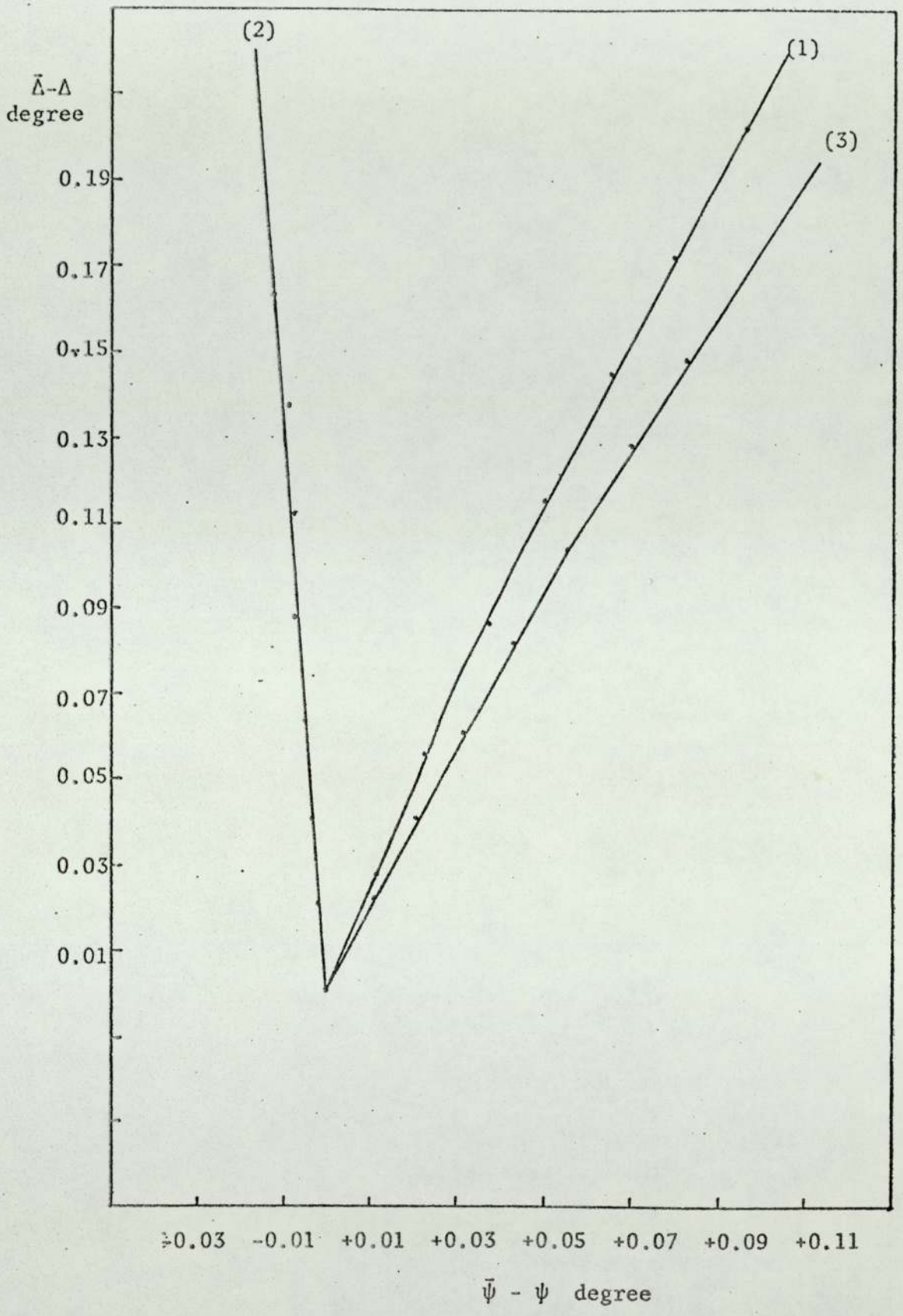


Fig. (4.3.1e) Changes of $\delta\Delta$ and $\delta\psi$ as a function of wavelength for adsorbed neon gas on polycrystalline gold film held at liquid nitrogen temperature.
Wavelengths: (1)7500 A, (2)5500 A, (3)5800 A.

### 4.3.2 Adsorption of neon and argon on polycrystalline gold films

In studying many surface phenomena, it is useful to visualize a particular model of the atomic structure. The presence of different crystal planes on a metal surface results in a heterogeneous distribution of adsorption forces on the face. This heterogeneity of metal surfaces may be seen from experimental results such as physical and chemical adsorption.

The adsorption of inert gases (neon and argon) on polycrystalline gold film has been studied with the specimen held at liquid nitrogen temperature. The increase of the gas pressure increases the probability of the gas being adsorbed. The magnitude and sign of the changes of the values of $\Delta$ and $\psi$ were found to be similar for both gases and the results are shown in Figs.(4.3.2a,b) which give the change of ellipsometric parameters $\Delta$ and $\psi$ as the gas pressure increases for argon only. The measurements were made at wavelength corresponding to the strongest emission line of each gas indicated on the graph. As mentioned before the sensitivity of the measurements at these wavelengths is the highest.

### 4.3.3 Adsorption of neon and argon on <110> single crystal gold films

The adsorption of neon and argon gases as observed by the change of the ellipsometric parameters $\Delta$ and $\psi$ were found to be similar. For single crystal <110> gold film, the change of the value of $\Delta$ on adsorption was found to be higher than for polycrystalline gold film. Measurements are made at the same wavelengths as in the previous section. Figs. (4.3.3a,b) show the change of both $\Delta$ and $\psi$ with argon gas pressure for a substrate held at liquid nitrogen temperature (see also section 4.4).

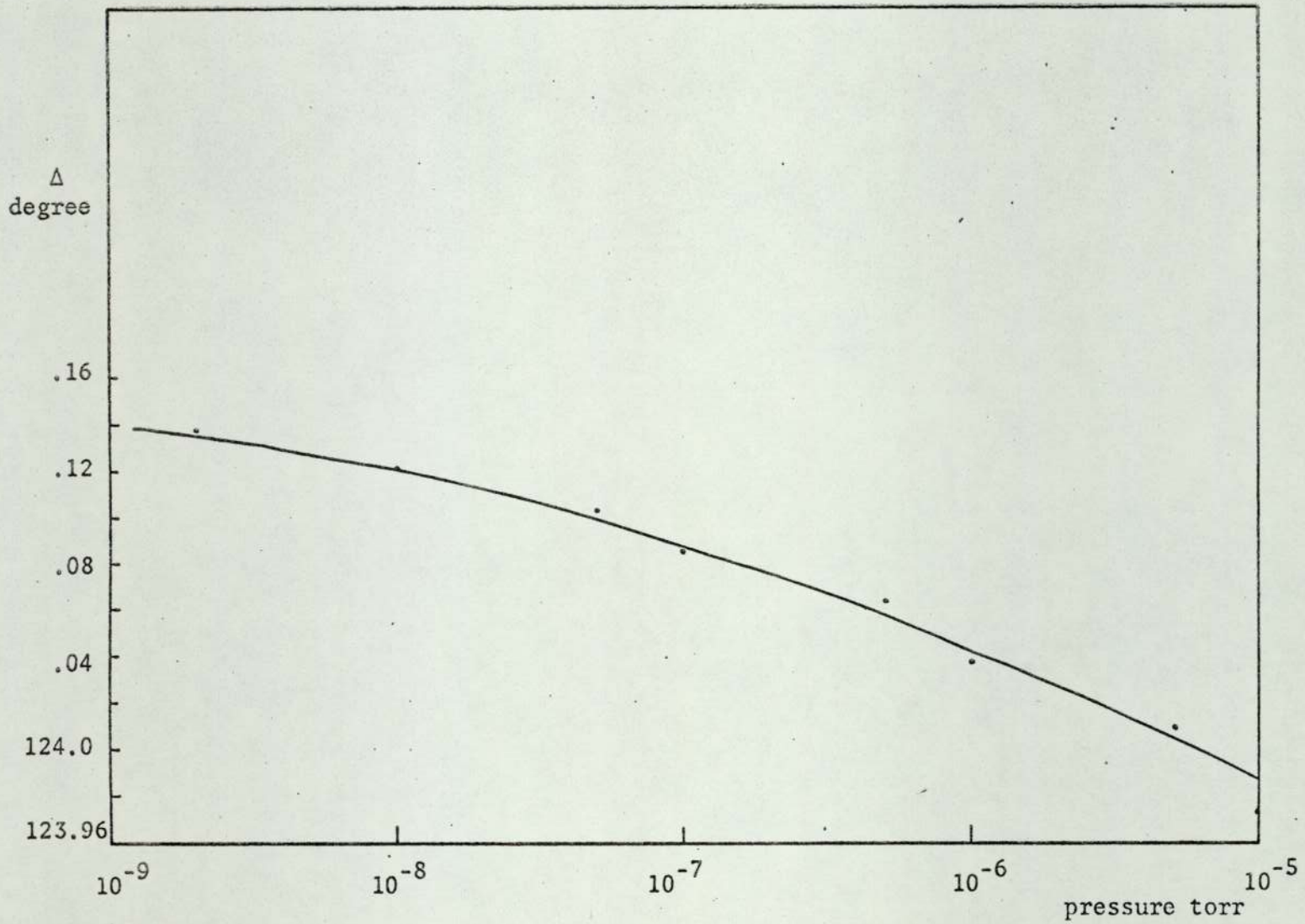


Fig. (4.3.2a) Change of Δ for adsorbed argon gas on polycrystalline gold film held at liquid nitrogen temperature at wavelength 6500 A.

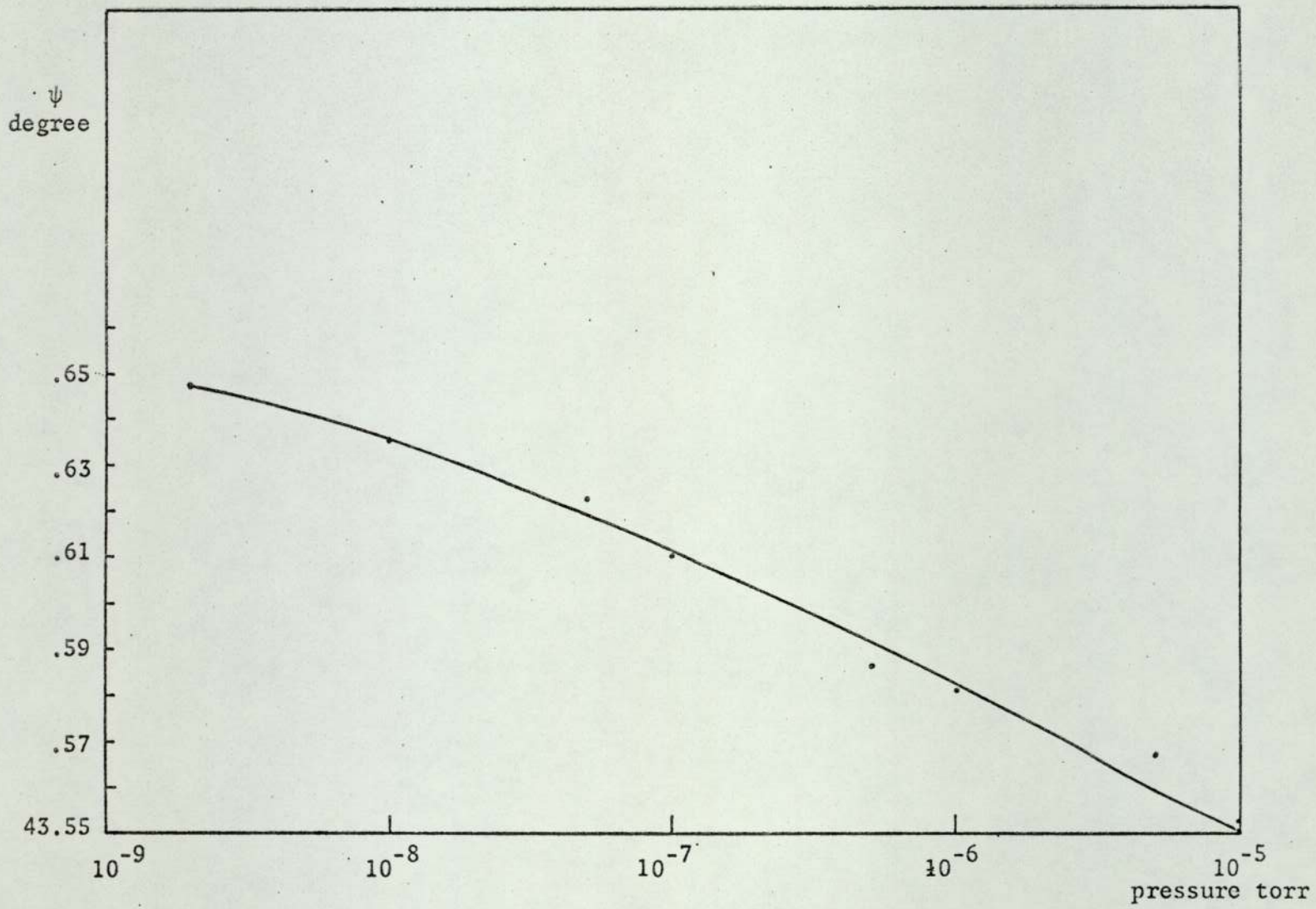


Fig.(4.3.2b) Change of ψ for adsorbed argon gas on polycrystalline gold film held at liquid nitrogen temperature at wavelength 6500 A.

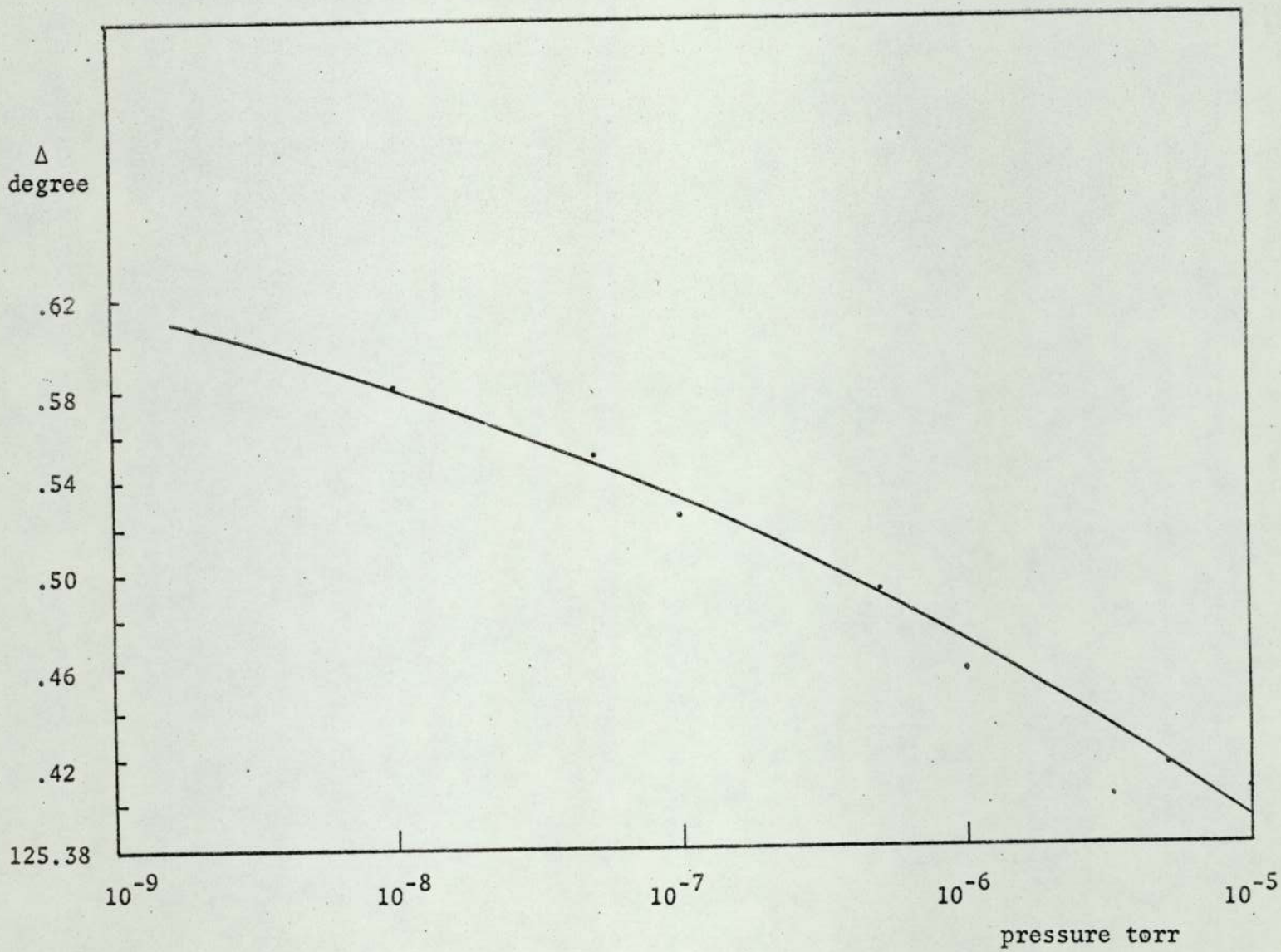


Fig. (4.3.3.a) Change of Δ for adsorbed argon gas on < 110 > single crystal gold film held at liquid nitrogen temperature at wavelength 6500 Å.

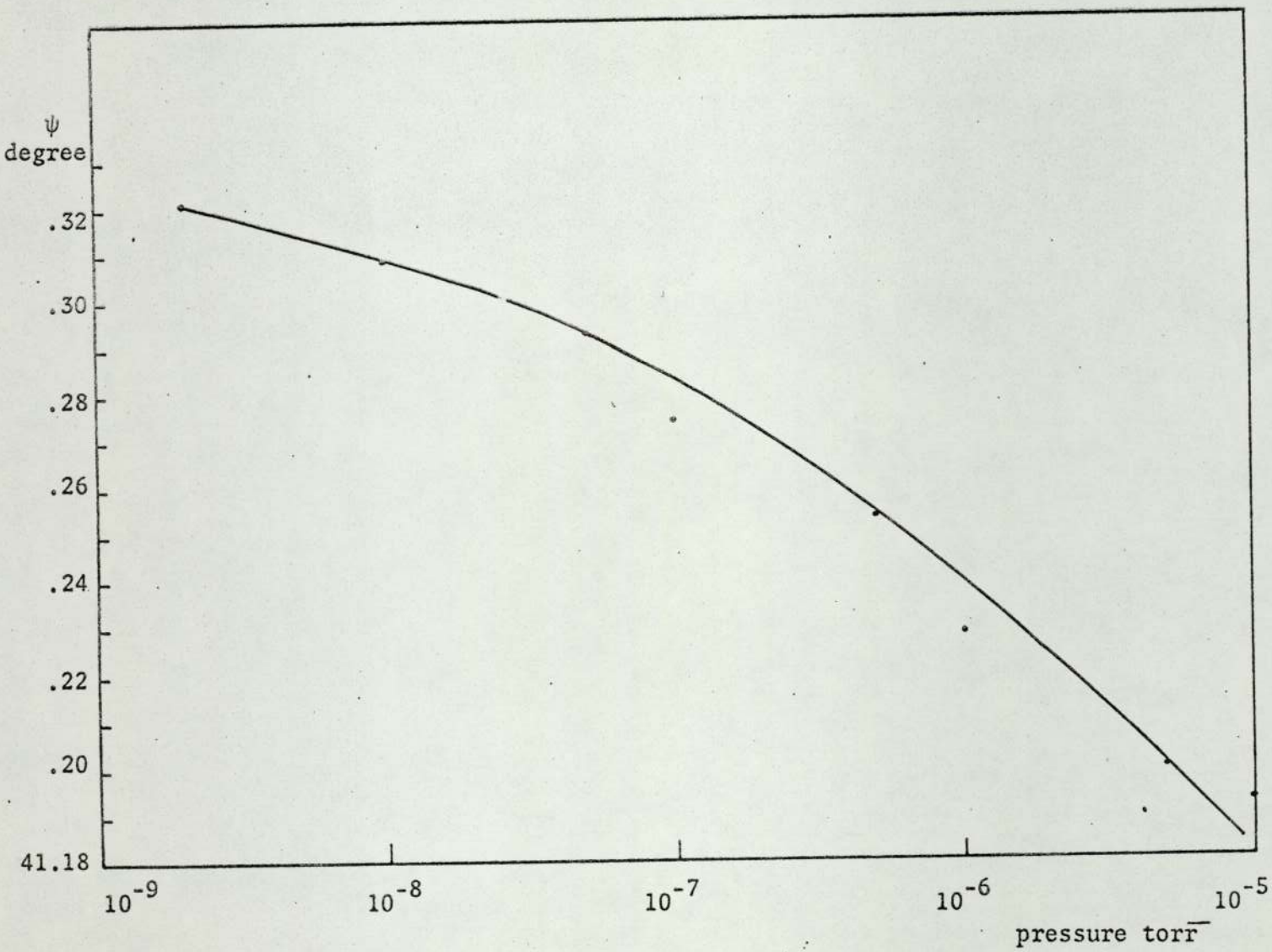


Fig.(4.3.3b) Change of ψ for adsorbed argon gas < 110 > single crystal gold film held at liquid nitrogen temperature at wavelength 6500 A.

4.3.4 Adsorption of neon and argon on <100> single crystal gold films

For single crystal <100> gold film, the change of the ellipsometric values $\psi$ and $\Delta$ were found to be less than both previous measurements. As mentioned in the previous two sections the amount of change of $\psi$ and $\Delta$ upon adsorption was found to be the same for neon and argon for the same conditions. Figs.(4.3.4a, 4.3.4b) show the adsorption of argon on <100> surface.

Investigation of the arrangements of atoms on such surfaces shows that the number of sites available to hold a foreign atom in the <110> direction is nearly twice as much as those in the <100> direction as illustrated in Fig. (4.3.4c). The change of the value of $\Delta$ in <100> film upon adsorption is found to be nearly half that for <110> orientation.

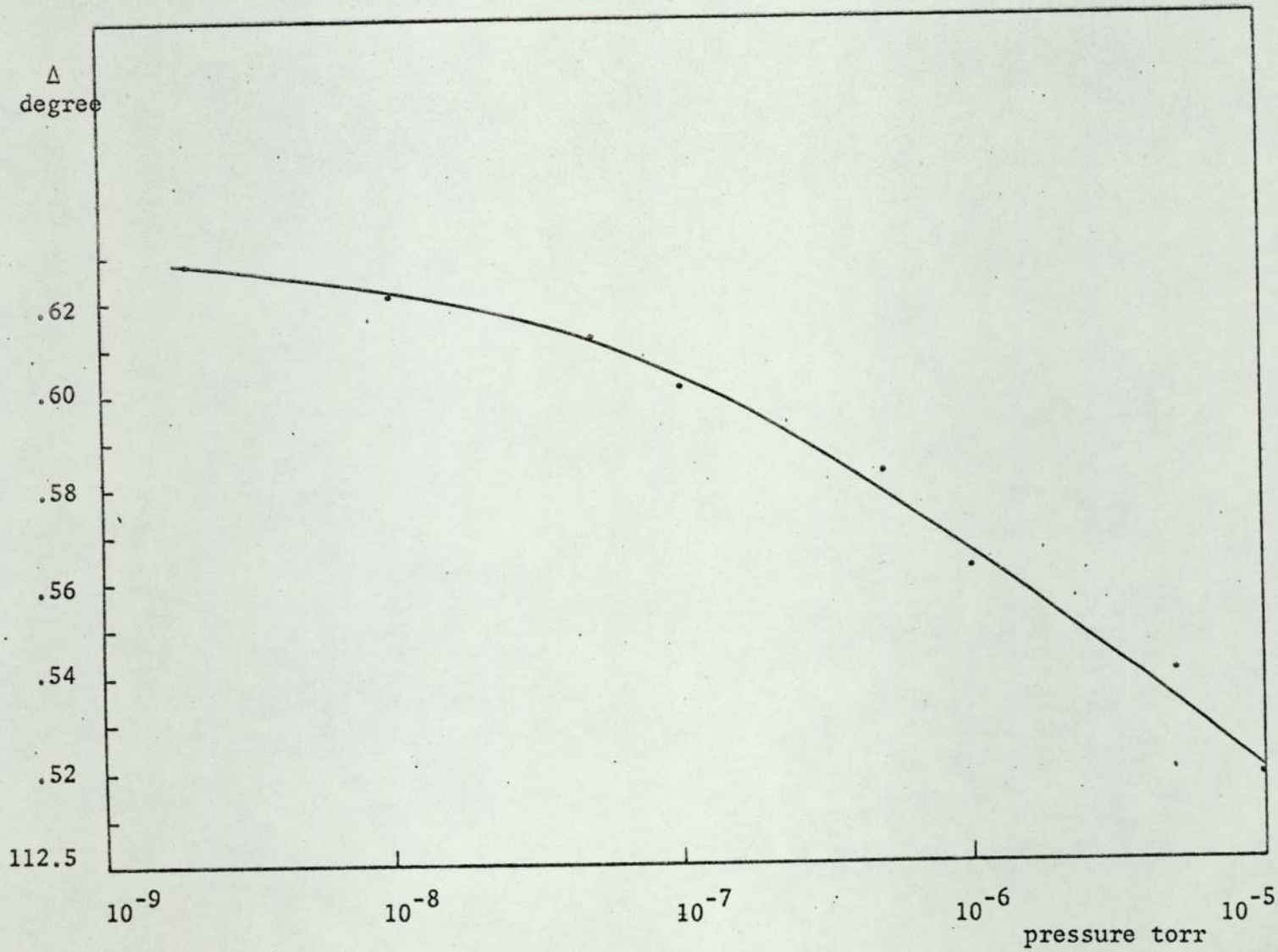


Fig.(4.3.4a) Change of Δ for adsorbed argon gas on < 100 > single crystal gold film held at liquid nitrogen temperature at wavelength 6500 A.

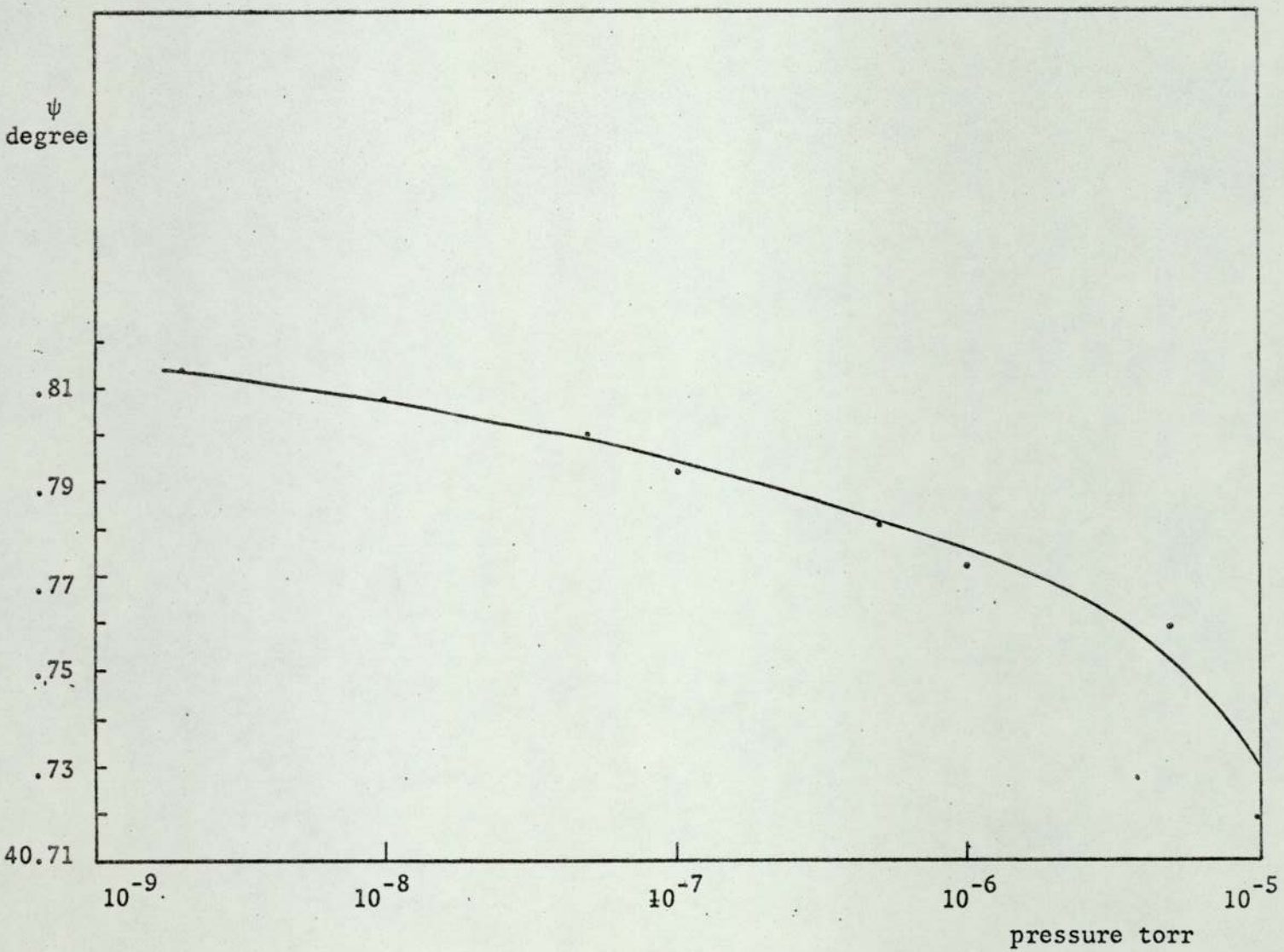


Fig.(4.3.4b) Change of ψ for adsorbed argon gas on < 100 > single crystal gold film held at liquid nitrogen temperature at wavelength 6500 A.

Fig. 4.3.4c. Models of (a) an ideal <100> surface, and
(b) an ideal <110> surface of a face-centres cubic crystal.

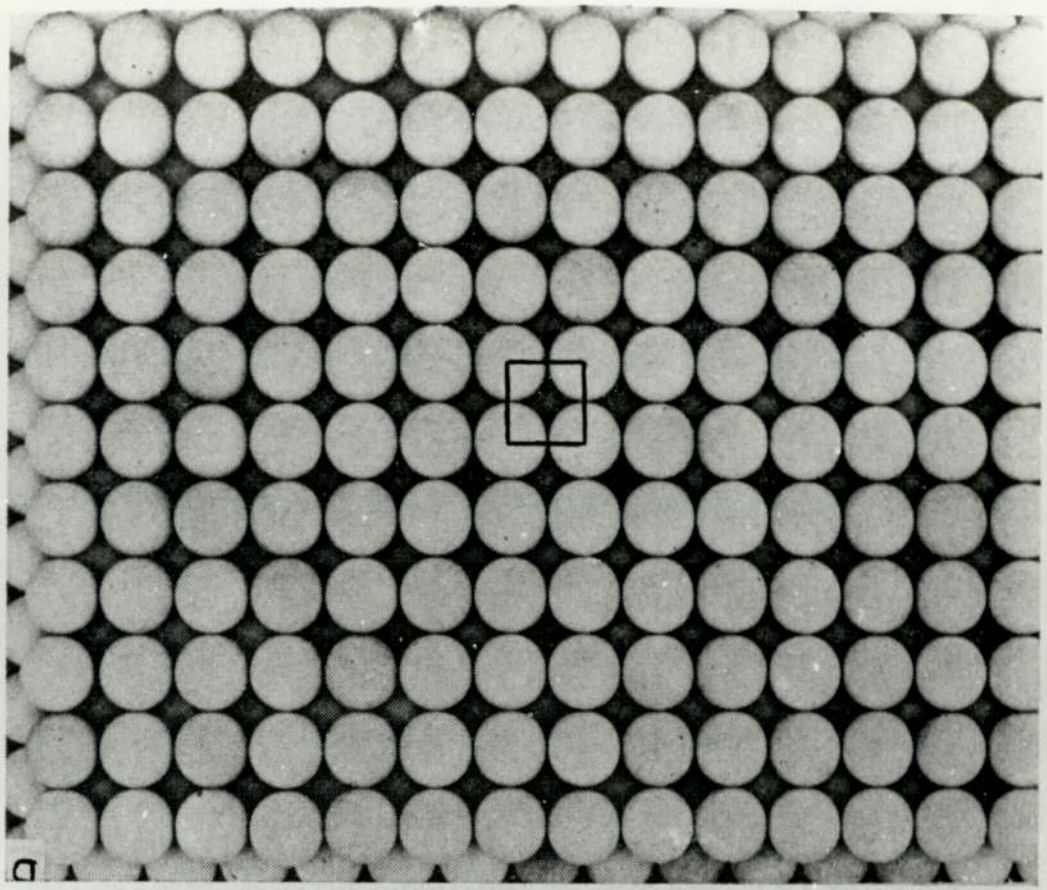
a

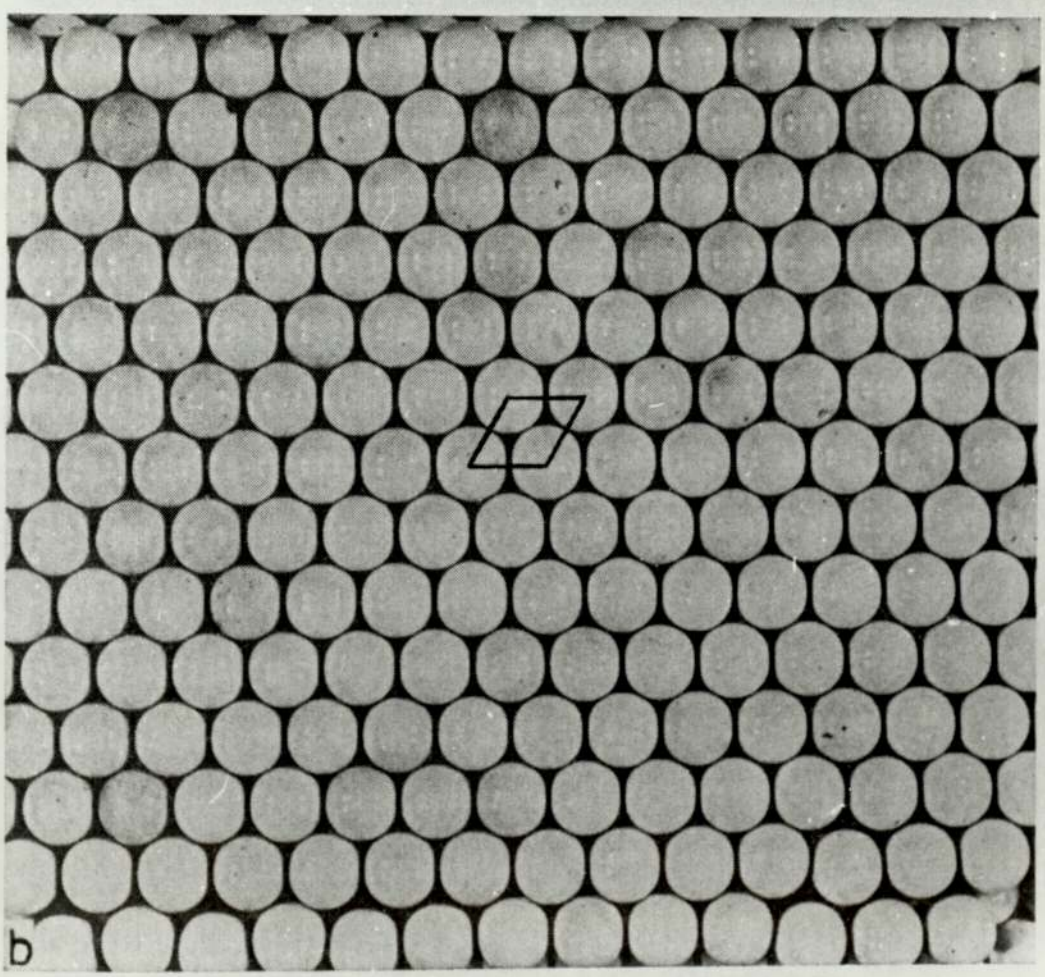
b

4.4 Binding forces of an atom on surface and gas desorption

The Van der Waals adsorption depends very strongly on the physical heterogeneity of the surface as shown by Polanyi (1932), Lennard-Jones (1932) and De Boer and Custers (1934).. They showed that the binding forces for adatoms adsorbed in small holes in the surface (as shown schematically in the diagram, Fig. (4.4a-1) are much greater than those for adatoms on a flat surface.

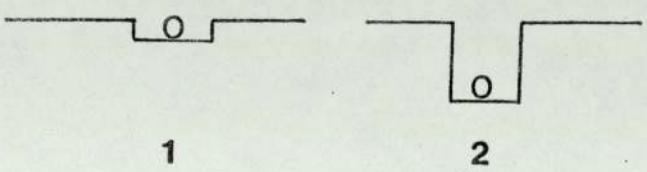


Fig. (4.4a) Schematic diagram of the adsorption of adatoms in small holes in the surface (1) and in deeper cracks (2).

For adatoms in cracks (2 in the daigram) the binding forces are still greater than those for atoms adsorbed in holes. On the other hand, the Van der Waals forces are very weak at peaks and corners on the surface. The maximum binding forces occur in positions where the adatoms are surrounded by the maximum number of lattice atoms.

In the present work, annealing of the adsorbed samples to room temperature did not return $\psi$ and $\Delta$ to the values for the clean surface as observed before adsorption. Even increasing the film temperature to 100°C was not sufficient in some cases to desorb all adsorbed gases which suggeststhat the amount of change of $\Delta$ and corresponding desorption largely depends on the surface roughness of the film.

## 4.5 Calculation of the optical constants of clean gold film (Freshly evaporated)

The optical constants of a freshly evaporated gold film were measured at room temperature after annealing the film to 300°C in vacuum for five hours. A computer programme with the graph plotter as described in Appendix 1 b was used. In this programme the calculated values of either n or k are plotted as a function of $\Psi$ at constant values of $\Delta$. From the experimentally determined ($\Psi$ and $\Delta$) values, the correct values of n and k can be determined from the graph as shown in Fig. (4.5a,b). The values determined in this experiment are in good agreement with the published values as shown in section 4.2.

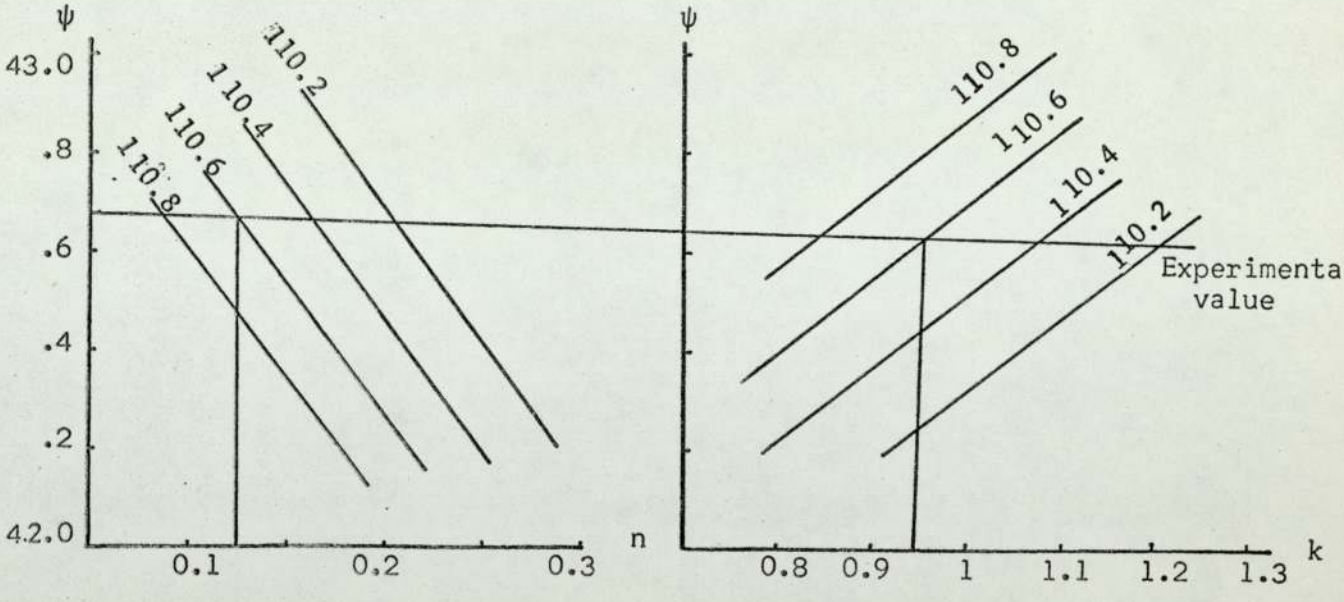


Fig.(4.5a) Relation between n and $\Psi$ at constant values of $\Delta$.

Fig.(4.5b) Relation between k and $\psi$ at the same constant values of $\Delta$.

4.6 Calculations of gas adsorbed layer and refractive index of the gas used.

The programme used in this calculation is described by O'Shea (Ph.D.thesis 1971). The programme solves the problem of a film of refractive index ($n_1$, $k_1$) on substrate ($n_2$, $k_2$). Values of ($n_2$, $k_2$) are first determined for freshly evaporated metal film as described in the previous section. The change of the ellipsometric parameters $\psi$ and $\Delta$ are then observed as the gas pressure in the system is increased. Values of ($n_1$, $k_1$) and the film thickness are assumed and fed to the computer programme from which the values of $\psi$ and $\Delta$ are calculated. Comparisons of the experimentally determined values ($\psi$ and $\Delta$) and calculated values of ($\psi$ and $\Delta$) yield the refractive index of the gas used at a particular wavelength and the film thickness. An example for the calculations is shown in Table (4.6a).

| $\lambda$ Å | Calculated | | Assumed | | Measured | | n | k |
|---|---|---|---|---|---|---|---|---|
| | $\delta\psi^o$ | $\delta\Delta^o$ | n | k | $\delta\psi^o$ | $\delta\Delta^o$ | | |
| 3900 | -0.051 | 0.084 | 1.18 | 0.0 | -0.007 | +0.11 | 1.18 | .13 |
| | -0.009 | 0.104 | 1.18 | 0.1 | | | | |
| | +0.01 | 0.129 | 1.18 | 0.2 | | | | |
| | +0.026 | 0.179 | 1.18 | 0.4 | | | | |
| 4700 | -0.031 | 0.081 | 1.14 | 0.0 | + .792 | 0.158 | 1.14 | 0.73 |
| | -0.01 | 1.04 | 1.14 | 0.1 | | | | |
| | +0.015 | 0.119 | 1.14 | 0.2 | | | | |
| | +0.034 | 0.134 | 1.14 | 0.4 | | | | |
| | +0.053 | 0.15 | 1.14 | 0.6 | | | | |
| | +0.076 | 0.164 | 0.14 | 0.73 | | | | |
| 6150 | -0.003 | 0.093 | 1.08 | 0 | +0.072 | 0.152 | 1.08 | 0.25 |
| | +0.015 | 0.116 | 1.08 | 0.1 | | | | |
| | +0.06 | 0.141 | 1.08 | 0.2 | | | | |
| | +0.091 | 0.168 | 1.08 | 0.3 | | | | |

Table (4.6a) Comparisons between theoretically calculated values of $\delta\psi$ and $\delta\Delta$ and experimentally determined values and the corresponding values of n, k for the gas used (argon).

Also shown in Table (4.6a) are some of the determined values of n and k for argon gas adsorbed on polycrystalline gold film held at liquid nitrogen temperature and a gas pressure of $10^{-7}$ torr.

The error in determining n and k values neglecting the gas layer is not very large as seen from Table (4.6b) where $\bar{n}$ and $\bar{k}$ are the values of the clean gold film at pressure $10^{-9}$ torr and n and k are the values for the composite surface of gold and gas after introducing the gas at pressure $10^{-7}$ torr, n and k represent pseudoconstants of the gold film .

| $\lambda$ A$^{o}$ | $\bar{n}$ | $\bar{k}$ | n | k |
|---|---|---|---|---|
| 4700 | 1.304 | 1.837 | 1.312 | 1.835 |

Table (4.6b) Real and pseudoconstants of gold film calculated from experimental values of $\Psi$ and $\Delta$ .

Measurements taken on films prepared at pressure of $10^{-7}$torr of the gas yielded higher discrepancies in the values of n and k which could be explained by assuming that gas atoms were trapped in the metal film during deposition.

4.7 Discussion

Thin films, present on most surfaces, were thought to be difficult to detect, and if not allowed for, can cause errors in the determination of the optical constants of pure surfaces. In some cases serious errors result for oxide films as thin as 10 $\overset{o}{A}$.

Young and Crowell (1962) concluded that below $P/P_o = 0.01$ no significant adsorption takes place, where P is the equilibrium pressure of the adsorbed film and $P_o$ is the vapour pressure of the bulk liquid at the temperature of the experiment. They made some exceptions with adsorbents having fine pores. This conclusion is quite at variance with many experiments on physical adsorption in physics and physical chemistry. Hobson and Armstrong (1963) obtained a drop in pressure of two orders of magnitude for $P/P_o = 10^{-10}$ in a flask of pyrex immersed in liquid nitrogen. In similar measurements on the physical adsorption of helium at 4.2$^{o}$K Hobson (1959) gave pressure drops of five orders of magnitude. Young and Crowell's conclusion is undoubtedly true within the meaning of the phrase "no significant adsorption", it conveys an impression quite at variance with experience in low pressure systems. As mentioned in a previous chapter, ellipsometry has proved to be a sensitive, non-destructive technique which can be used to detect very thin films on surface. Several factors affect the sensitivity of the measurements, among the most important is the angle of incidence, the sensitivity of the detection system and the wavelengths of the light used. The circumstances of the present experiment did not allow a study of the effect of the angle of incidence because measurements were to be made in an ultra high vacuum system, in which the window configuration had already been fixed. The detection system is found

to be very sensitive to any change in the surface as shown in Figs. (4.3.2a,b) where the value of the ellipsometric parameters $\Psi$ and $\Delta$ are shown to change as the gas pressure changes by small amounts i.e. as the gas surface layer is increasing.

The effect of the wavelengths of the light used was studied with the substrate held at liquid nitrogen temperature for two gases (neon and argon) at different wavelengths corresponding to some of the strong and weak emission lines of each gas. The sensitivity of the measurements was found to improve for a selective wavelength of the gas used. For each gas, the change in the value of $\Delta$ is found to be twice as much at a wavelength corresponding to a strong emission line of the gas as at any wavelength corresponding to a weak line. $\Psi$ was found to decrease upon increasing the gas pressure, i.e. increasing the film thickness for these particular wavelengths and to increase for other wavelengths as shown in Fig.(4.3.1e). The most probable explanation is that the gas film is slightly absorbing as seen from calculations of the thickness and refractive index of the adsorbed gas in the previous section.

Table (4.7a) shows the dependence of the sensitivity of measurements on the angle of incidence. The values of $\delta\Delta$ and $\delta\psi$ are taken for any chosen film thickness (4 $\mathring{A}$) and all calculations are made at the same wavelength and using the values of n's and k's for the film and substrate as determined experimentally. The optimum angle which gives the highest value of $\delta\Delta$ and $\delta\psi$ is around 72 degrees in which the sensitivity is increased by 18% for $\delta\Delta$ and 13% for $\delta\psi$ while the improvement due to selecting the optimum wavelength was one order of magnitude for $\delta\psi$ and twice as much for $\delta\Delta$ as described in

section 4.3.1. Consequently by selection of wavelength and angle of incidence, the sensitivity for a particular investigation could be improved.

| Angle $^{o}$ | $\delta\Delta$ | $\delta\psi$ | $\delta\Delta\%$ | $\delta\psi\%$ |
|---|---|---|---|---|
| 64 | 0.158 | 0.108 | | |
| 65 | 0.162 | 0.111 | 2.5 | 2.8 |
| 66 | 0.167 | 0.113 | 5.7 | 4.6 |
| 67 | 0.170 | 0.115 | 7.6 | 6.5 |
| 68 | 0.174 | 0.117 | 10.1 | 8.3 |
| 69 | 0.178 | 0.119 | 12.7 | 10.2 |
| 70 | 0.181 | 0.120 | 14.6 | 11.1 |
| 71 | 0.183 | 0.121 | 15.8 | 12.0 |
| 72 | 0.186 | 0.122 | 17.7 | 13.0 |
| 73 | 0.187 | 0.122 | 18.4 | 13.0 |

Table (4.7a) Computed values of $\delta\Delta$ and $\delta\psi$ for different angles of incidence using values of refractive indices of gold and argon as determined experimentally.

4.7.1 Explanations of the observed changes in $\psi$.

The calculation of the change of the ellipsometric parameters $\psi$ and $\Delta$ upon gas adsorption showed a positive value of $\delta\psi$ for an absorbing film on an absorbing substrate and a negative value for adsorption of non-absorbing film on an absorbing substrate (see section 4.3.1). Two explanations are given in the literatures.

1. Bootsma et al.(1969) found a positive change of $\delta\psi$ for adsorption of several gases on silicon surfaces at a particular

wavelength. They considered these positive values as anomalous and proposed three different models to account for the anomalous change in $\psi$.

Model (1) An optically absorbing layer on an unchanged substrate.

Model (2) Change in optical constants of the substrate as a result of chemisorption.

Model (3) Change in optical constants of thin surface layer of the substrate.

2. Dignam et al.(1971) considered that at low surface coverage (one monolayer or less), the adsorbed molecules are bound to be partially orientated relative to the normal to the surface, and if it is assumed that the molecules are randomly oriented with respect to rotation about a normal to the surface, then the adsorbed film would behave as a uniaxial medium with the optic axis oriented normal to the surface. The ellipsometric effect in the thin film approximation is shown to be identical to those of an isotropic film of complex refractive index $n_1$ which may be given by:

$$(1-\bar{n}_1^{-2})(n_2^2-n_1^2) = (1-\bar{n}_\perp^{-2}(n_\perp^2-n_2^2)(n_{//}^2-n_2^2)^{-1})(n_2^2-n_{//}^2)$$

where $n_\perp$ and $n_{//}$ are the refractive indices normal and tangential to the surface respectively. Real solutions were found only for $n_{//} > n_\perp$ leading to finite but small values of $k_1$, $n_1 = 1.4-0.03\,i$ leads to $\delta\psi = +0.003^\circ$ per Å which is too small to account for the present observed value of $\delta\psi$.

For physical adsorption, model (1) is the most reasonable since the adsorbed gas is only bound to the surface by the Van der Waal's forces of attraction and no exchange of electrons between substrate and adsorbed gas takes place to change the surface of the substrate and hence its optical constants as is the case for models (2 and 3). Model (3) would be suitable for semiconductor crystals where the surface atoms have one or more uncompensated bonds and the gas film may be considered as a separate layer parallel to the substrate surface. The present measurements did not show any change of the electrical resistance of the gold film upon adsorption of the gas layer, which confirms the chosen model and thickness of the film.

The adsorption process on different crystallographic planes has been considered theoretically by Lenel (1933). The maximum binding forces occur in positions where the adatoms are surrounded by the maximum number of lattice atoms, i.e. different crystallographic planes of a given crystal can show marked differences in catalytic activity. The experiments of Gwathmey et al.(1954) show that, in the case of copper single crystal spheres, those positions that are parallel to the most densely packed (111) planes show the highest catalytic activity.

The ellipsometric measurements in sections 4.3.2, 4.3.3 and 4.3.4 indicate that the change in $\Delta$ values depends on the density of

packing in the particular surface, in good agreement with the theoretical considerations and Gwathmey's experiments. For polycrystalline film surfaces, the experimental values of $\delta\Delta$ is nearly an average of the values of the two other planes (110) and (100). Also the value of $\delta\Delta$ is nearly twice as much for (110) as for (100) planes. It is assumed that polycrystalline films are combinations of all orientations in a random arrangement. This is also shown from the present ellipsometric measurements since the values of $\delta\Delta$ caused by adsorption on polycrystalline films lie between the values for $(\delta\Delta)_{110}$ and $(\delta\Delta)_{100}$ upon adsorption, this can be seen from Figs.(4.3.2a), (4.3.3a) and (4.3.4a). The amount of gas adsorbed on the surface depends on the number of sites available to accommodate the gas as shown in Fig. (4.3.4c). In the case of monolayer all available sites are occupied. Fractions of monolayer can be defined by the ratio $\frac{\text{number of sites occupied}}{\text{number of sites available.}}$

# CHAPTER 5

## EXPERIMENTAL RESULTS AND DISCUSSIONS : LOW ENERGY ION BOMBARDMENT

## 5.1 Introduction

Changes in optical properties and electrical conductivity of ion bombarded samples have been measured. These changes have been interpreted in terms of gas adsorption and damage.

The samples were evaporated gold films, on glass to produce polycrystalline films and on sodium chloride single crystal to produce single crystal gold films.

Difficulties arose when attempting to combine both electrical and optical measurements simultaneously. The magnitude of the change in the electric conductivity with bombardment was found to be small. In order to achieve reasonable percentage changes, it was necessary to prepare thin films, a requirement not consistent with that for optical measurements in which thicker films were needed to eliminate the influence of the substrate on measurements. Films of thicknesses 300 - 400 $\mathring{A}$ were used.

In the study of low energy ion bombardment, two important parameters are involved, the incident total ion dose and the ion energy E. The following results describe the effect of these parameters on both electrical and optical measurements and the corresponding desorption of trapped ions of the inert gas used.

## 5.2 Optical measurements

### 5.2.1 Argon and neon ion bombardment of polycrystalline gold films

Polycrystalline gold films were irradiated at room temperature. The bombarding ion current was kept constant for the whole range of measurements at $2 \times 10^{-11}$ A over a film area of 0.96 $cm^2$, and samples were irradiated for the same length of time, 60 minutes. The gases were spectroscopically pure gases (British Oxygen Co.). Figs. (5.2.1.a,b) show the changes of the ellipsometric parameter $\Delta$ with the bombarding ion energy, for argon and neon respectively. For low energies, the value of $\Delta$ decreased initially, and then started to increase. For argon ion bombardment the value of energy at which the value of $\Delta$ changes sign was about 130 eV while that for neon ions was about 150 eV as shown in the figures.

The corresponding changes in the values of $\psi$ are shown in Figs. (5.2.1.c,d). The values of $\delta\Delta$ and $\delta\psi$ at zero energy, correspond to the values at a gas pressure of $5 \times 10^{-5}$ torr and room temperature before irradiation, were found to be very small compared with measurements at liquid nitrogen temperature which have already been shown in the previous chapter. Table (5.2.1a) illustrates the difference between the adsorption of argon gas on a polycrystalline gold film at room temperature and liquid nitrogen temperature. When the sample (following adsorption at liquid nitrogen) was warmed to room temperature, there was less than 6% change in $\delta\psi$ and 4% in $\delta\Delta$. Also, at a particular ion energy, the change of both $\Delta$ and $\psi$ values were higher for argon ions than for neon ions.

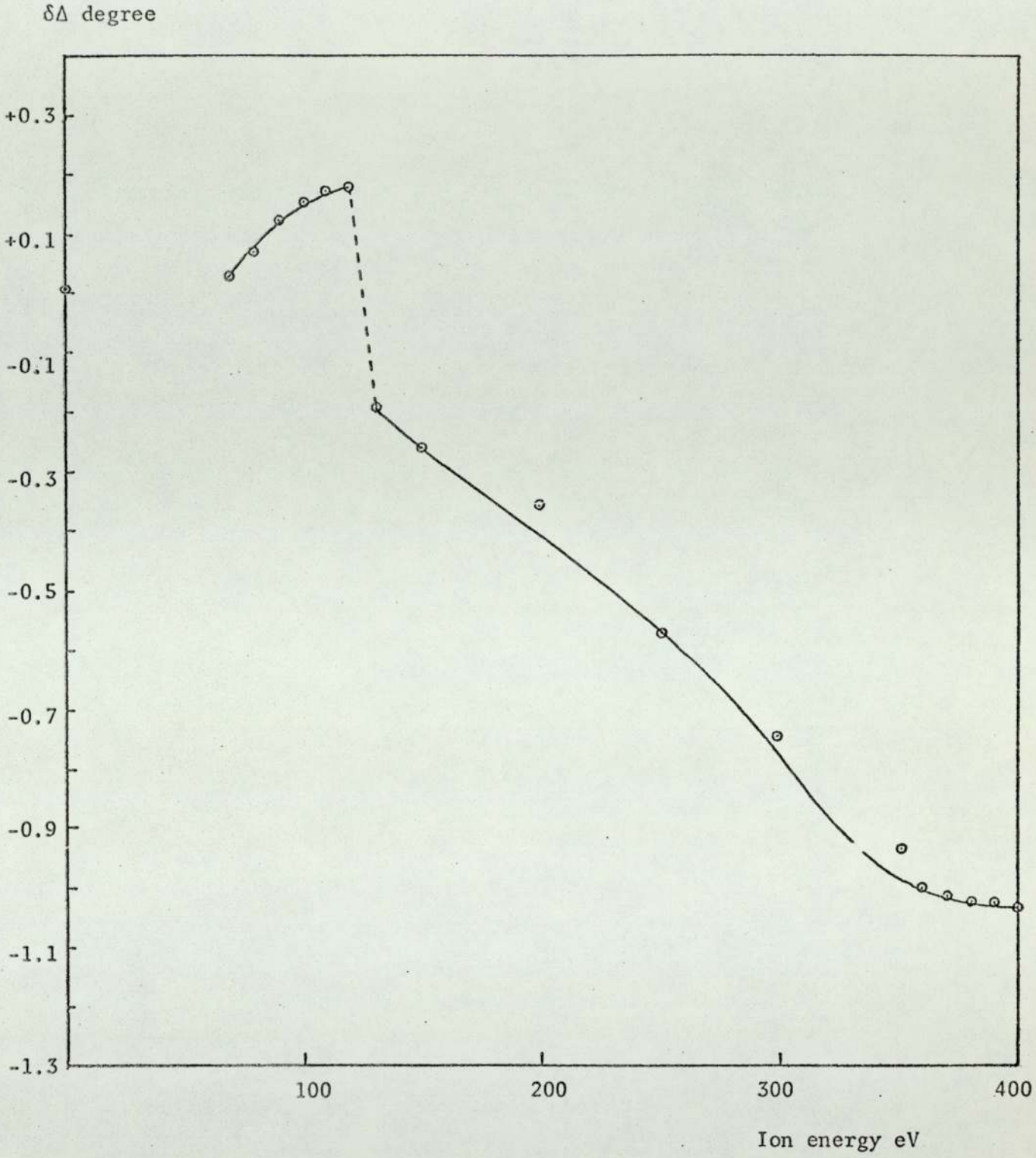


Fig. (5.2.1a) Change of ellipsometric parameter Δ with bombarding ion energy for argon ions on polycrystalline gold film at wavelength 6400 A.

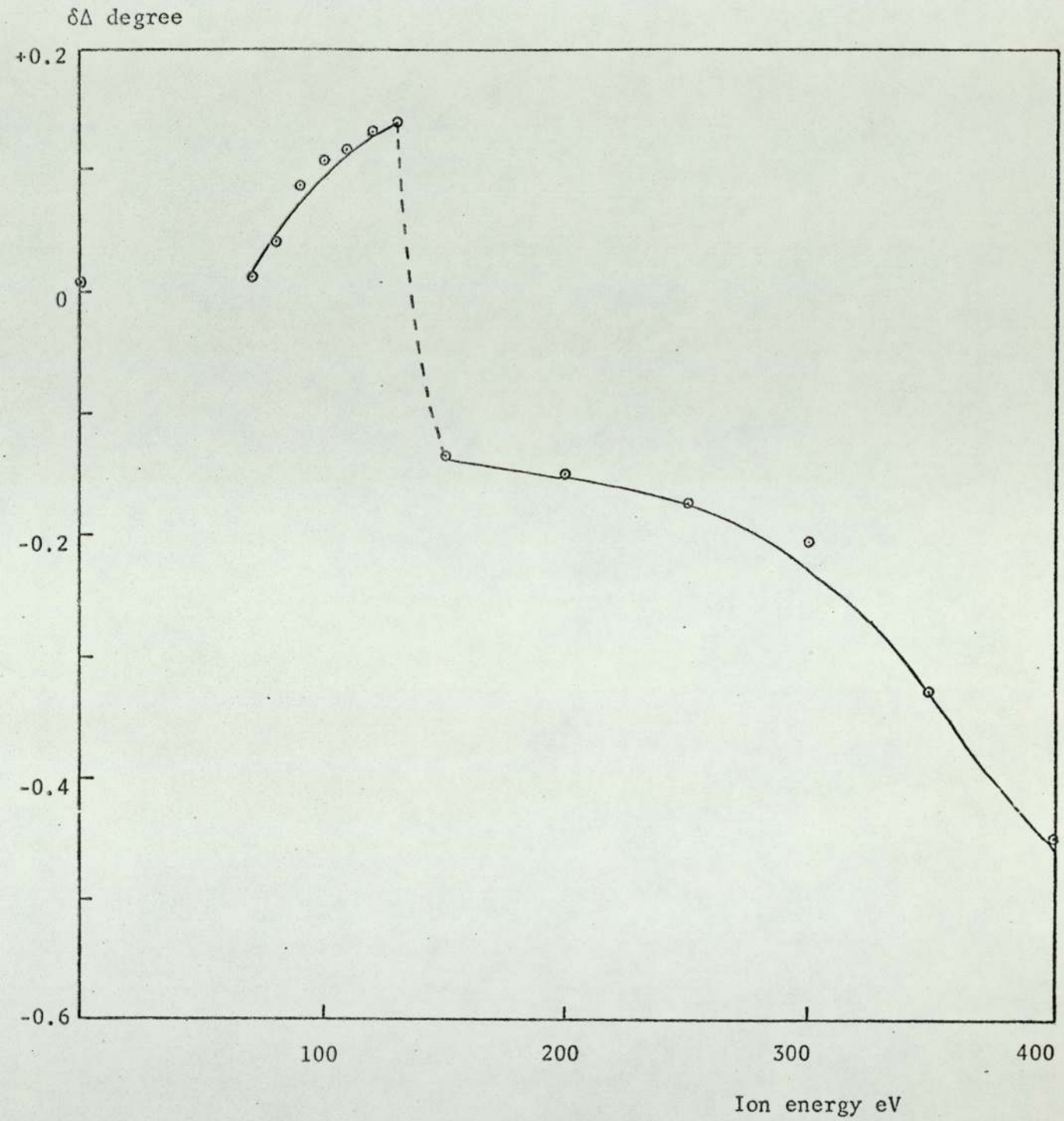


Fig.(5.2.1b) Change of ellipsometric parameter Δ with bombarding ion energy for neon ions on polycrystalline gold films at wavelength 6400 A.

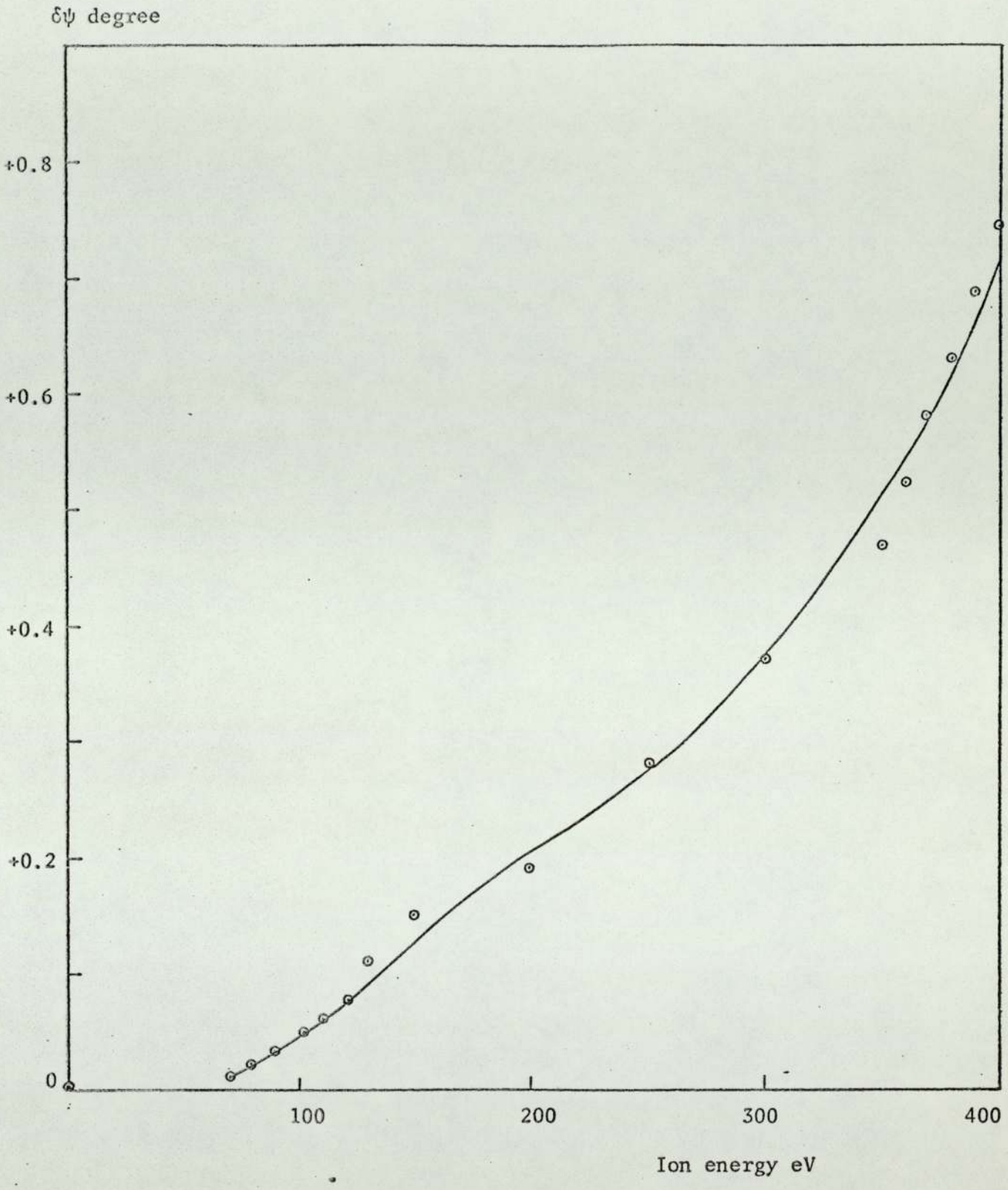


Fig. (5.2.1c) Change of ellipsometric parameter $\psi$ with bombarding ion energy for argon ions on polycrystalline gold film at wavelength 6400 A.

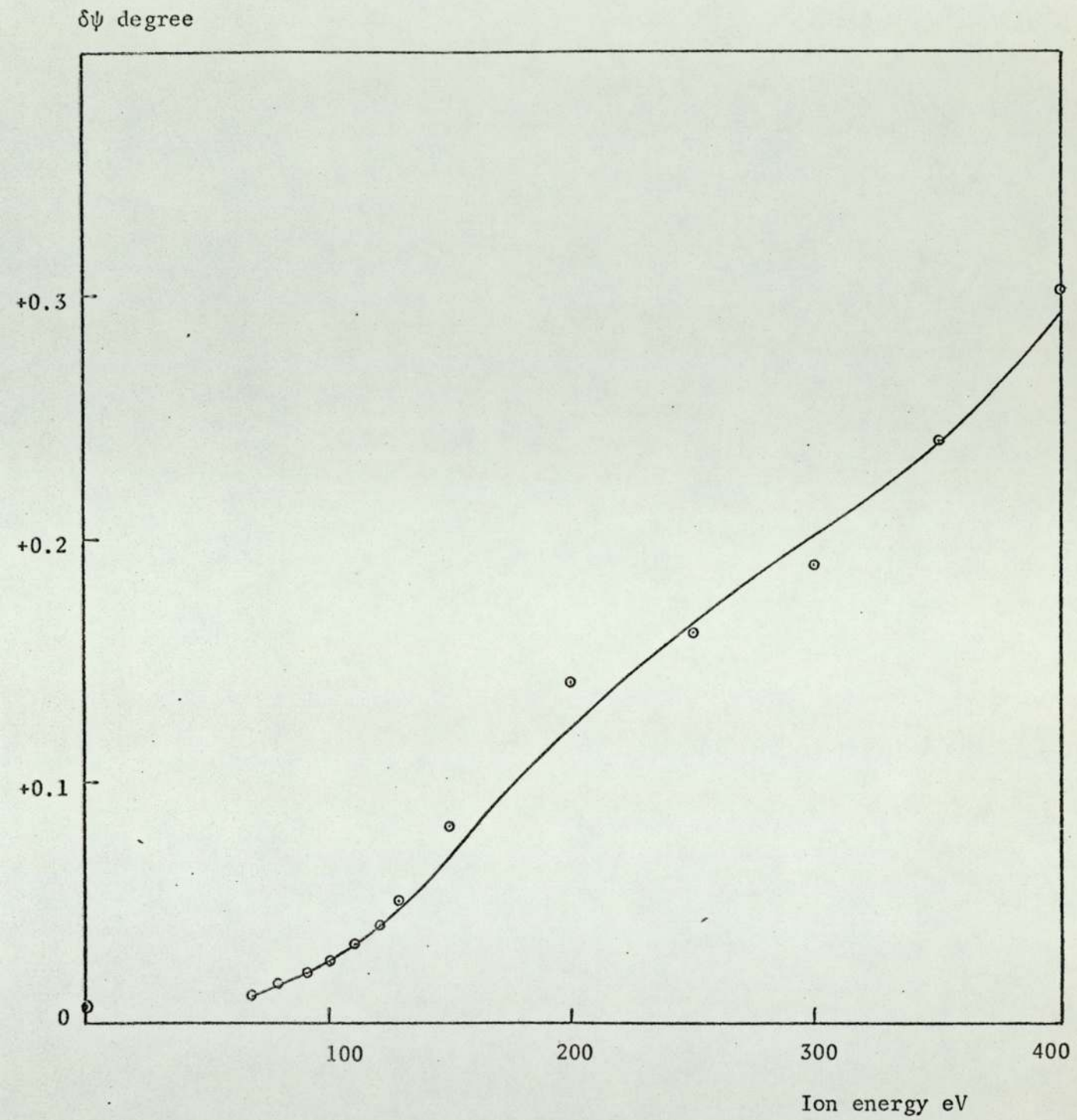


Fig. (5.2.1d) Change of ellipsometric parameter ψ with bombarding ion energy for neon ions on polycrystalline gold film at wavelength 6400 A.

| Temperature $^{o}C$ | $\delta\psi$ degree | $\delta\Delta$ degree |
|---|---|---|
| r.t. | 0.009 | 0.01 |
| liq. $N_2$ | 0.095 | 0.15 |

Table (5.2.1.a) The experimental ellipsometric changes of $\delta\psi$ and $\delta\Delta$ at pressure of $5 \times 10^{-5}$ torr of argon at two temperatures.

5.2.2 Argon and neon ion bombardment of <110> single crystal gold films

Single crystal gold film of <110> orientation was bombarded under the same conditions as described in the previous section. The values of $\delta\Delta$ and $\delta\psi$ for the same values of energies were found to be less than $\delta\Delta$ and $\delta\psi$ for polycrystalline films as shown in Figs. (5.2.2.a-d), $\delta\Delta$ takes the same shape as before. Also, the changes of $\delta\Delta$ and $\delta\psi$ for argon ion bombardment were much higher than those for neon. At an ion energy of 400 eV; $(\delta\Delta)_{argon} = (4\delta\Delta)_{neon}$ and $(\delta\psi)_{argon} = (3\delta\psi)_{neon}$. The threshold for neon was 130 eV while for argon it was 110 eV as shown in Figs.(5.2.2.a,b) and Table (5.2.3.a). The effect on optical constants n and k are shown in section (5.5)

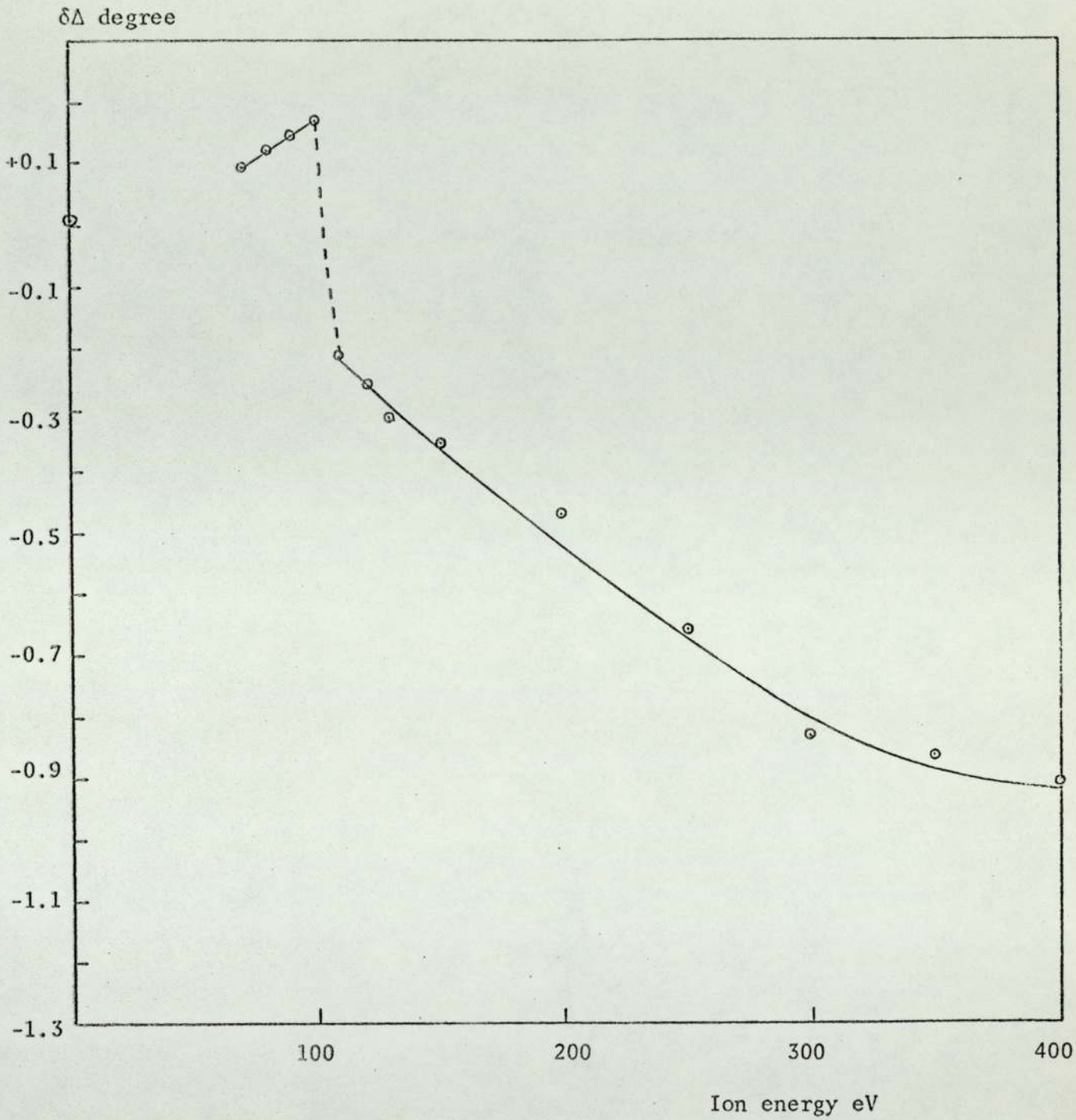


Fig. (5.2.2a) Change of ellipsometric parameter Δ with bombarding ion energy for argon ions on < 110 > single crystal gold film at wavelength 6400 A.

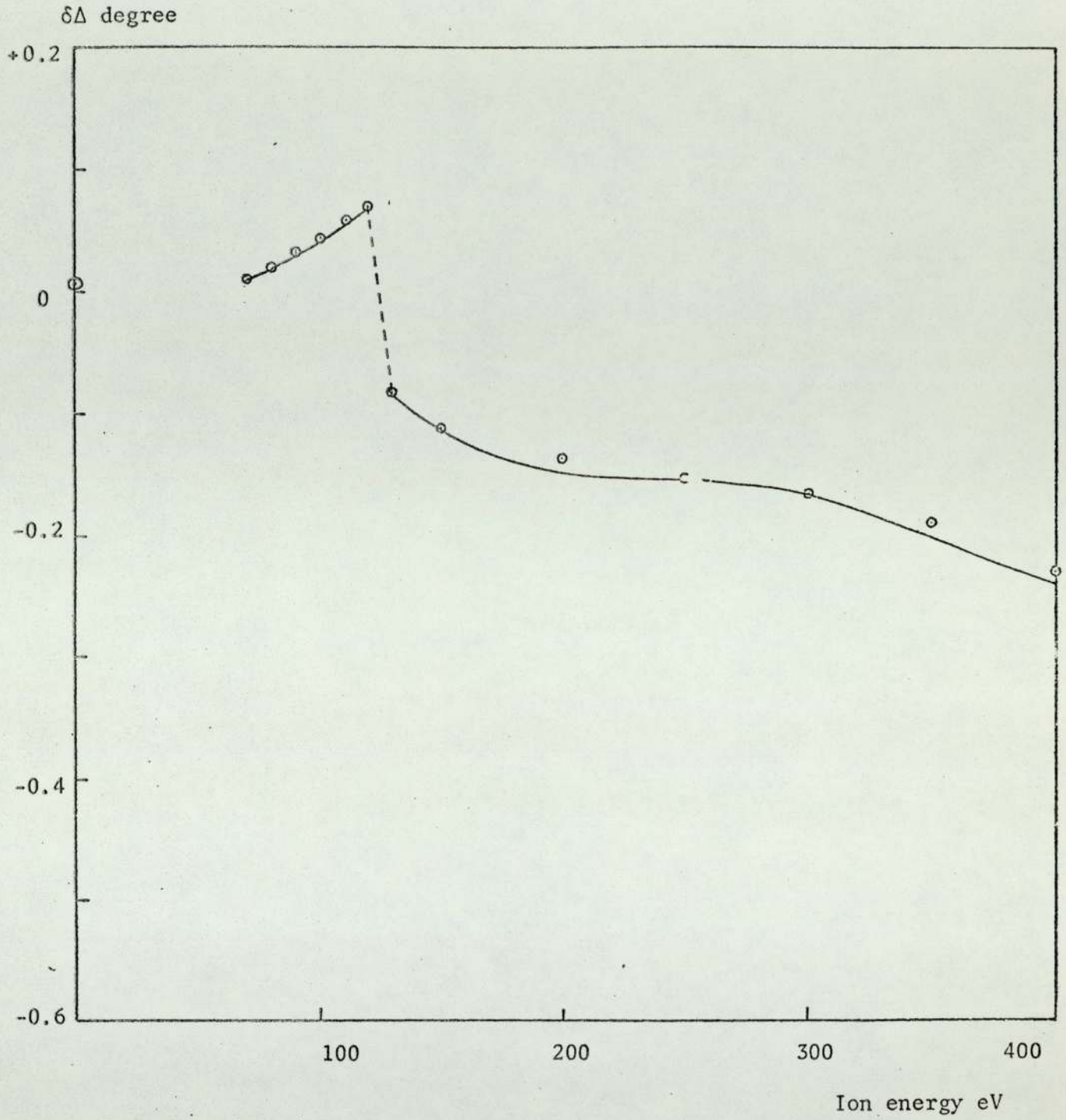


Fig. (5.2.2b) Change of ellipsometric parameter Δ with bombarding ion energy for neon ions on < 110 > single crystal gold film at wavelength 6400 A.

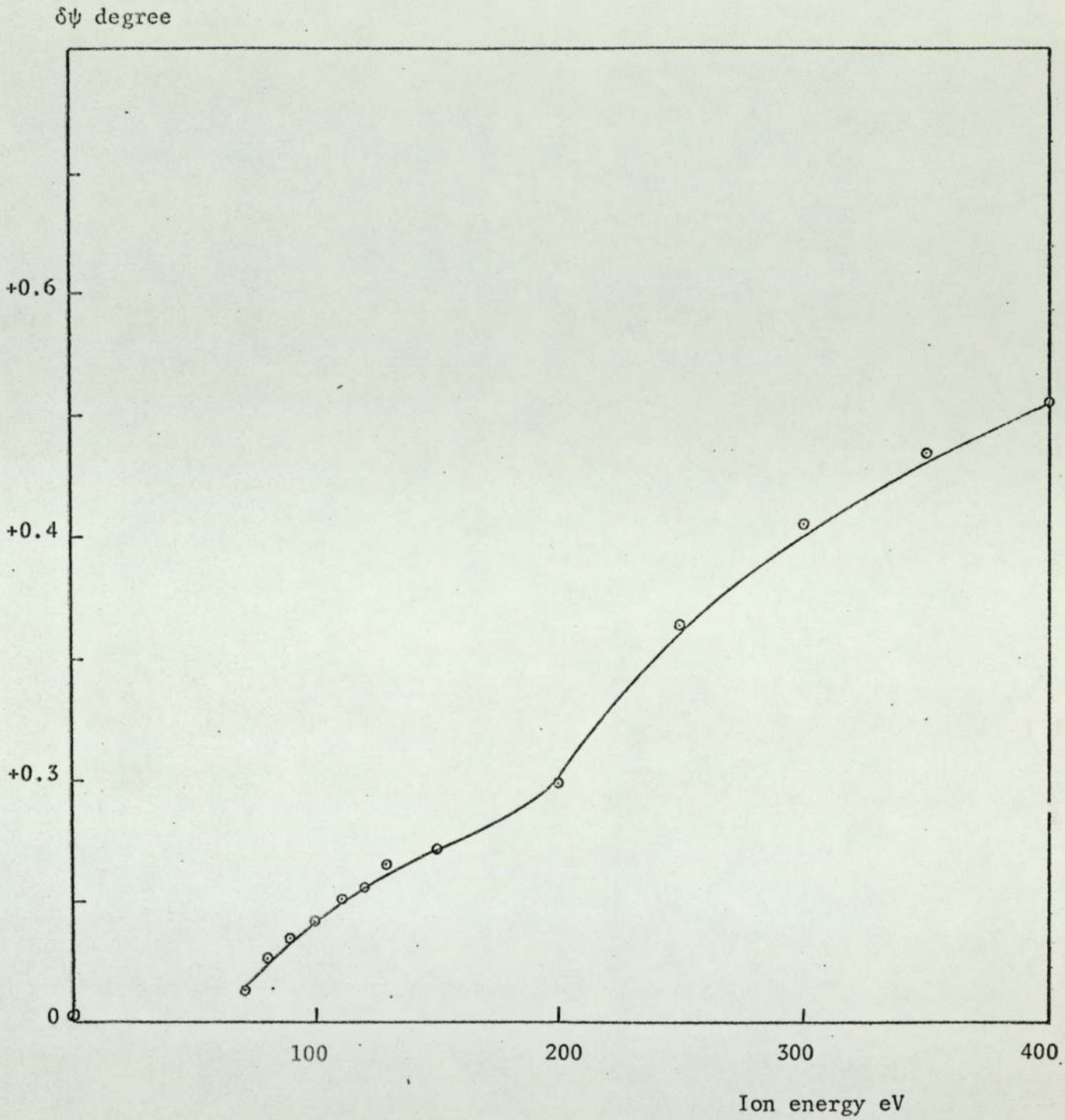


Fig. (5.2.2c) Change of ellipsometric parameter ψ with bombarding ion energy for argon ions on < 110 > single crystal gold film at wavelength 6400 A.

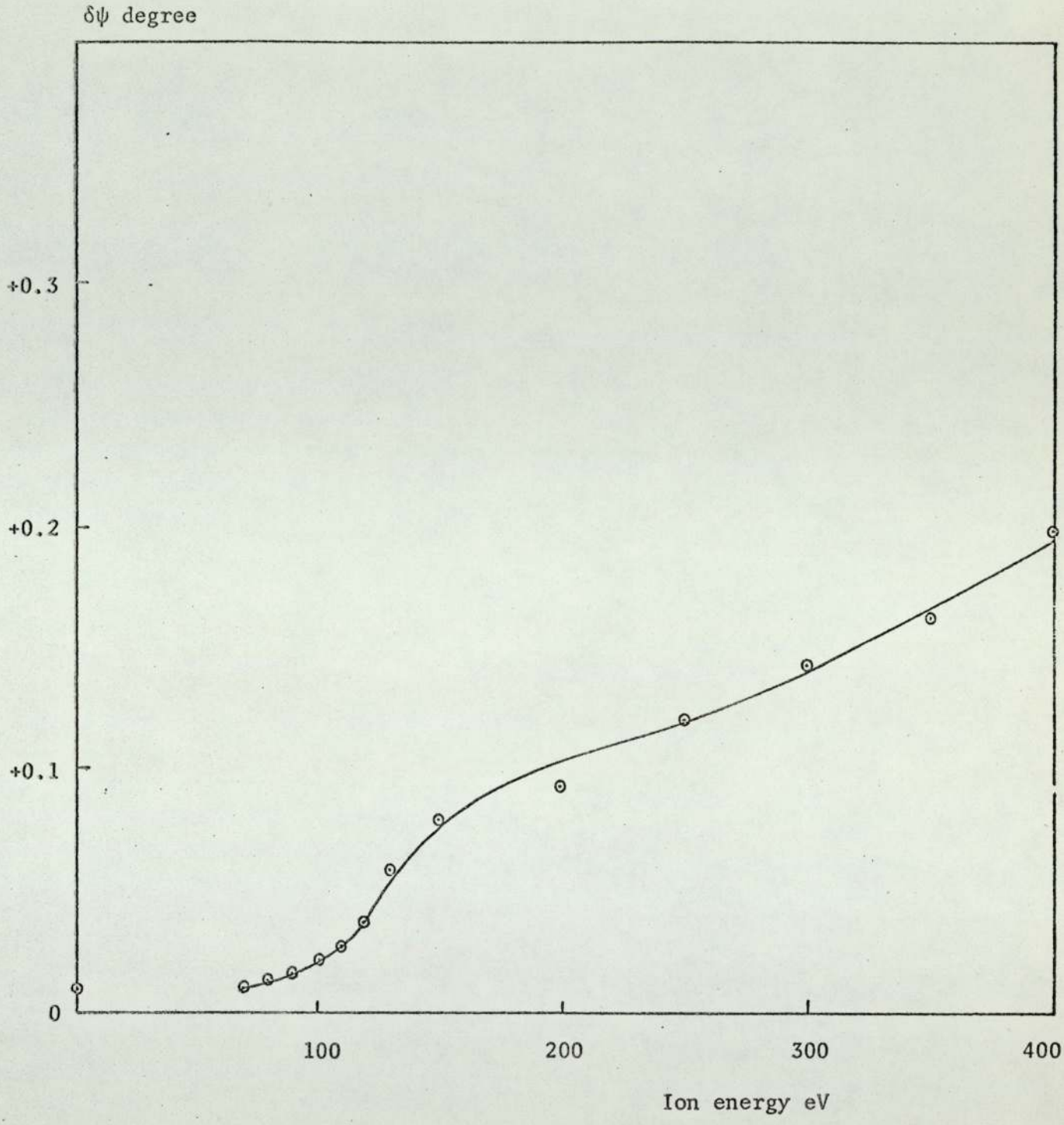


Fig. (5.2.2d) Change of ellipsometric parameter ψ with bombarding ion energy for neon ions on < 110 > single crystals gold film at wavelength 6400 A.

5.2.3 Argon and neon ion bombardment of single crystal <100> gold film

For single crystal <100> film, the values of $\delta\Delta$ follow the same pattern as in polycrystalline film and single crystal <110> as shown in Figs.(5.2.3.a,b) for argon and neon ion bombardment.

For argon ion bombardment, the values of $\delta\Delta$ and $\delta\psi$ were found to be less than both previous measurements for polycrystalline and single crystal <110> gold films. For neon ion bombardments, those values were found to be less than polycrystalline film but higher than that for the <110> single crystal film. The value of argon ion energy at which $\delta\Delta$ changes sign was 100 eV and for neon it was 120 eV.

Table 5.2.3.a summarizes the experimentally determined values of the energy at which the value of $\delta\Delta$ changes sign. The momentum transferred from neon atoms to target atoms are less than that from argon, if it is assumed that the change in sign of $\Delta$ corresponds to the same damaged condition for both types of ions.

| Crystal surface | Ion Energy eV | |
|---|---|---|
| | Neon | Argon |
| Polycrystalline | 150 | 130 |
| Single Xtal <100> | 120 | 100 |
| Single Xtal <110> | 130 | 110 |

Table (5.2.3.a). Measured values of threshold energies for different surfaces for neon and argon ion bombardment.

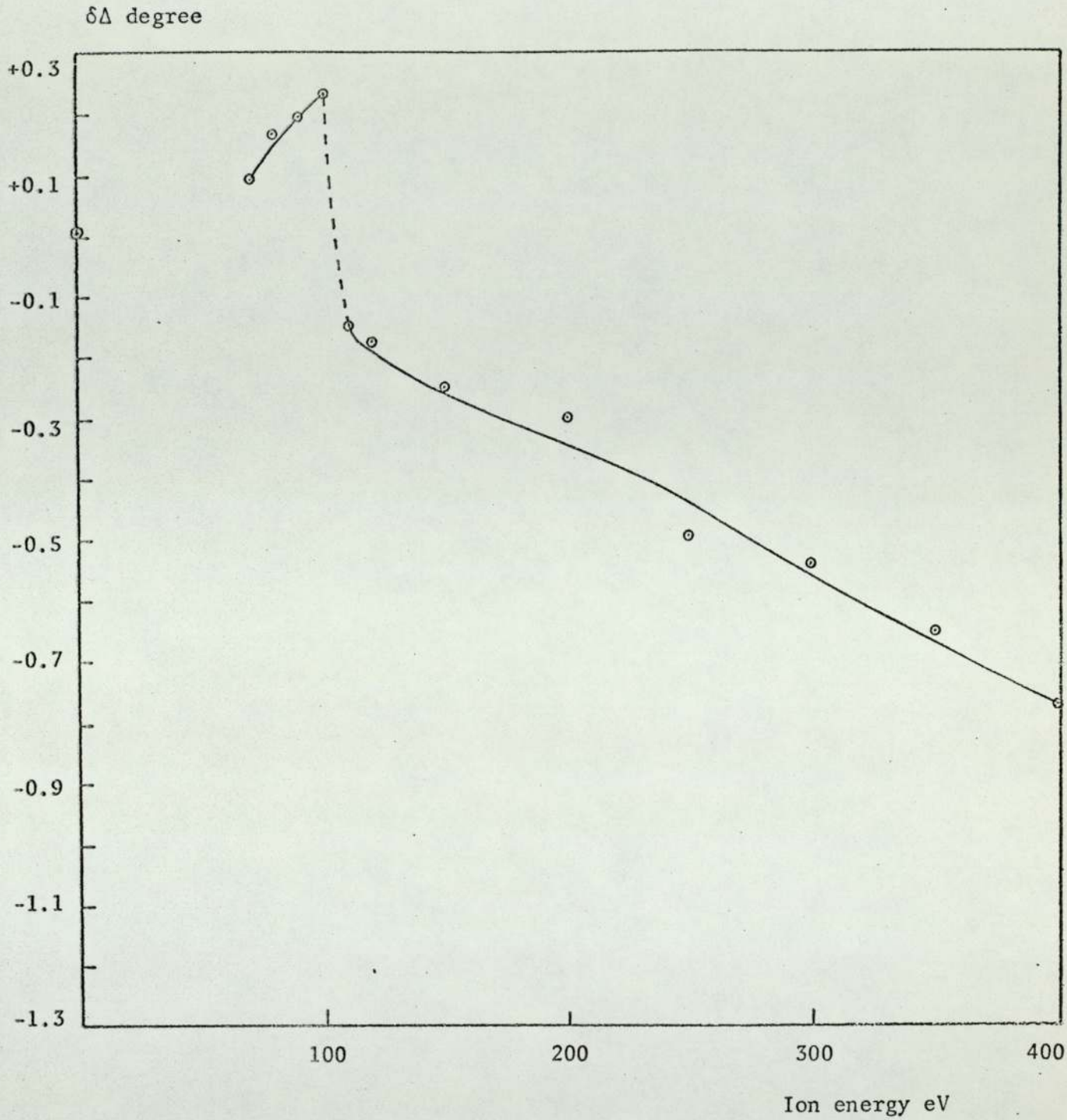


Fig. (5.2.3a) Change of ellipsometric parameter Δ with bombarding ion energy for argon ions on < 100 > single crystal gold film at wavelength 6400 A.

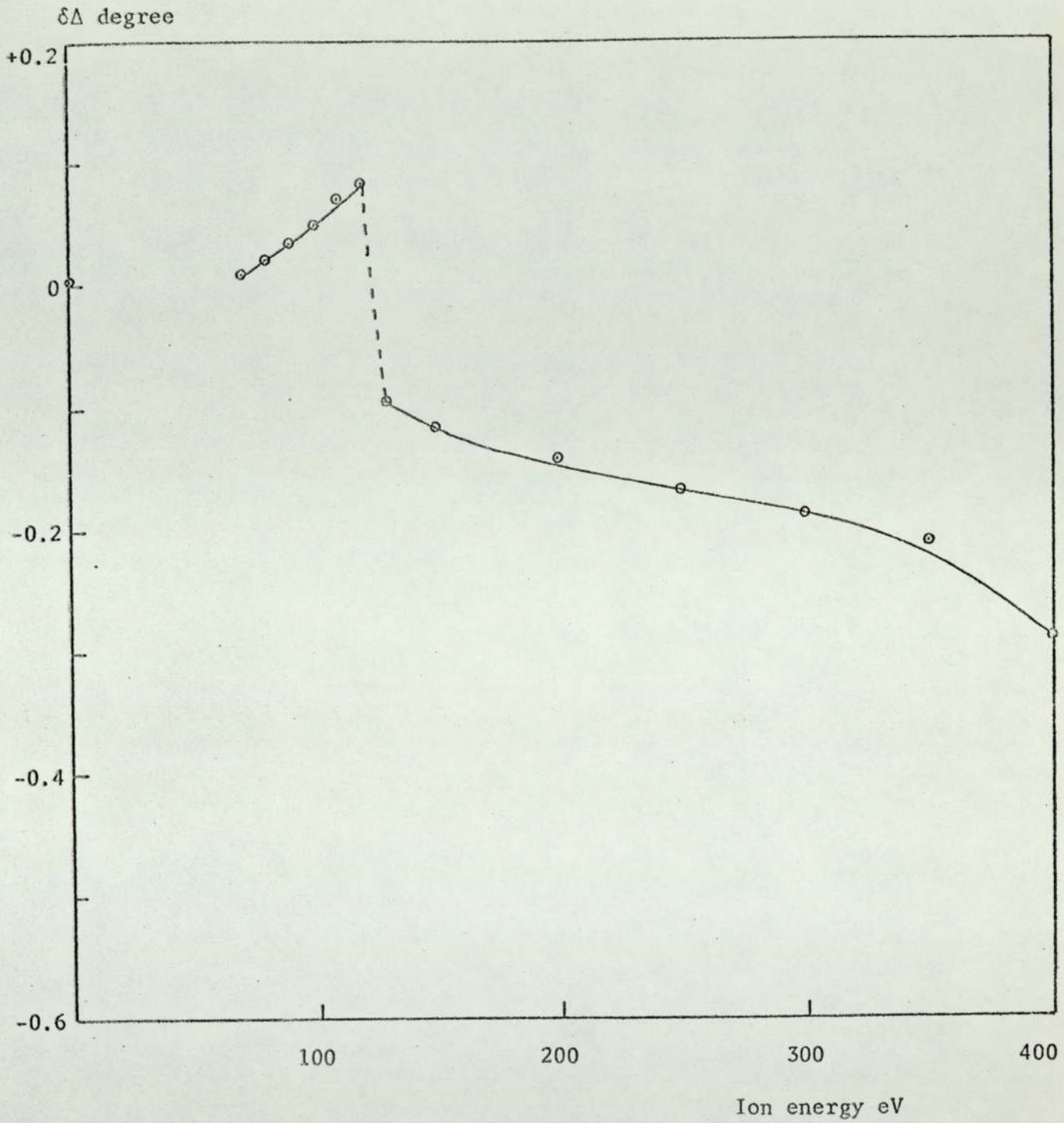


Fig. (5.2.3b) Change of ellipsometric parameter Δ with bombarding ion energy for neon ions on < 100 > single crystal gold film at wavelength 6400 A.

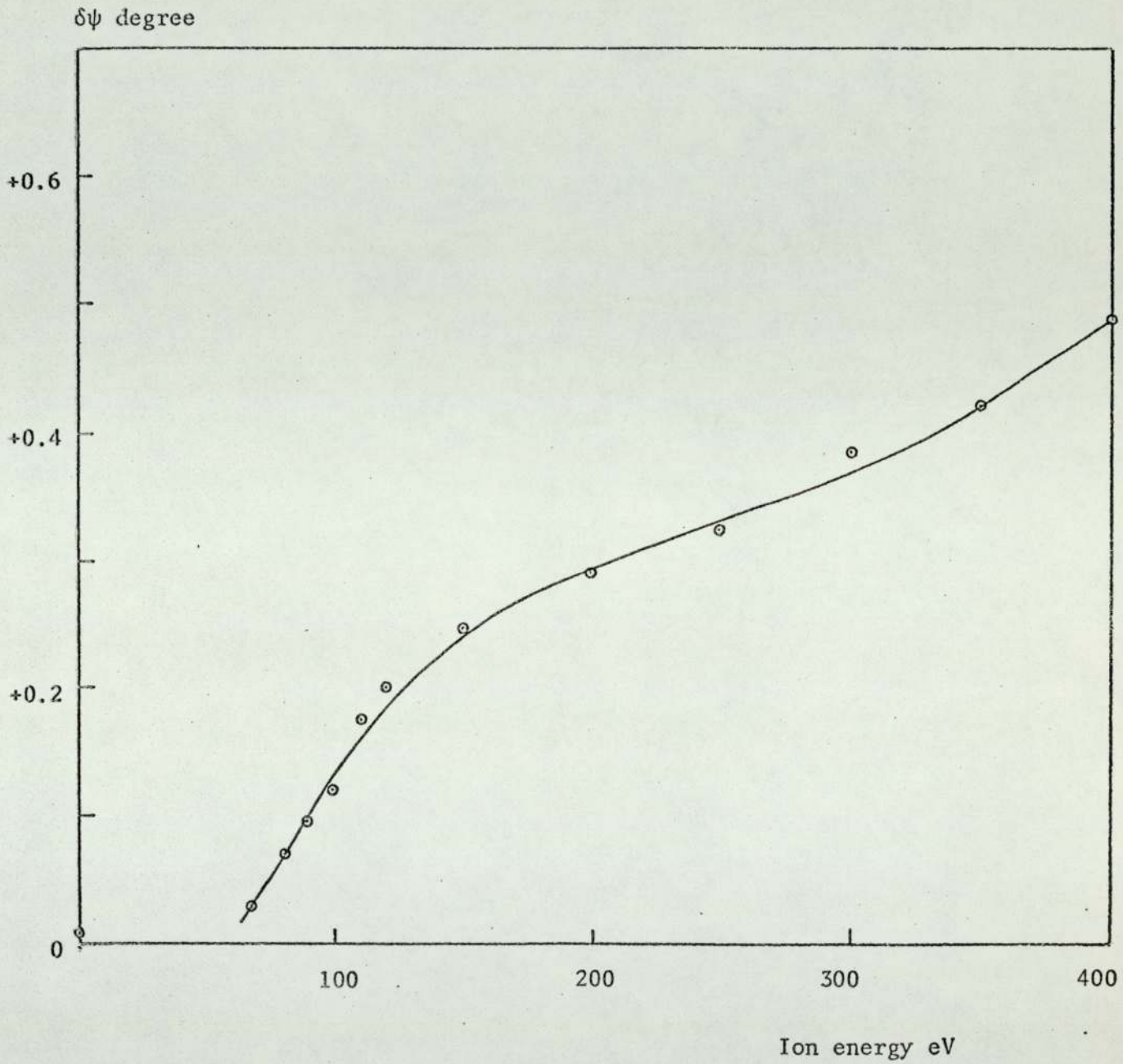


Fig. (5.2.3c) Change of ellipsometric paremeter ψ with bombarding ion energy for argon ions on < 100 > single crystal gold film at wavelength 6400 A.

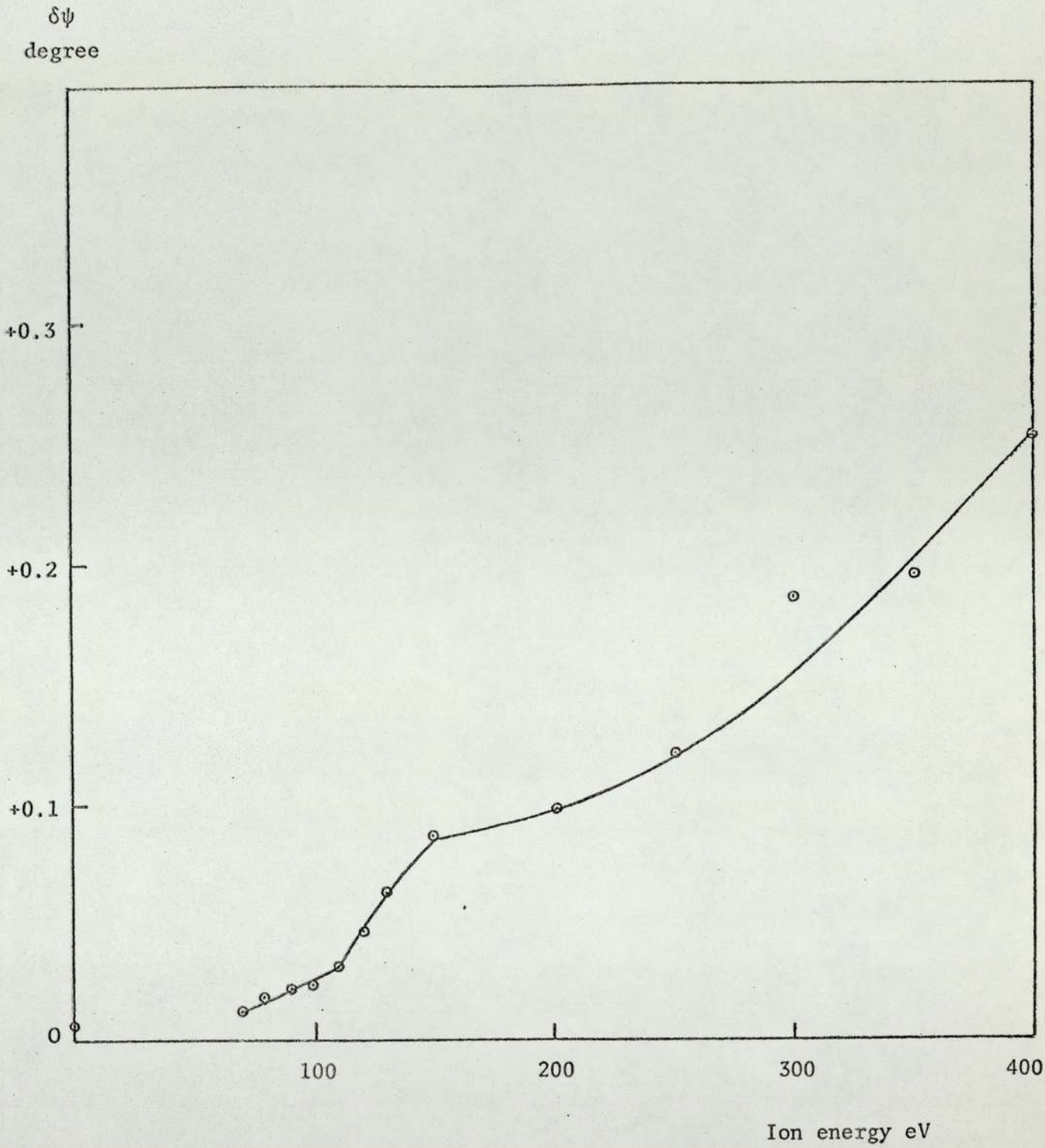


Fig. (5.2.3d) Change of ellipsometric parameter $\psi$ with bombarding ion energy for neon ions on < 100 > single crystal gold film at wavelength 6400 A.

## 5.3 Electrical measurements

The electrical resistance was found to increase as a result of bombardment. Fig.(5.3.a) shows the increase of the resistance of a polycrystalline gold film bombarded at room temperature, with increasing ion energy. Optical measurements of the film were made simultaneously. The ion dose was the same for all tests using an ion current of $2 \times 10^{-11}$ A for one hour. The contaminated surface layer due to very low ion energy bombardment did not cause any change in the electrical resistance whereas changes in ellipsometric parameters were observed. For energies less than approximately 200 eV, the resistance did not change. After each bombardment, the samples were heated to 200 $^{o}$C for one hour and left to cool for eight hours. This annealing did not restore the film resistance to its value, prior to bombardment. Fig. (5.3.b) shows the remaining value of the resistance after heating. Up to 55% of the increase of the resistance was recovered as shown in Fig.(5.3c). The residual resistivities measured at 4 $^{o}$K, of two films of different thickness prepared in the same run were measured. Measurements at this temperature eliminate resistivity effects of the gold lattice and gives the resistivity due to imperfections and impurity. Two pairs of films were prepared at the same time (as explained in chapter 2), each pair of films were of the same thickness. Two films (one from each pair) were bombarded at the same time, at gas pressure of $5 \times 10^{-6}$ torr and at an ion current of $2 \times 10^{-11}$ A at 400 eV for one hour. After bombarding the two films, all four films were transferred to another system to measure the residual resistivities. Fig.(5.3.d) shows two films of the same thickness prepared at the same time under identical conditions. Film (1) was not bombarded and film (2) was bombarded at room temperature. The value of the resistance of the bombarded film is increased as shown in the figure.

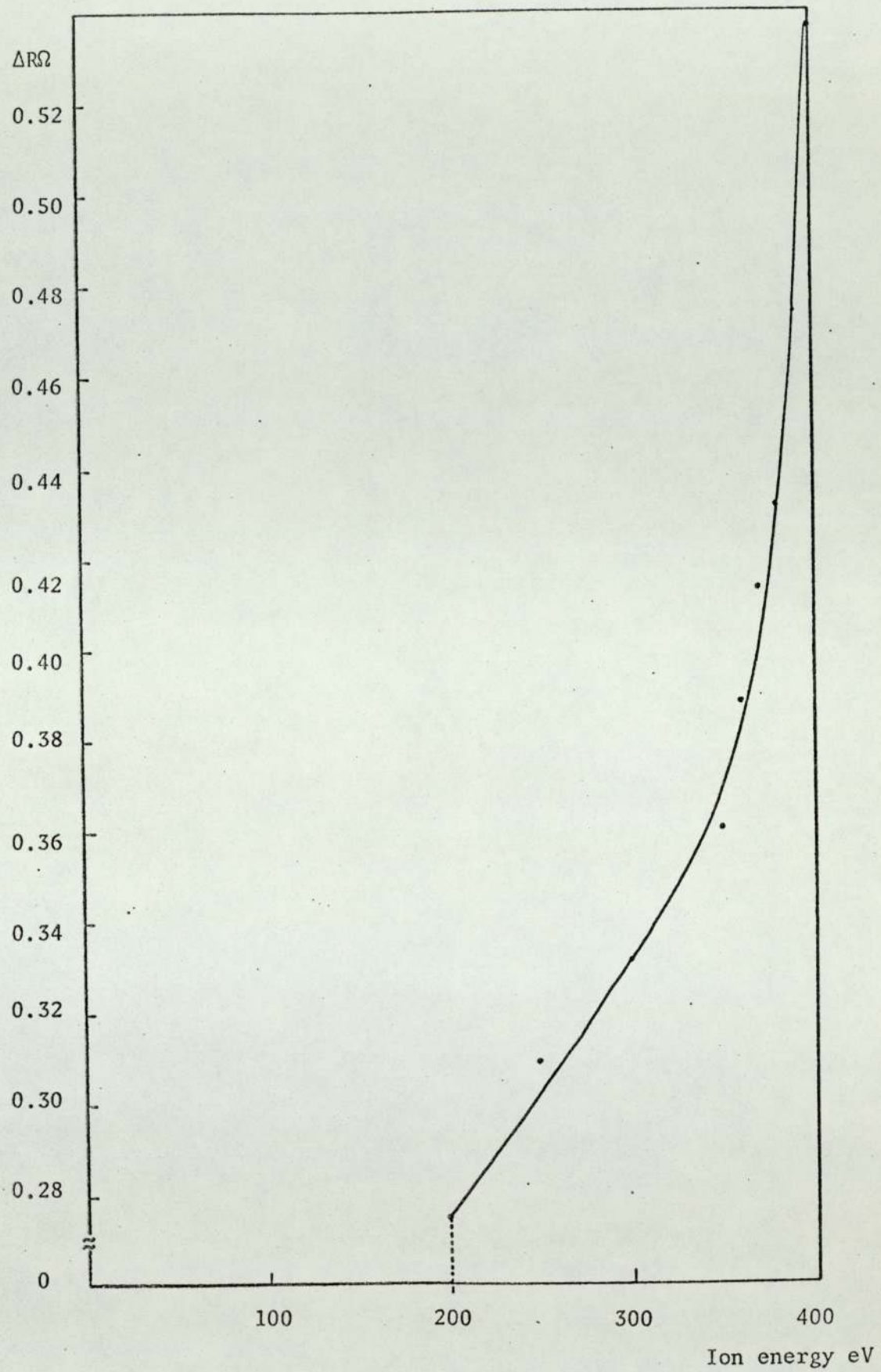


Fig. (5.3a) The change in the resistance of polycrystalline gold film with increasing bombarding ion energy (argon ions)

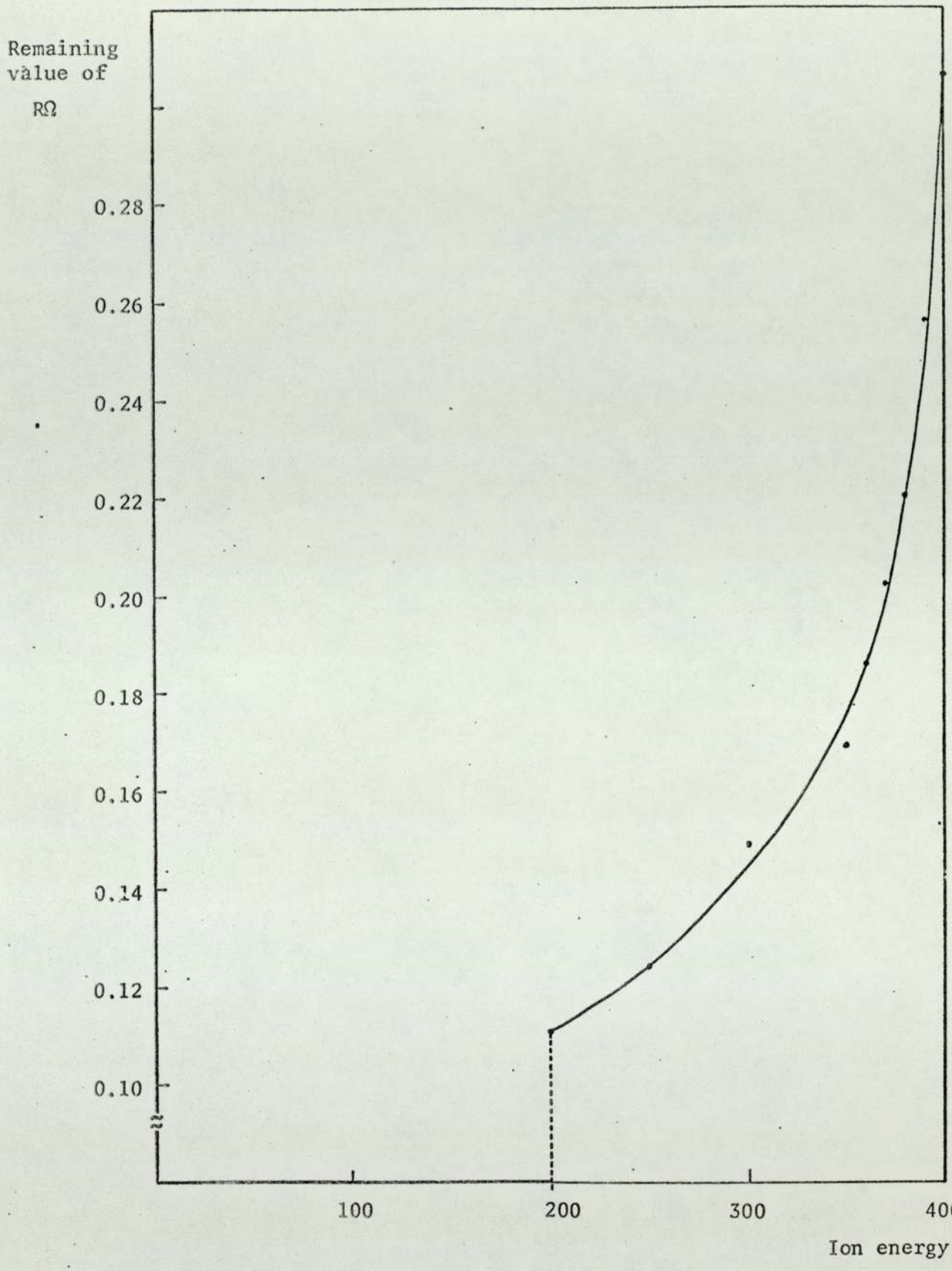


Fig. (5.3b) The change in resistance remaining in polycrystalline gold film after annealing following argon ion bombardment.

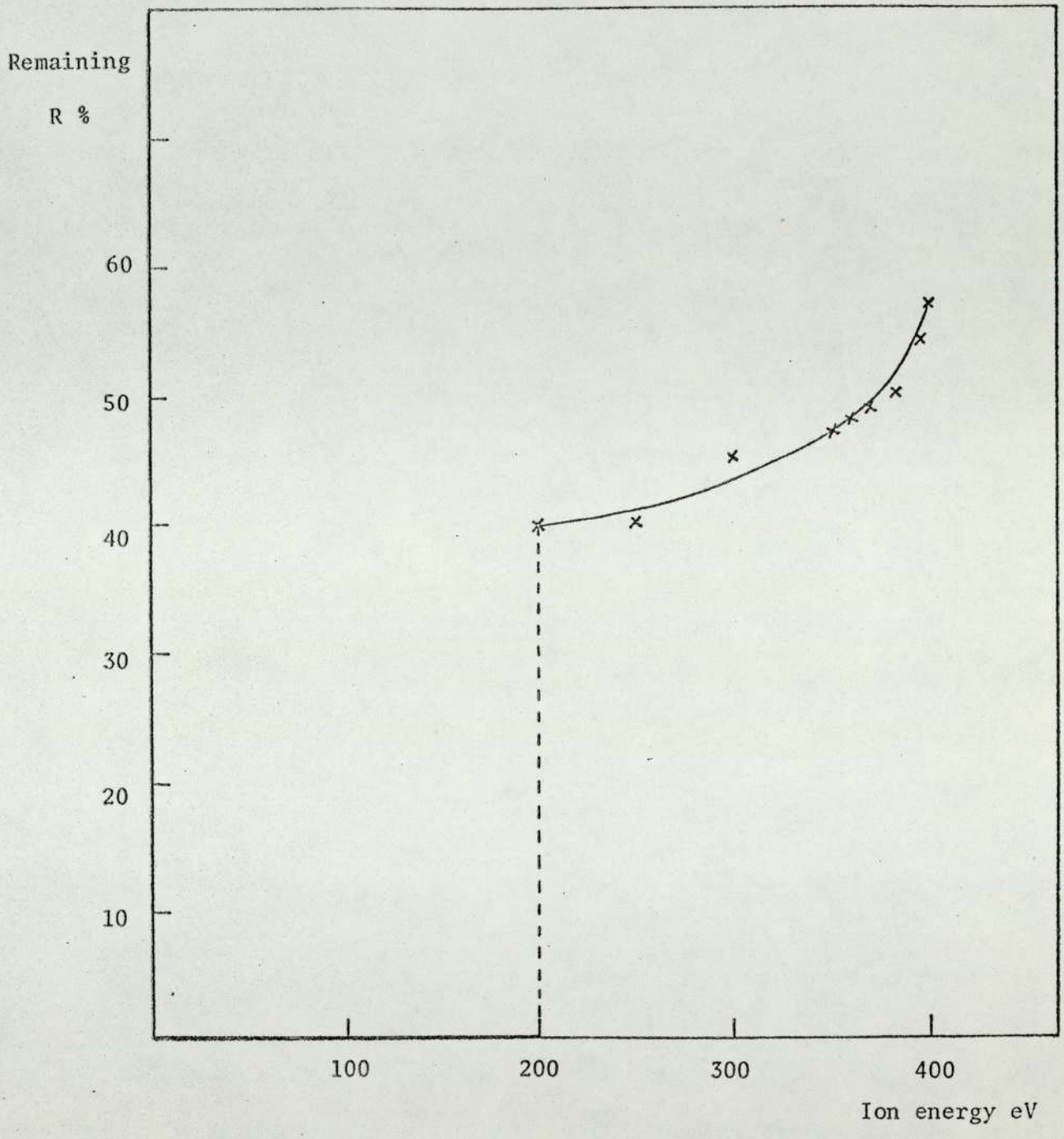


Eig.(5.3c) Percentage of the remaining resistance after annealing following argon ion bombardment on polycrystalline gold film.

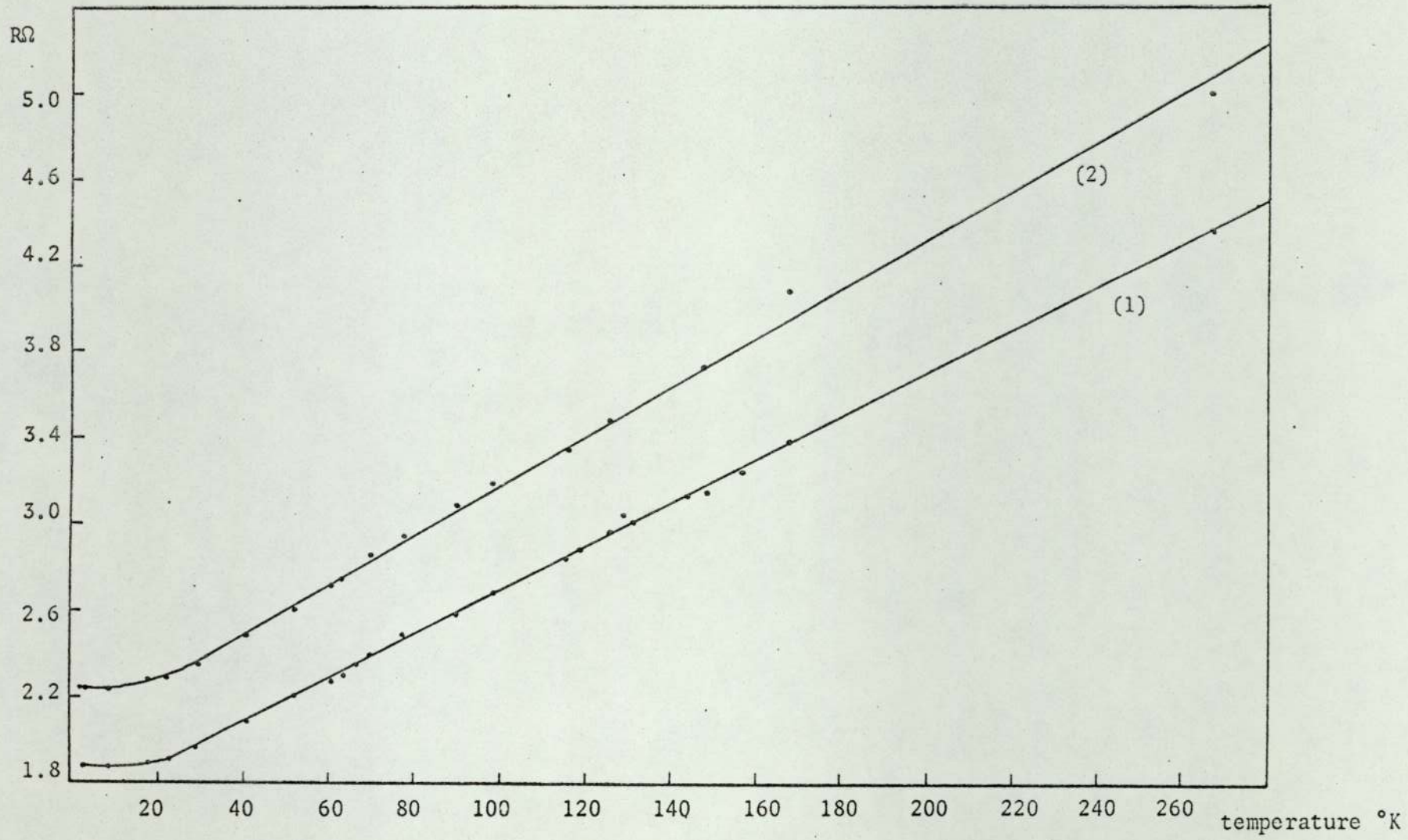


Fig. (5.3d) Residual resistance of polycrystalline gold film. Film (1) not bombarded
Film (2) after bombardment with argon ions of energy 400 eV.

## 5.4 Dose dependence measurements

The change of the values of $\psi$ and $\Delta$ are found to be dose dependent. The bombardment was conducted at constant ion currents for varying periods of time, i.e. the total ion dose incident on the target was adjusted by varying the bombardment time keeping the ion current constant. Figs.(5.4.a,b) illustrate the relation between the ion dose and the change in the values of $\Delta$ and $\psi$ respectively. As is expected the change in both $\psi$ and $\Delta$ is linearly dependent on the bombarding time because by increasing the bombardment time, the number of ions striking the surface is higher.

## 5.5 Calculation of some electrical properties and the damaged layer thickness from optical measurements

Two constants, the index of refraction and the extinction coefficient describe the optical properties of a system. For metals, these optical properties depend on the behaviour of conduction electrons in response to the incident electromagnetic radiation. An absorbing medium is characterized by a complex refractive index (n-ik) and a complex dielectric constant $\varepsilon = \varepsilon_1 - i\varepsilon_2$. When electromagnetic waves are absorbed as a result of interaction with conduction electrons, the Drude theory may be used to express the optical constants in terms of the fundamental constants of the metal,

$$\varepsilon_1 - i\varepsilon_2 = (n-ik)^2 \qquad 5.5a$$

In the far infra-red, the optical absorption is dominated by the conduction electrons and one can assume that the current is almost in phase with the electric vector and hence

$$nk = \sigma_o/\nu$$

where $\sigma_o$ is the conductivity measured for static fields and $\nu$ is the frequency. For intermediate wavelength, account must be taken of the resistance and hence of the absorption of energy by the medium. The classical formulae for the optical constants expressed in terms of the frequency $w/2\pi$ and the time of relaxation $\tau$ are

$$n^2 - k^2 = 1 - \frac{4\pi N^* e^2}{m} \left(w^2 + \frac{1}{\tau^2}\right)^{-1} \qquad 5.5b$$

$$2nk = \frac{4\pi N^* e^2}{m} \left(\frac{1}{w\tau}\right) \left(w^2 + \frac{1}{\tau^2}\right)^{-1} \qquad 5.5c$$

where $N^*$ is the effective electron density

$\tau$ is their relaxation time

$w$ is the angular frequency of the incident light

If $\frac{1}{w} >> \tau$ i.e. the period of the light is large compared with the time of relaxation, then from equations 5.5b, 5.5c

$$nk = \sigma/\nu$$

$$n^2 - k^2 << nk$$

On the other hand if $\frac{1}{w} << \tau$ the following approximate equations are valid,

$$n^2 - k^2 = 1 - 4\pi N^* e^2/mw^2 \qquad 5.5d$$

$$2nk = 4\pi N^* e^2/mw^3\tau \qquad 5.5e$$

$$\sigma_o = \frac{N^* e^2 \tau}{m} \qquad 5.5f$$

$\sigma_o$ is the d.c. electrical conductivity

In general, for good conductors, the wavelength $\lambda_\tau$ at which $w = \frac{1}{\tau}$ lies in the far infra-red and relations (5.5d,e) are good approximations when applied in the visible region. $\lambda_\tau$ for gold, calculated from the bulk values of $\sigma_o$ and N* is 51.529 $\mu$ ($\sigma_o = 4.55 \times 10^5 (\text{ohm cm})^{-1}$ and $N^* = 5.9 \times 10^{22} \text{cm}^{-3}$).

In the present experiment, the change in the values of n and k of the bombarded film as a function of ion energy is shown in Figs. (5.5a,b) for a typical polycrystalline gold film. A two layer computer programme described by O'Shea (Ph.D. thesis, Aston University, 1971) is used to determine the values of the damaged layer thickness, n and k as described in Chapter 4 section 6. Table (4.6b) in Chapter 4 shows that the error in determining the values of the optical constants for films, neglecting the adsorbed gas layer, is very little (as can be seen from the values of the pseudoconstants) compared with the change produced by the ion bombardment. The fact that ion bombardment produces greater changes in $\Psi$ and $\Delta$ suggests that the surface layer of the bombarded film is significantly affected by the incident ions. Table (5.5a) summarizes the calculated values of the effective number of conduction electrons and the corresponding resistivity and relaxation time as calculated from equations (5.5d,e,f) for a typical polycrystalline gold film, using the experimentally determined n and k values. The decrease in the value of N* with increasing ion energy may be due to the formation of holes in the film. The decrease in the relaxation time may be due to enhanced scattering of electrons caused by disorder produced by the foreign or displaced atoms.

The value of the resistivity ($\rho_{opt.} = 5.24 \times 10^{-6}$ ohm cm) calculated from the optical measurements and equation (5.5f) did not agree with the measured d.c. resistivity ($3.13 \times 10^{-6}$ ohm cm) for unbombarded film, but the increase in $\rho_{opt.}$ due to ion bombardment is in the same direction as the measured steady current resistance and corresponds to poorer quality film. Mott and Jones (1958) compared optical measurements of a polished gold surface with bulk conductivity of gold and found that the observed electrical conductivity for steady fields was an order of magnitude less than the value calculated on the basis of equations (5.5b,c). They attributed this difference to the high absorption of an amorphous surface layer produced by the polishing. In the present case the films were prepared under ultra high vacuum conditions giving smooth surfaces. The lack of significant broadening of the lines in the X-ray diffraction patterns of the films indicated a large grain size. These factors probably account for the fact that the discrepancy in optically calculated and experimental values is only reduced to approximately 40% as is shown in the last two columns of Table 5.5a.

The damaged thickness determined optically for an argon ion beam is shown in Fig.(5.6b). For the maximum energy used (400eV), the thickness was found to be 38 Å. Figs.(5.5c,d,e) show the change of the values of n,k and 2nk with wavelength of the light used. The full line is the annealed film before bombardment and the dots correspond to the values after ion bombardment with argon ions of energy 400 eV, the minimum of the curves in the bombarded case is less deep which indicates a deterioration of the film quality in good agreement with Abeles (1969).

Also there was no change in the band structure or the nature of the interband transitions by the introduction of the defects because the characteristic values are located at approximately the same wavelength as seen from Fig.(5.5e).

The damage produced in single crystal gold film is less than that for polycrystalline film as seen from the change of $\delta\Delta$ and $\delta\psi$ with ion energy which suggests easier penetration of the ions with less disturbance of the lattice because as the film quality is deteriorating, the values of n increase and values of k decrease as calculated before.

Tables (5.5b,c) show the change of the value of $N^*$ and $\tau$ and $\rho$ as in Table (5.5a), for single crystal (110),(100) respectively. The lower part of the table demonstrates the depth of damage produced by bombarding ions (argon) in both surfaces as calculated optically and electrically as explained in Section 5.6. The depth of damage in single crystal films is less than in polycrystalline. The change in $\rho$(optical) from ion energy 200 eV is 33% for $\langle 110 \rangle$ single crystal while the change in $\rho$ from electrical measurement is only 8.5%, and the corresponding values for $\langle 100 \rangle$ single crystal are 23% and 7.8% respectively. The difference in the optical and electrical measurements could be due to gas adsorption in the first few layers of the surface which did not affect the electrical measurements. This view is supported by microscan analysis of the bombarded samples which showed traces of argon in the gold film. Quantitative analysis was difficult because of the difficulty in preparing solid samples of the gas to be used as a standard. Comparison between the remaining values of $\delta\Delta$ and $\delta\psi$ after annealing are shown in Figs.(5.7a-f) in section 5.7.

| Energy eV | $N^* \times 10^{22}/cm^3$ | $\tau \times 10^{-16}$ sec. | $\rho_{opt.} \times 10^{-6}\ \Omega$ cm | $\rho \times 10^{-6}$ electrical $\Omega$ cm |
|---|---|---|---|---|
| 0 | 2.4446 | 9.246 | 5.237 | 3.13 |
| 70 | 2.3964 | 8.948 | | |
| 80 | 2.3200 | 8.480 | | |
| 90 | 2.3101 | 8.404 | | |
| 100 | 2.2952 | 8.229 | | |
| 110 | 2.2889 | 8.164 | | |
| 120 | 2.2746 | 8.033 | | |
| 130 | 2.2568 | 7.901 | | |
| 150 | 2.2442 | 7.779 | | |
| 200 | 2.2276 | 7.704 | 6.898 | |
| 250 | 2.2061 | 7.557 | 7.100 | |
| 300 | 2.1847 | 7.415 | 7.308 | |
| 350 | 2.1665 | 7.205 | 7.584 | |
| 400 | 2.1469 | 7.017 | 7.858 | |

Table (5.5a) Calculated values of electron density $N^*$ and relaxation time $\tau$ and resistivity $\rho$ from experimental measurements of the change of optical constants n's and k's of a bombarded polycrystalline golf film.

| Energy eV | $N^* \times 10^{22}/cm^3$ | $\tau \times 10^{-16}$ sec. | $\rho_{opt.} \times 10^{-6}$ $\Omega$ cm | $\rho \times 10^{-6}$ electrical $\Omega$ cm |
|---|---|---|---|---|
| 0 | 2.5088 | 9.524 | 4.89 | 2.9 |
| 200 | 2.47 | 9.35 | 5.197 | |
| 250 | 2.42 | 8.94 | 5.547 | |
| 300 | 2.37 | 8.54 | 5.929 | (1) |
| 350 | 2.32 | 8.12 | 6.371 | |
| 400 | 2.27 | 7.64 | 6.92 | |

| E ev | $d_{opt.}$ Å | $d_{min.}$ Å | $d_{max.}$ Å | |
|---|---|---|---|---|
| 200 | 15 | 7 | 15 | |
| 250 | 20 | 12 | 25 | |
| 300 | 27 | 16 | 36 | |
| 350 | 29 | 21 | 46 | (2) |
| 400 | 32 | 27 | 55 | |

single crystal <110>

Table (5.5b)

(1) Calculated values of electron density N* and relaxation time $\tau$ and resistivity $\rho$ from experimental measurements of the change of optical constants n's and k's of a bombarded single crystal (110) gold film.

(2) Damage layer thickness calculated from optical and electrical measurements for the same film.

| Energy eV | $N^*$ x $10^{22}/cm^3$ | $\tau$ x $10^{-6}$ sec. | $\rho_{opt}$ x $10^{-6}$ $\Omega$ cm | $\rho$ x $10^{-6}$ electrical cm |
|---|---|---|---|---|
| 0 | 2.5243 | 9.56 | 4.97 | 2.95 |
| 200 | 2.49 | 9.28 | 5.194 | |
| 250 | 2.46 | 9.01 | 5.415 | |
| 300 | 2.43 | 8.7 | 5.677 | |
| 350 | 2.39 | 8.36 | 6.006 | |
| 400 | 2.34 | 8.02 | 6.395 | |

(1)

| E ev | $d_{opt.}$ Å | $d_{min.}$ Å | $d_{max.}$ Å |
|---|---|---|---|
| 200 | 14 | 7 | 17 |
| 250 | 17 | 12 | 21 |
| 300 | 22 | 17 | 26 |
| 350 | 26 | 22 | 31 |
| 400 | 29 | 28 | 36 |

(2)

single crystal <100>

Table (5.5c)

(1) Calculated values of electron density $N^*$ and relaxation time $\tau$ and resistivity $\rho$ from experimental measurements of the change of optical constants n's and k's of a bombarded single crystal (100) gold film.

(2) Damage layer thickness calculated from optical and electrical measurements for the same film.

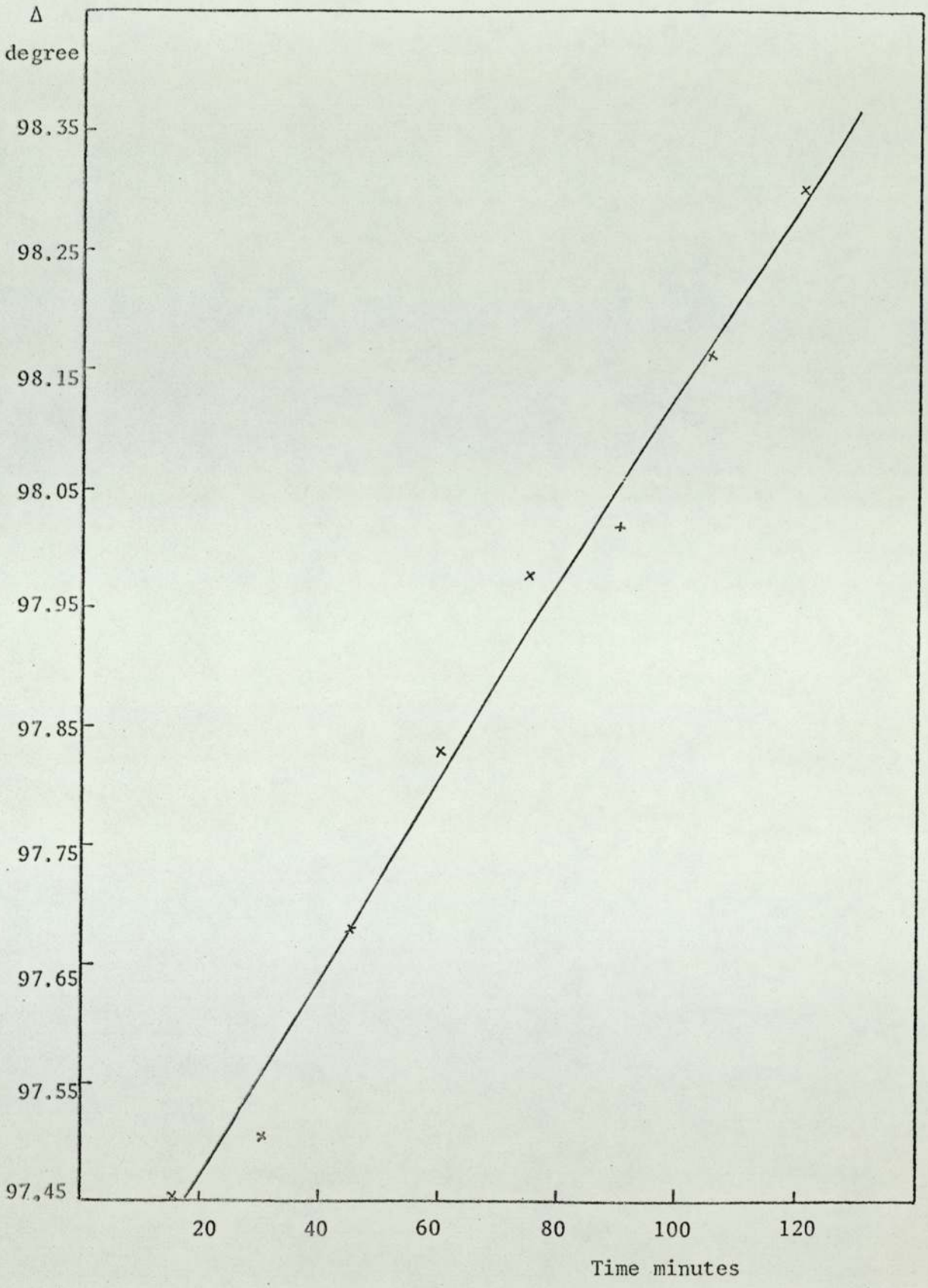


Fig.(5.4a) The change of Δ values with bombarding time for polycrystalline gold film and argon ions.

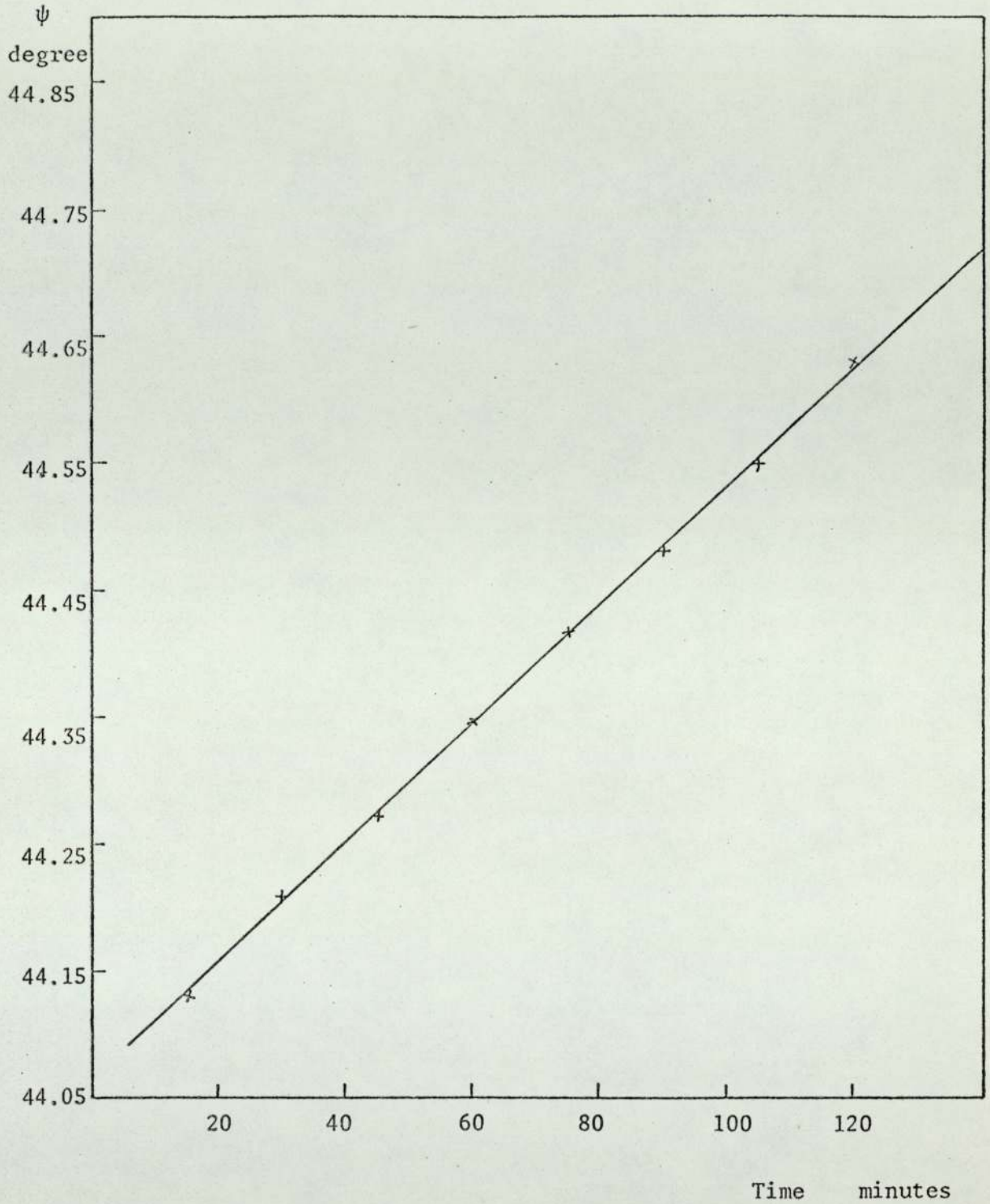


Fig.(5.4b) The change of ψ values with bombarding time for polycrystalline gold film and argon ions.

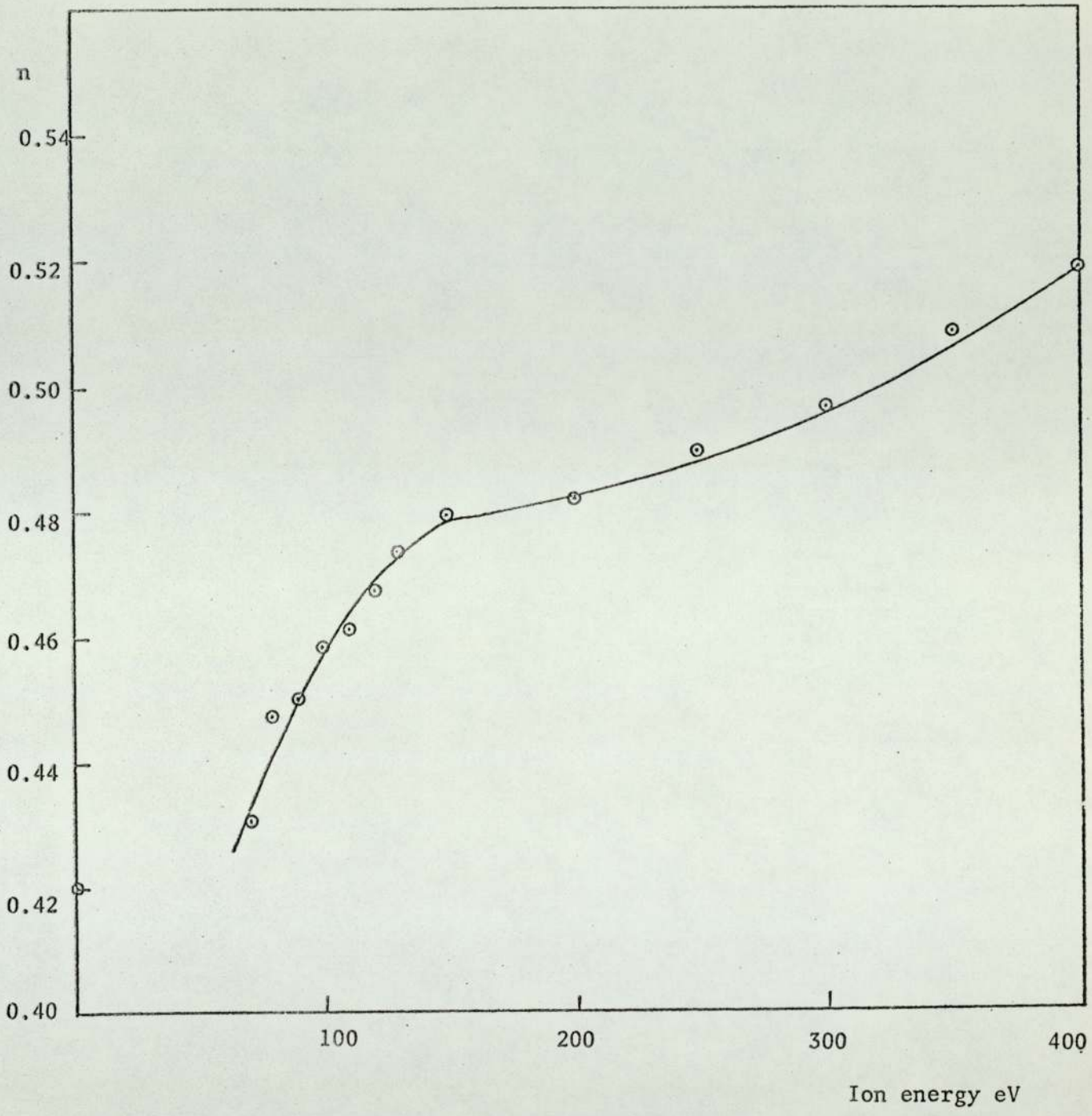


Fig.(5.5a) The change of n values for polycrystalline gold film as a function of ion energy (argon ions)

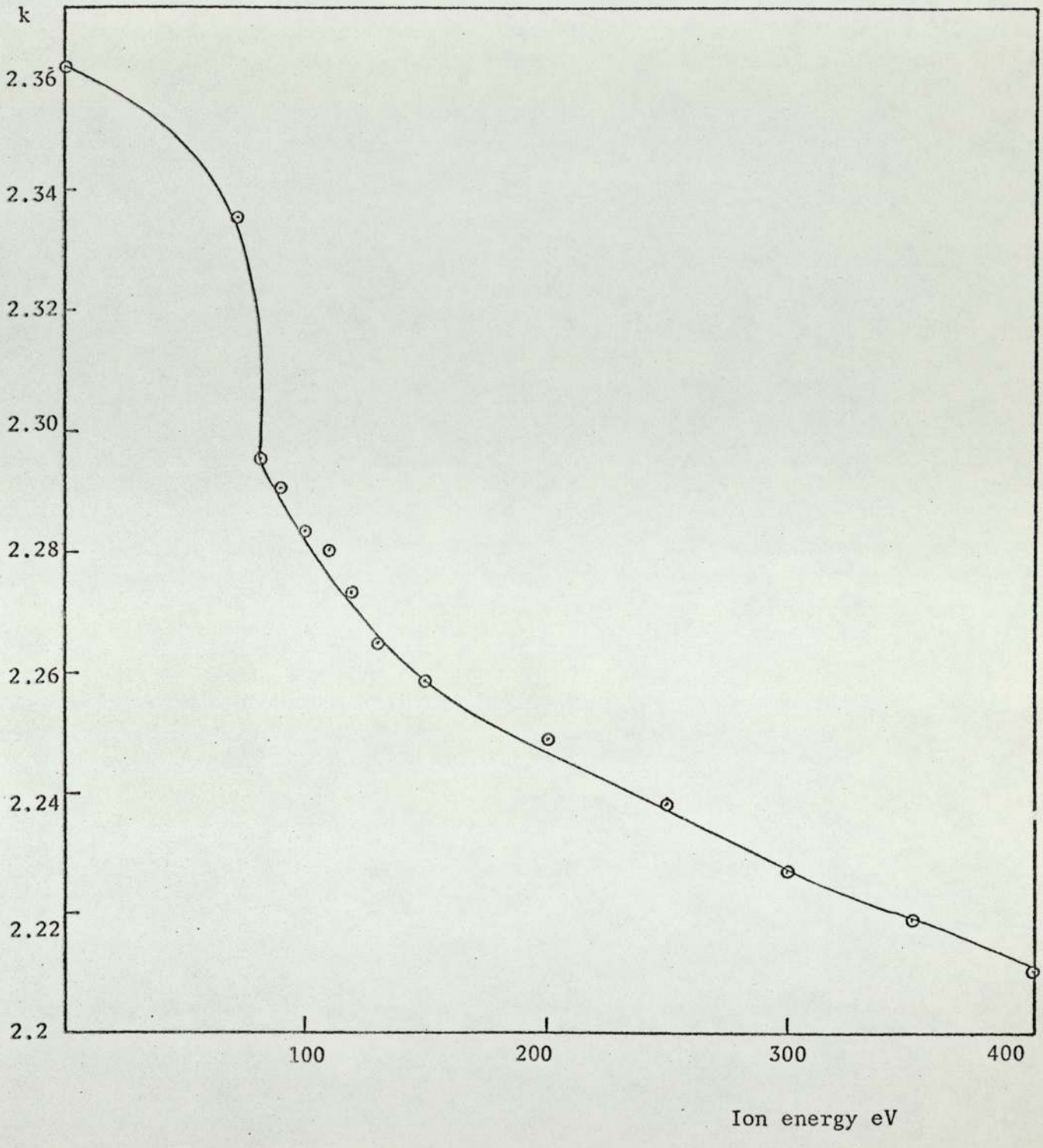


Fig.(5.5b) The change of k values for polycrystalline gold film as a function of ion energy (argon ions)

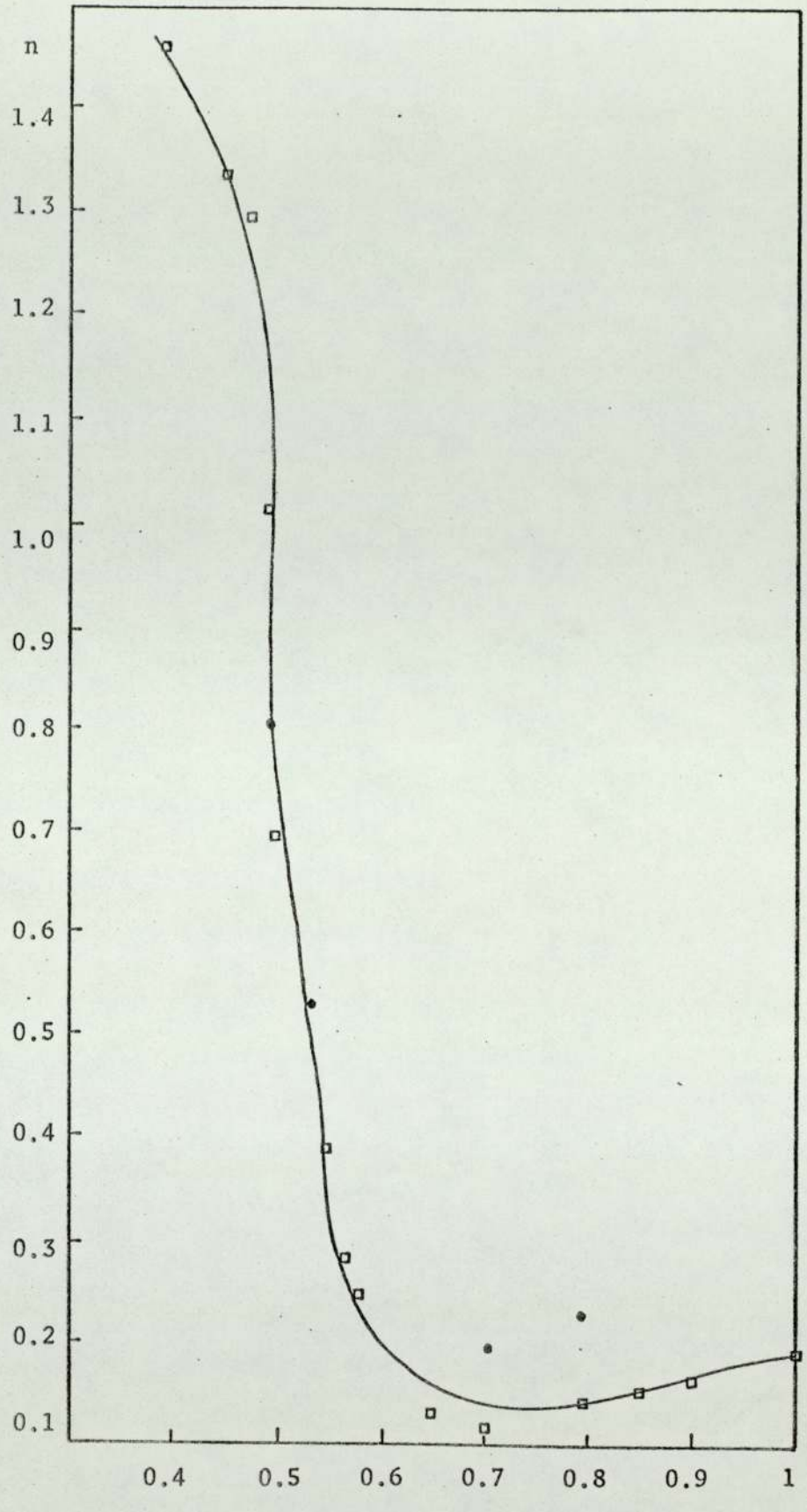


Fig.(5.5c) The change of the value of n as a function of wavelength of light used for a polycrystalline gold film at a bombarding argon ion energy of 400 eV.

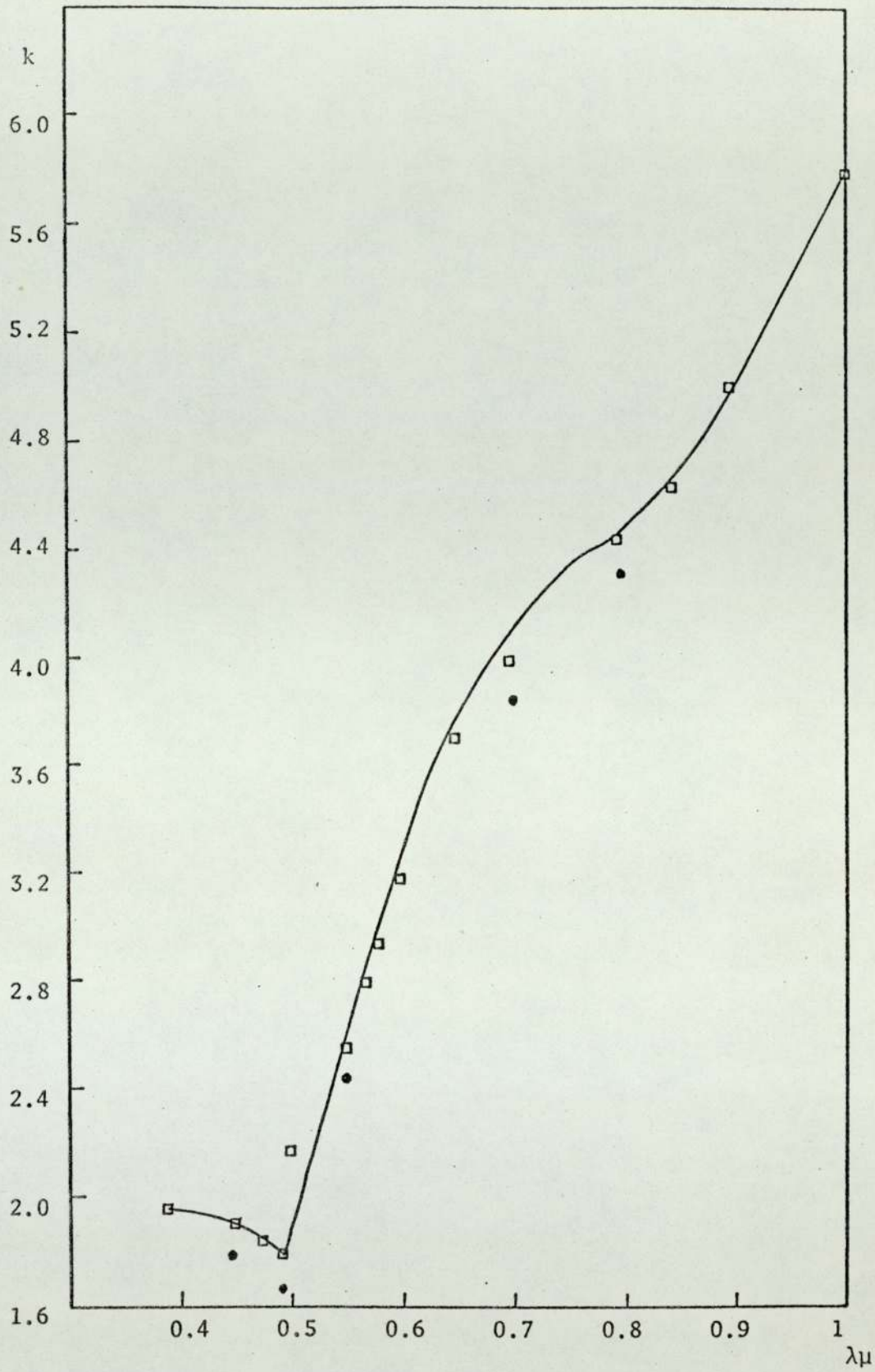


Fig. (5.5d) The change of the value of k as a function of wavelength of light used for a polycrystalline gold film at bombarding argon ion energy of 400 eV.

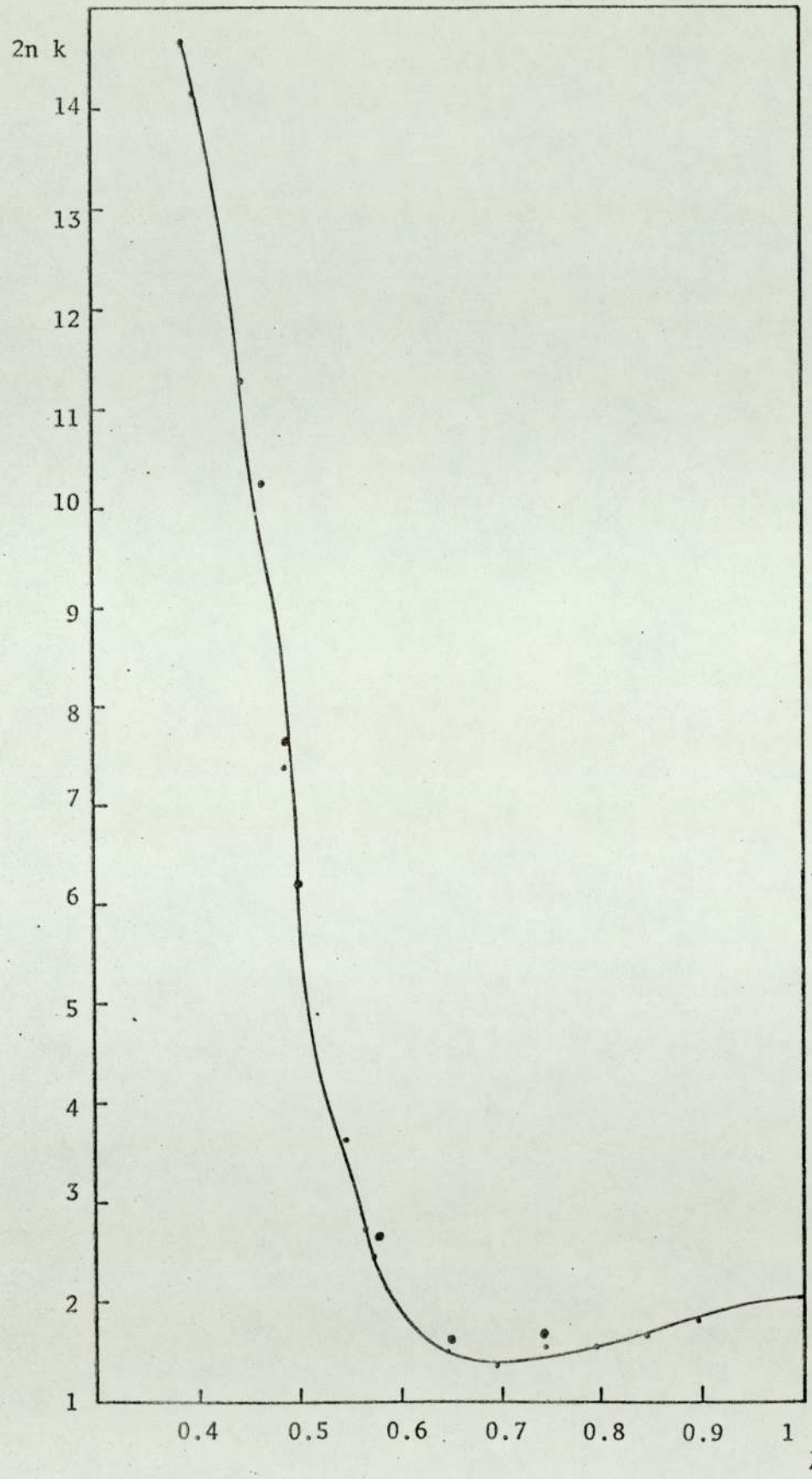


Fig. (5.5e) The change of the value of 2nk as a function of wavelength of light used for a polycrystalline gold film at bombarding argon ion energy of 400 eV.

## 5.6 Estimation of the damaged layer thickness from electrical measurements

There is no accepted method of calculation of damage layer thickness from electrical resistance measurements. The following two methods were used to give approximate values;

a) Assuming that the damaged layer had a very high resistance with respect to the whole film, a rough estimation of the damaged layer thickness could be determined from the percentage change of the resistance upon bombardment. Fig.(5.6a) shows the percentage increase of the resistance R with applied ion energy. An ion of energy 400 eV causes the resistance of the film of thickness 310 $\mathring{A}$ irradiated and held at room temperature to increase by 9.58%. On this basis the minimum damaged layer thickness is of the order of 30 $\mathring{A}$. This value is in good agreement with the optical measurements made on the same film (38 $\mathring{A}$).

(b) Assuming the resistivity of the film did not change, the increase in the resistance of the bombarded film was as if the film had been thinned by irradiation. The effective thickness of the irradiated film of thickness 310 $\mathring{A}$ was found to be 265 $\mathring{A}$, for ions of energies 400 eV, using the relation

$$R = \rho \frac{l}{A}$$

where

$$A = w\, t$$

and $\rho$ is the resistivity of the freshly evaporated golf film, l its length, A the cross sectional area, w is the width and t the thickness of the film. This indicates the upper limit of the damage produced by irradiation to be $\sim$ 45 $\mathring{A}$.

In view of the assumptions which have been made the fact that the optically measured thickness lies between these extremes, as estimated electrically, is considered to be satisfactory. Fig.(5.6b) shows

comparison between damaged layer thickness as estimated from optical and electrical measurements and that calculated using the method and programme due to Armstrong and Chandler (1973). They considered the stopping power of the material and calculated the range of ions as a function of energy.

The temperature coefficient of resistance of the unbombarded film ($4.2 \times 10^{-3}/^{o}C$) is very close to the value of perfect bulk gold material ($4.3 \times 10^{-3}/^{o}C$) while that of the bombarded film is decreased to $4.04 \times 10^{-3}/^{o}C$ which indicates a deterioration of the film quality.

At ion energies less than the threshold energy for each gas, no change of the electrical resistance was observed. These results combined with the optical measurements indicate that at an energy less than the threshold energy, the change observed in the optical measurements is due to gas contamination of the film surface which did not affect the resistance.

## 5.7 Defect annealing and migration and desorption of gas atoms from the target on heating

After point defects have been created, they will tend to migrate and cluster or anneal out at all temperatures except very low temperatures. Typical activation energies for migration in crystals are 0.5 eV for vacancies and 0.2 eV for interstitials. Within a few atomic layers of the surface, defects interact with an effective "image" defect via elastic strain and thereby move to the surface. Within the bulk material, both types of defects aggregate to form discs oriented along a crystal plane.

After each bombardment, the film has been heated to 200°C for one hour and left to cool down for eight hours, the values of $\Psi$ and $\Delta$ did not return to the initial values measured before bombardment. The residual values of $\Psi$ and $\Delta$, which may be considered as a measure of the damage, are found to depend on the surface structure, as shown in Figs.(5.7a-f) for polycrystalline, <100> and <110> single crystal respectively. For polycrystalline films, approximately 50% of the value of $\Delta$ was found to be recovered, in agreement with the electrical measurements shown in Fig.(5.3c).

It is clear that for single crystal film the structure looked more open, and easier movement of the gas atoms is possible.

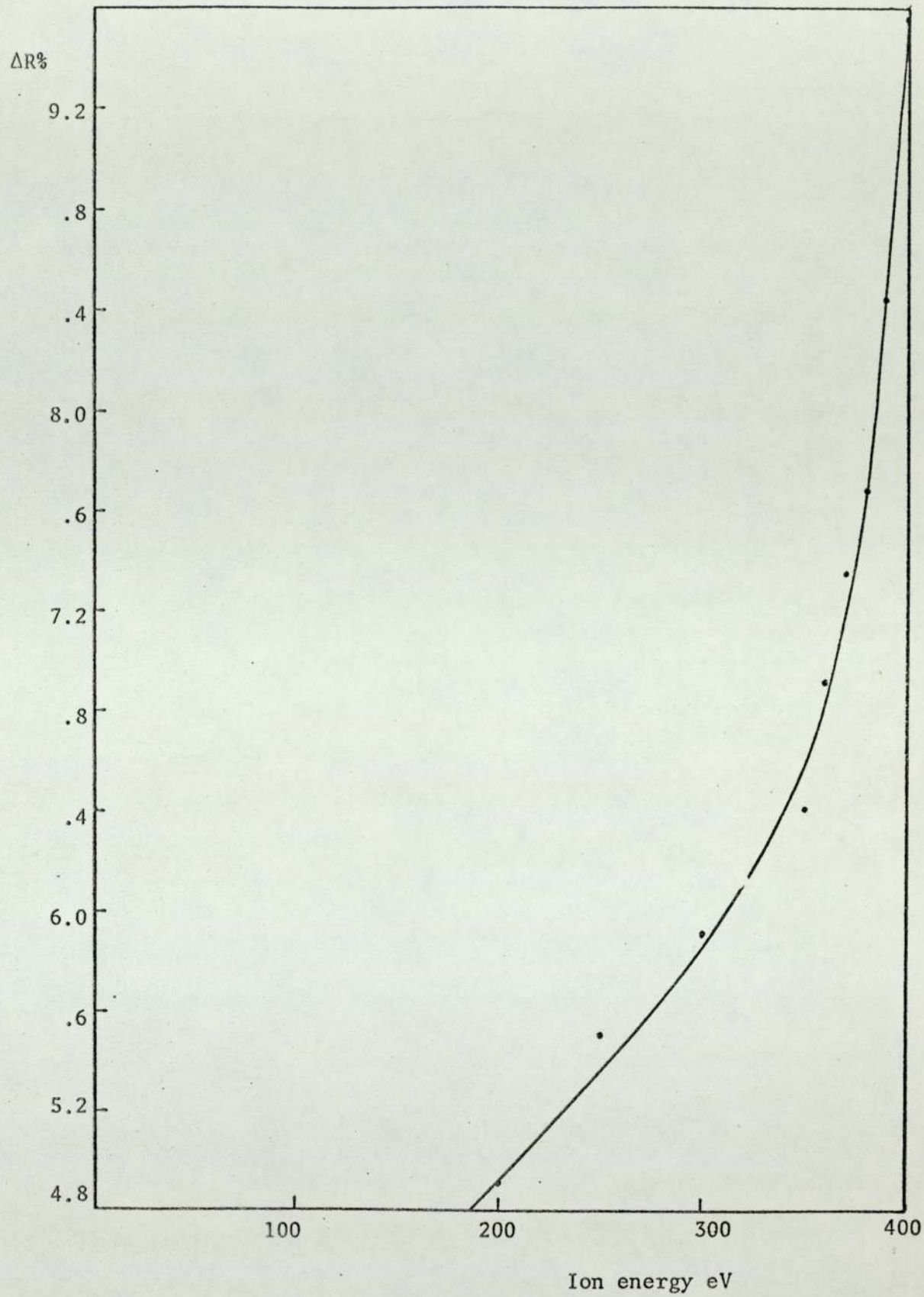


Fig.(5.6a) Percentage increase of the resistance R with increasing bombarding ion energy for argon ions on polycrystalline gold film.

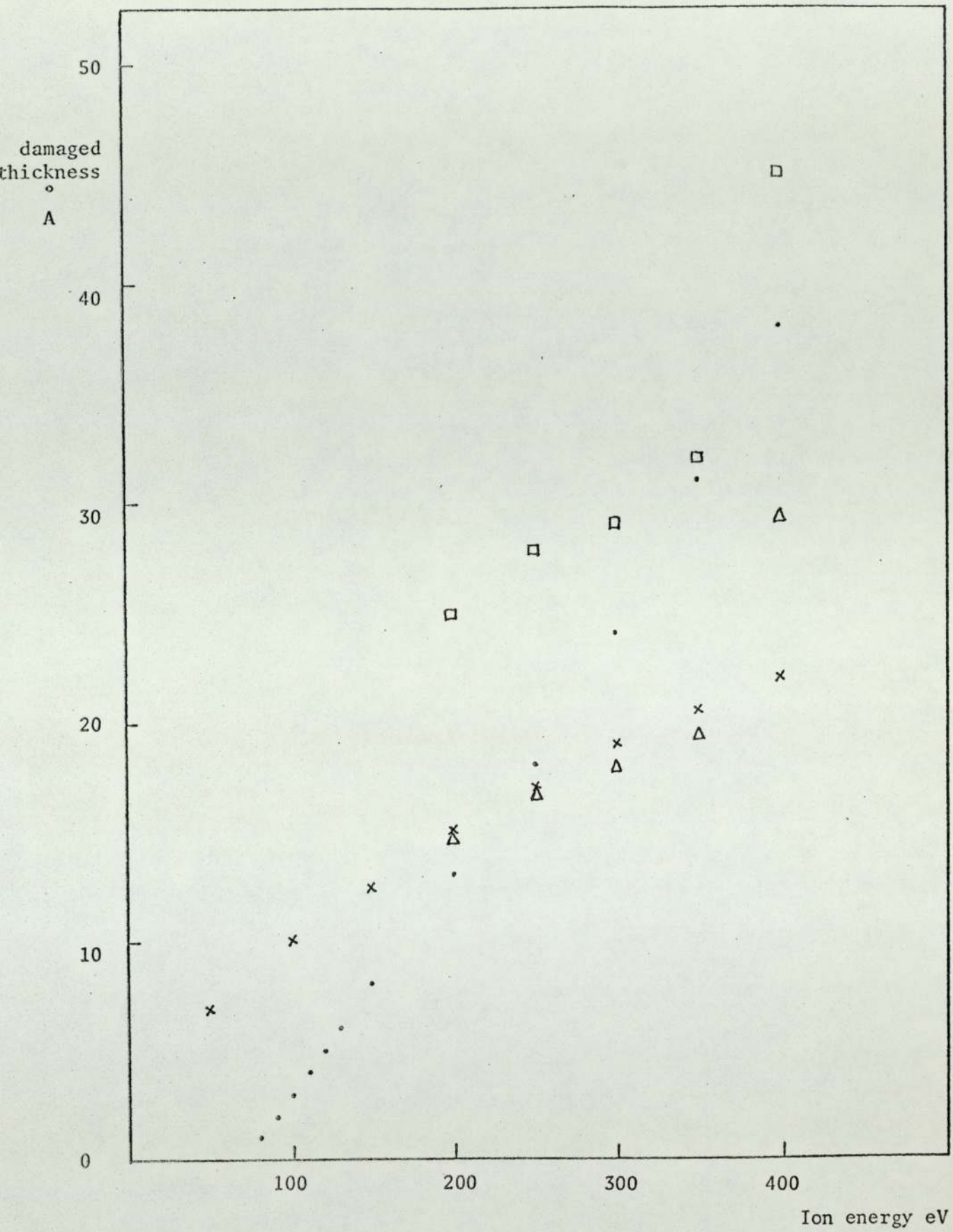


Fig. (5.6b) The damaged layer thickness as a function of bombarding ion energy for argon ions on polycrystalline gold film.

• Optically measured

Δ lower limit of electrical measurement.

▫ Upper limit of electrical

x theoretically calculated

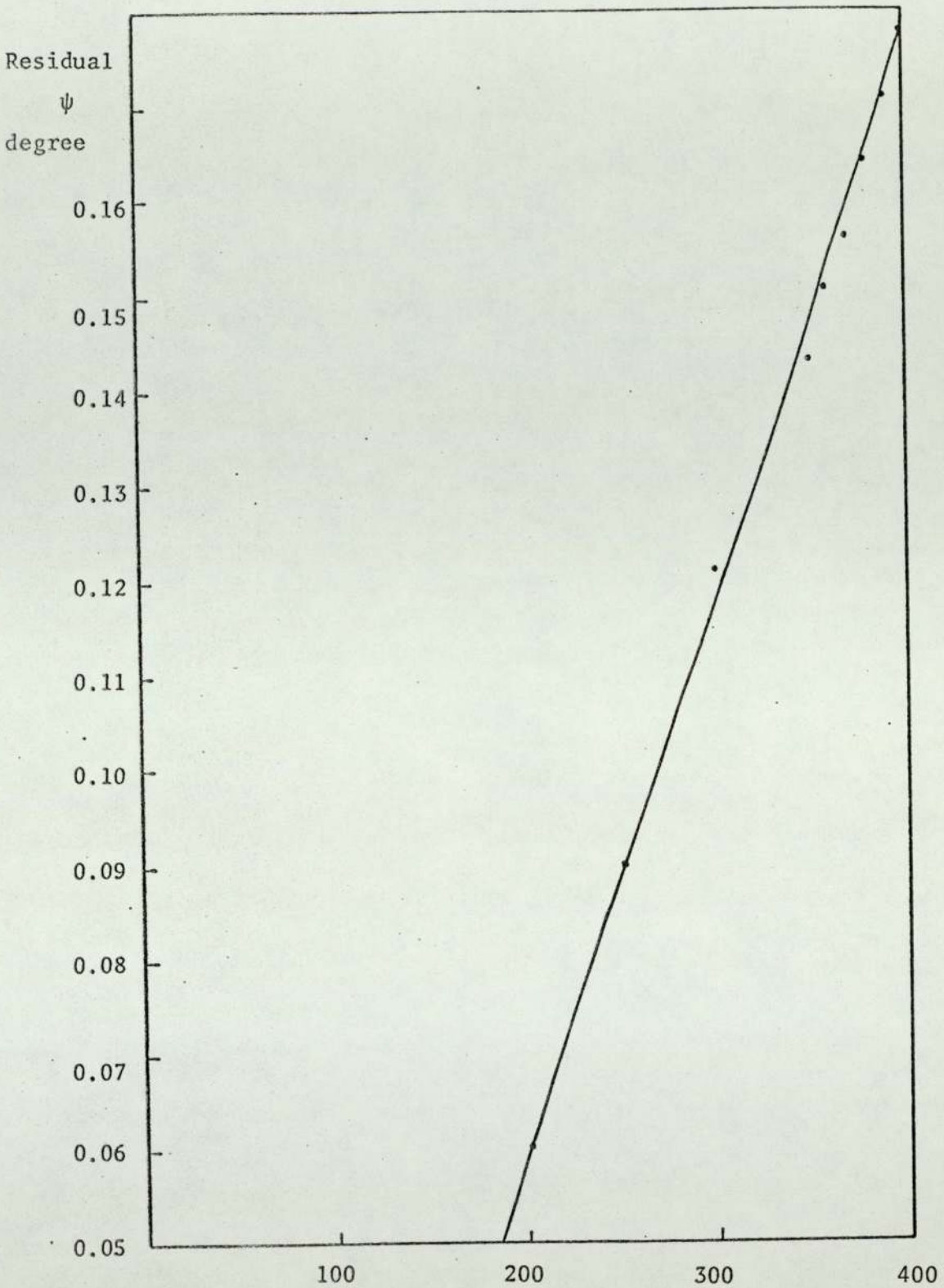


Fig.(5.7a)

The value of $\delta\psi$ remaining after annealing following argon ion bombardment on polycrystalline gold film.

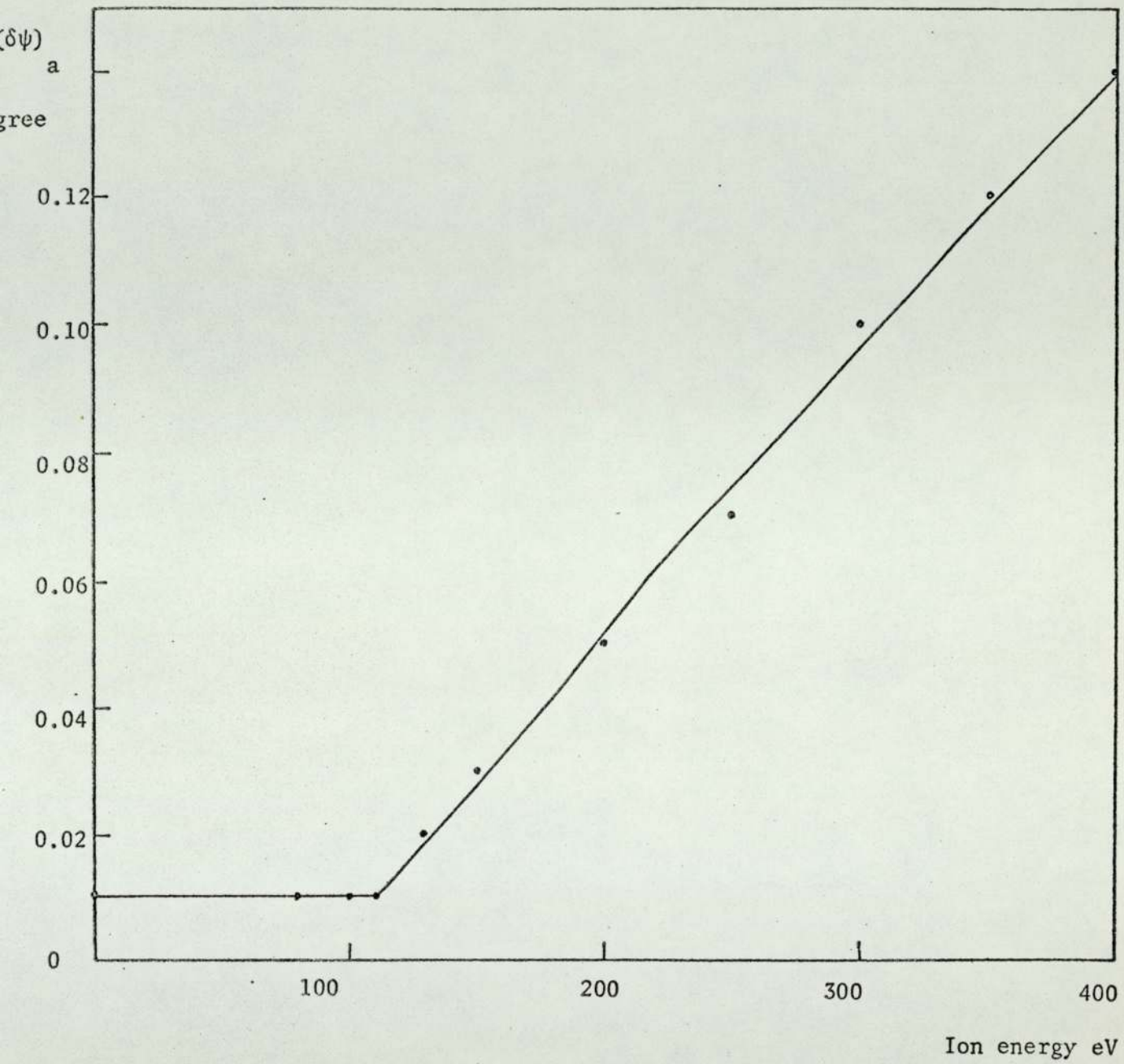


Fig. (5.7b) The values of δψ remaining after annealing following argon ion bombardment on < 100 > single crystal gold film.

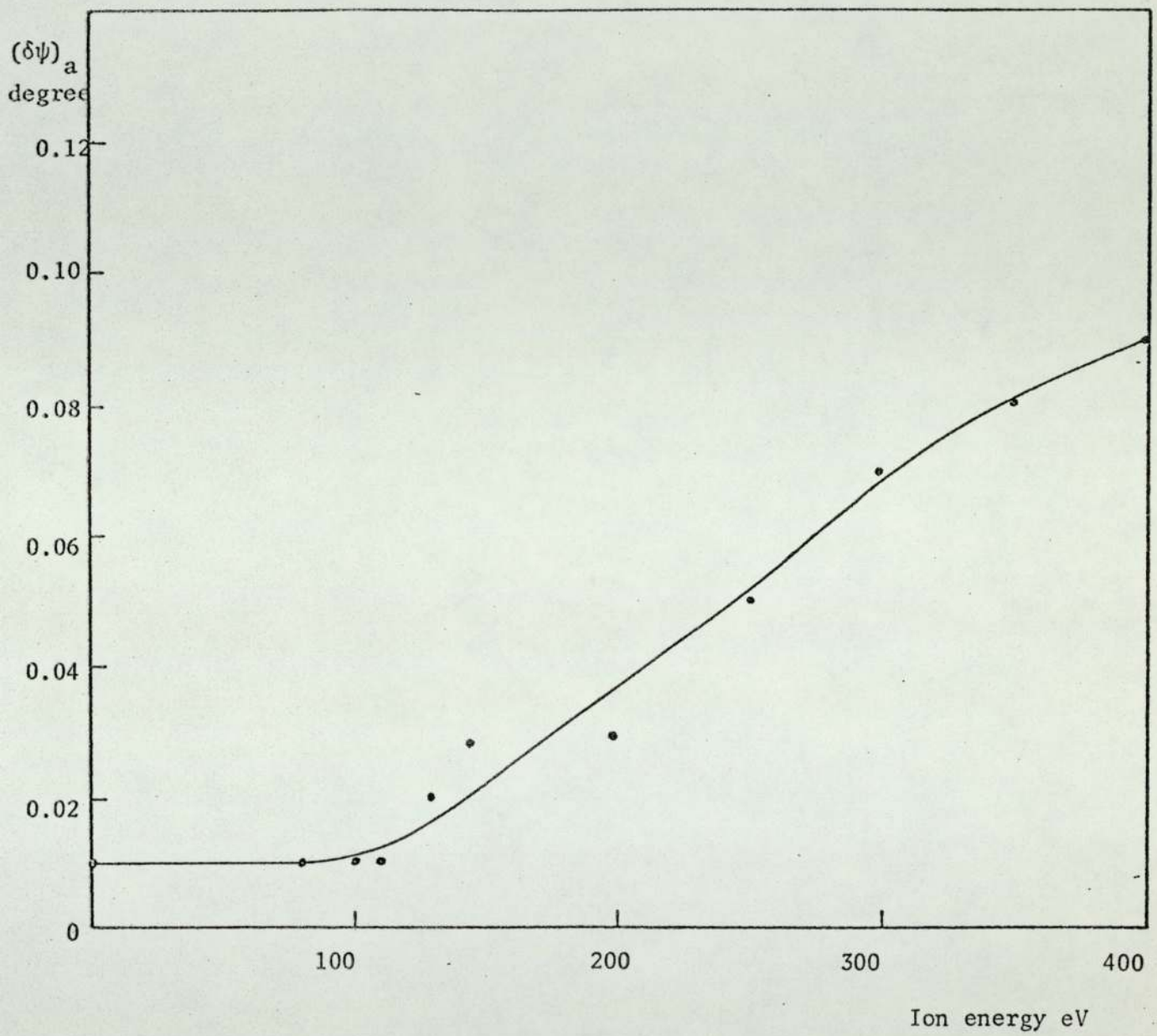


Fig. (5.7c) The value of δψ remaining after annealing following argon ion bombardment on < 110 > single crystal gold film.

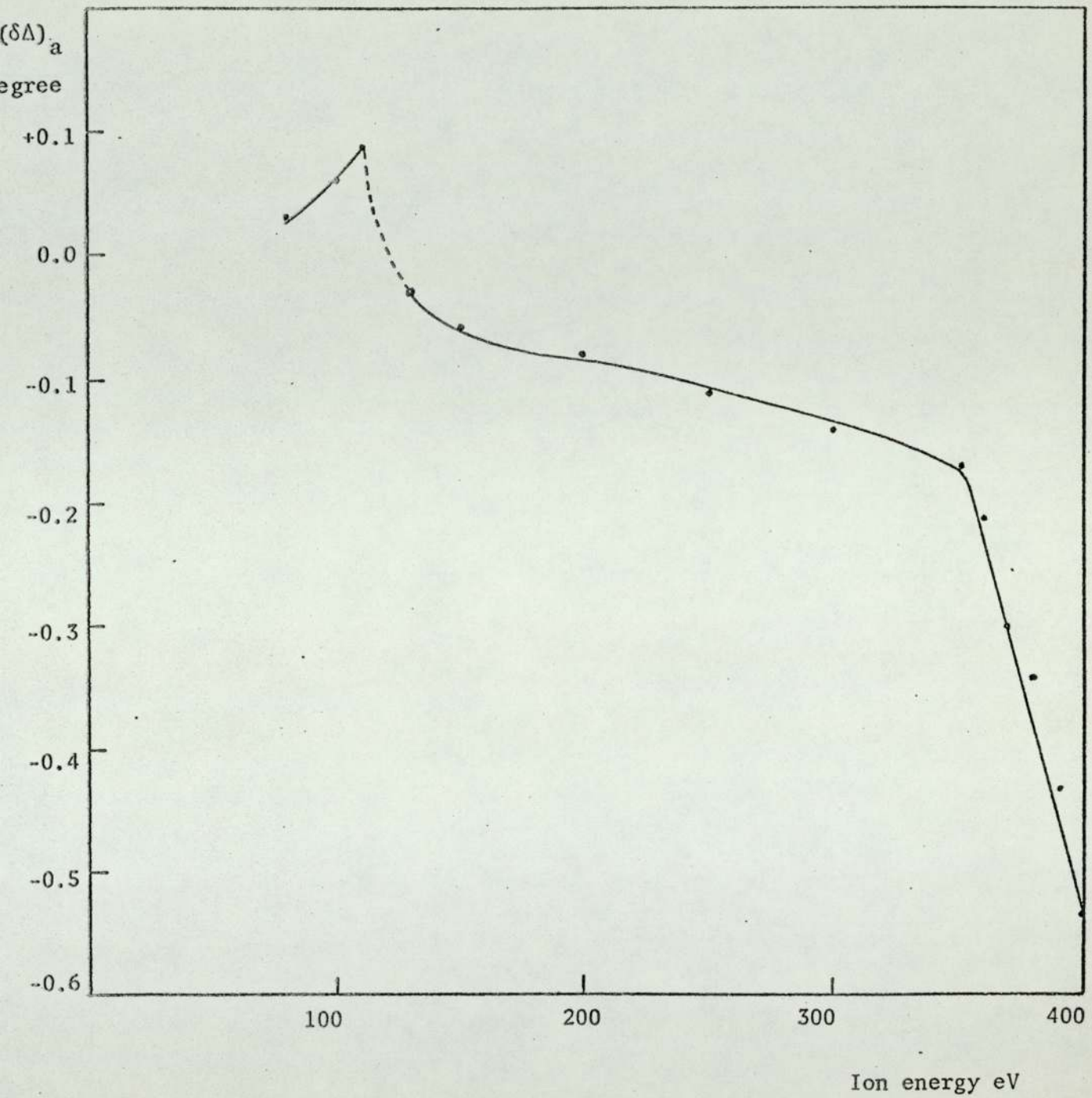


Fig. (5.7d) The value of $\delta\Delta$ remaining after annealing following argon ion bombardment on polycrystalline gold film.

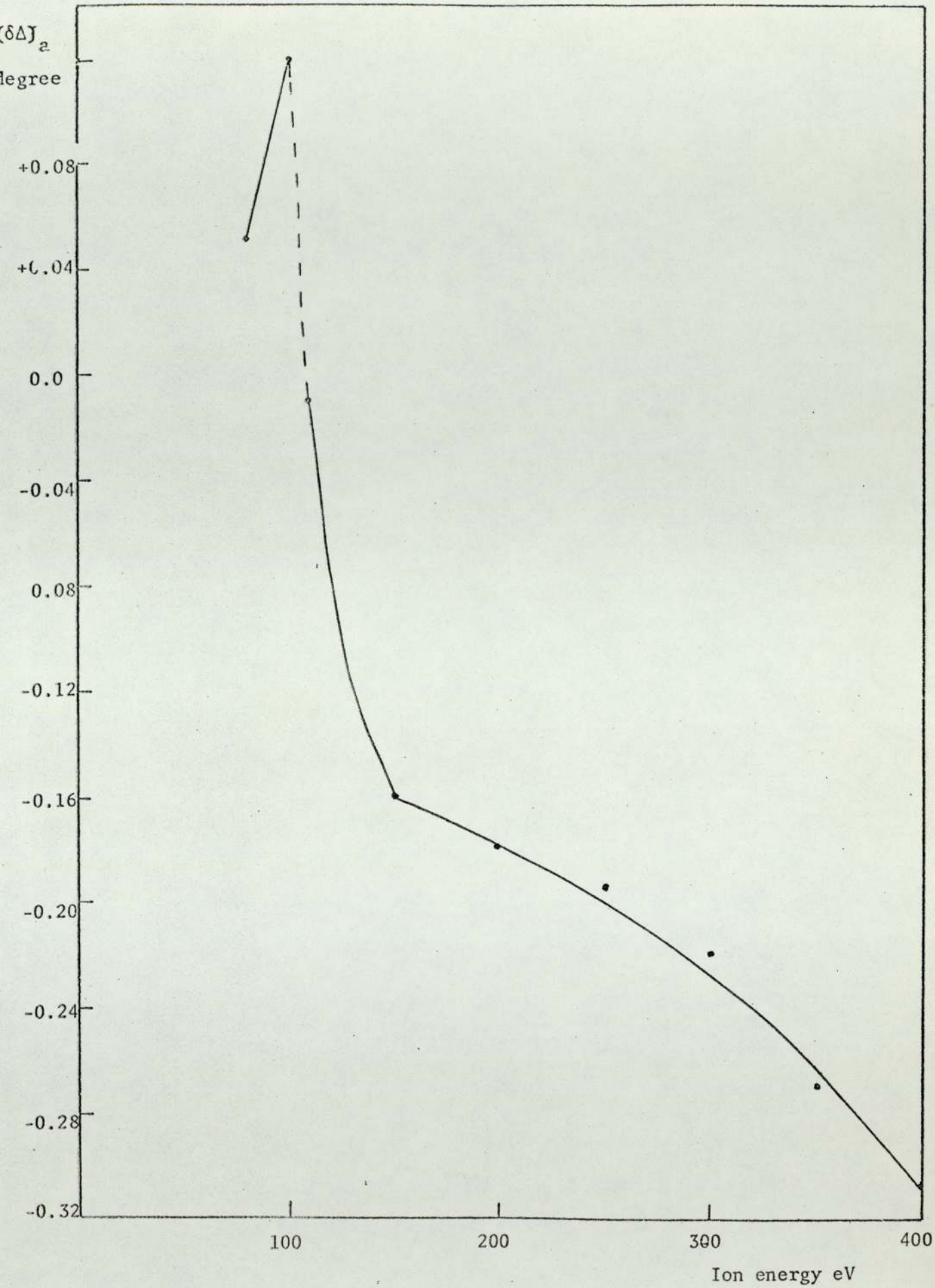


Fig.(5.7e) The value of $\delta\Delta$ remaining after annealing following argon ion bombardment on < 100 > single crystal gold film.

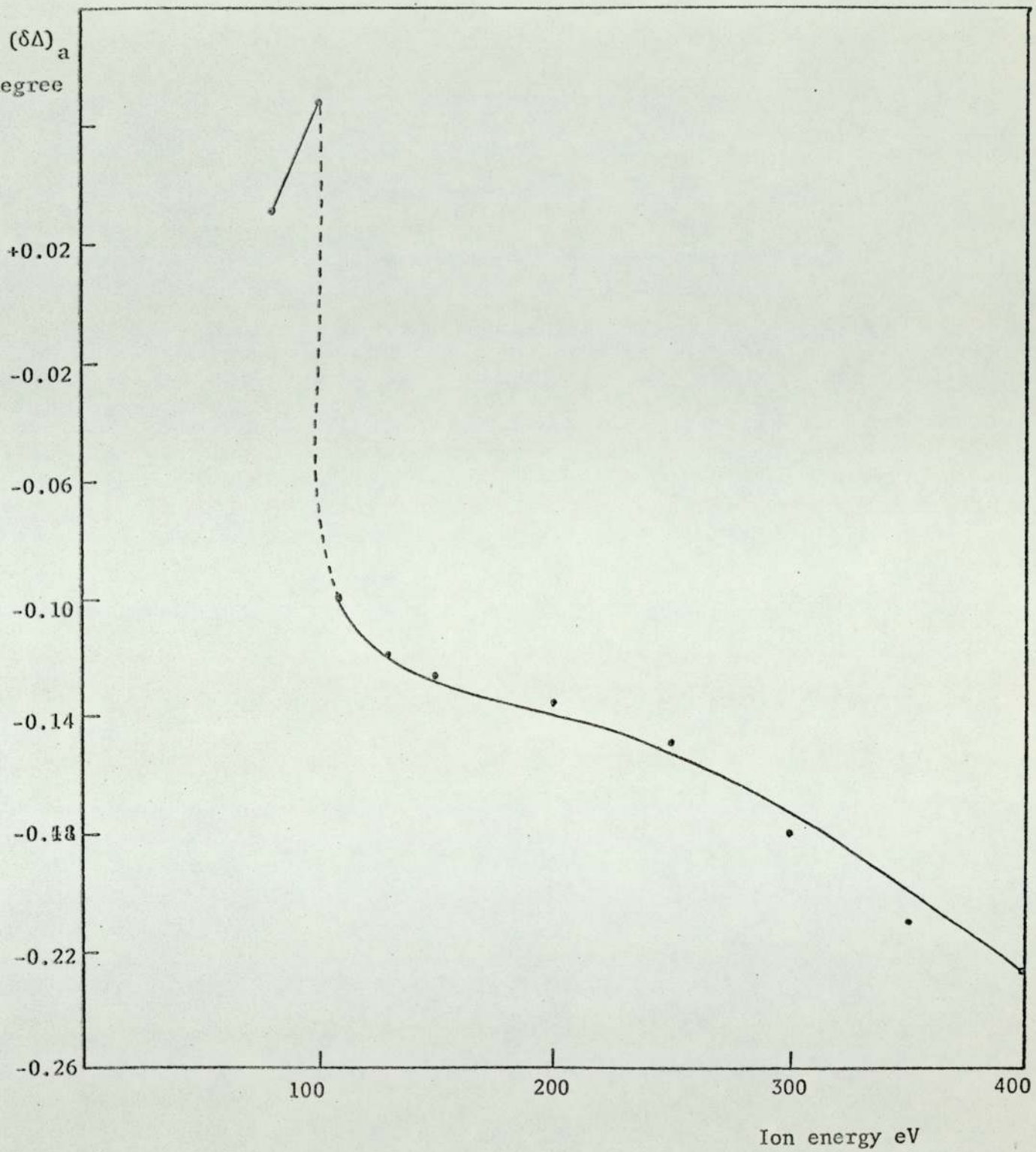


Fig. (5.7f) The value of δΔ remaining after annealing following argon ion bombardment on < 110 > single crystal gold film.

## 5.8 Distribution of defect production

The average number of Frenkel pairs $N_{fp}$ produced by each incident ion of energy E can be estimated, using a Kinchin and Pease model and neglecting electronic losses (Kinchin 1955).

$$N_{fp} = E/2E_d \qquad 5.8a$$

The ordered nature of the lattice can result in the long-range transfer of energy and matter and so influence the distribution of atomic displacements. As mentioned in chapter 3, this effect is better understood by considering focusing collisions, which are most important at low ion energies (usually $<$ 1 KeV). The atoms were considered as hard spheres of radii (R) related to the distance of closest approach. Since R is energy dependent, it was found that R must be matched to a more realistic interatomic potential such as the Born-Mayer potential.

$$V(r) = A \exp(-r/B) \qquad 5.8b$$

where

$$R(E) = \tfrac{1}{2}B \ln (2A/E) \qquad 5.8c$$

On the basis of focusing collision, if D is the separation between two atoms then:

$D > 4R$ for $f > 1$ and $|\theta_1| < |\theta_2|$

$D < 4R$ for $f < 1$ and $|\theta_1| > |\theta_2|$

So that if $D > 4R$ and $f > 1$, $\theta_n$ increases until an atom no longer collides with its neighbour in the row. If, however, $D < 4R$ and $f < 1$, $\theta_n$ decreases to zero and the momentum transfer is then perfectly efficient.

Table (5.8a) shows the calculated values of $N_{fp}$ and R(E) where values of A and B in equation 5.8c are taken from the work of Abrahamson (1969) and assuming $E_d$ to be 25 eV.

The number of Frenkel pairs produced, increases as the ion energy increases which will accumulate the damage produced by incident ions. Also, for single crystal gold film, the value of 4R is always higher than the separation between the atoms in the plane ($D_{100}$ = 2.03 Å, $D_{110}$ = 1.44 Å) which means the ions could penetrate deeper in the lattice and may cause less damage and explain the fact that the change of $\delta\psi$ and $\delta\Delta$ for single crystal gold film is less than that for polycrystalline film. The diameter of the neon and argon atoms being 2.3 Å and 2.8 Å respectively, also indicates that the damage produced by an argon ion will be higher than that produced by neon ions. This is confirmed by the calculations of the average energy $\bar{T}$ and the maximum energy $T_m$, transferred to target atoms, as shown in Table (5.8b)

Table 5.8a

| E ev | $N_{fp}$ / ion | R(E) Å |
|---|---|---|
| 70 | 1.4 | 1.06 |
| 80 | 1.6 | 1.04 |
| 90 | 1.8 | 1.03 |
| 100 | 2 | 1.01 |
| 110 | 2.2 | 0.998 |
| 130 | 2.6 | 0.97 |
| 150 | 3 | 0.95 |
| 200 | 4 | 0.91 |
| 250 | 5 | 0.58 |
| 300 | 6 | 0.86 |
| 350 | 7 | 0.83 |
| 360 | 7.2 | 0.83 |
| 370 | 7.4 | 0.83 |
| 380 | 7.6 | 0.82 |
| 390 | 7.8 | 0.82 |
| 400 | 8 | 0.81 |

Table 5.8a. Calculated values of Frenkel pairs $N_{fp}$ produced by each incident ion using Kinchin and Pease model and calculated value of R(E).

Table 5.8b

| E eV | $\bar{T}$ | | $T_m$ | |
|---|---|---|---|---|
| | Neon | Argon | Neon | Argon |
| 70 | - | 31.06 | 23.66 | 39.25 |
| 80 | 23.43 | 33.02 | 26.97 | 44.86 |
| 90 | 27.08 | 34.61 | 30.35 | 50.47 |
| 100 | 28.36 | 36.43 | 33.72 | 56.07 |
| 110 | 30.23 | 37.86 | 37.09 | 61.68 |
| 120 | 31.19 | 39.39 | 40.46 | 67.29 |
| 130 | 32.67 | 40.71 | 43.83 | 72.9 |
| 150 | 34.83 | 43.16 | 50.58 | 84.11 |
| 200 | 39.33 | 48.28 | 67.43 | 112.15 |
| 250 | 43.2 | 52.46 | 84.29 | 140.19 |
| 300 | 48.24 | 55.98 | 101.15 | 168.22 |
| 350 | 49.23 | 59.03 | 118.01 | 196.26 |
| 360 | 49.75 | 59.6 | 121.38 | 201.87 |
| 370 | 50.26 | 60.18 | 124.75 | 207.48 |
| 380 | 50.76 | 60.69 | 128.12 | 213.08 |
| 390 | 51.25 | 61.22 | 131.5 | 218.69 |
| 400 | 51.72 | 61.73 | 134.87 | 224.3 |

Table 5.8b. Calculated values of the average $\bar{T}$ and the maximum $T_m$ value of energy transferred to target atoms during ion bombardment.

## 5.9 Discussion

The changes in the physical properties of a metal resulting from irradiation with charged particles are difficult to interpret because the types and numbers of imperfections produced by the bombardment are not accurately known. Interstitial atoms and vacant lattice sites are expected to be the predominant types produced (Seitz 1949) and this view is supported by the observed annealing properties of the damage (Overhauser 1953). In order to understand or explain the reason for the change of the physical properties of the bombarded samples, we have to visualize what is happening when an ion impinges on the surface. By following a collision cascade, there appears to be a mechanism which focuses momentum along the simple rows. The dominant features of the cascade are focused replacement sequences where replacements are involved, and focused energy packets where only energy is transported. As mentioned in chapter 3, the displacement energy $E_d^{hkl}$ may be defined as the minimum energy required to produce a stable interstitial-vacancy pair in the <hkl> direction. For a particular direction, the number of displaced atoms will rise sharply from zero to one at $E_d^{hkl}$. In the present work $E_d$ for polycrystalline film was found to be 130 eV and $E_d^{110}$, $E_d^{100}$ is 110 eV as shown from the results in sections 5.2.1, 5.2.2, 5.2.3 and summarized in Table (5.2.3a). The initial change of the values of $\Delta$ as the ion energy increased shows contamination of the surface layer of the order of 6Å thick as computed up to energy $E_d$. Then the values of $\delta\Delta$ change sign as the bombarding energy starts to produce damage of the surface. This bombardment produces two monolayers on the surface initially. The change observed is identical with adsorbed gas when the gold substrate is held at 77°K; namely the addition of two monolayers as mentioned in chapter 4. It therefore appears that two monolayers is the limit of adsorption at $5 \times 10^{-5}$ torr.

The simplest type of focused collision sequence propagates along the closest packed rows of atoms such as <110> in the f.c.c. lattice. Focused collision sequences arise because the lattice is then able to impose more rigid conditions on the possible modes of momentum transfer, for when penetration of the channels in the lattice becomes impossible, a struck atom receives its momentum from one of its near neighbours. A simple focused collision sequence cannot travel indefinitely. There are some important ways in which they can lose energy:

a) Energy loss directly to the rings of atoms surrounding the focusing axes, this effect may be enhanced by thermal vibration of the lattice.

b) Scattering by structural defects in the crystal for instance dislocation lines.

c) Scattering of energy out of the line by misalignment of atoms caused by lattice vibration.

If we consider mechanism (a) as seen from Fig. (5.9a) B is one of the four atoms which lie in a {110} plane and form a ring around the <110> line, when $A_n$ reaches C with $CA_{n+1} = 2R$ and $CB = c$, the hard sphere collision occurs but the potential energy gained by $A_n$ in moving to C is lost to the sequence. Eventually this energy appears as thermal energy in the lattice when the four B atoms and $A_n$ relax and then oscillate about equilibrium positions.

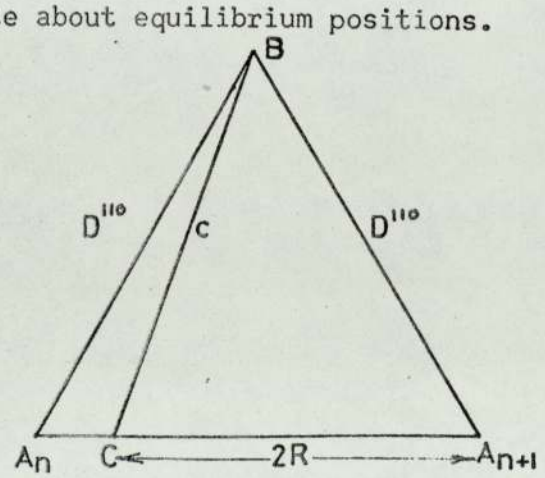


Fig.(5.9a) Energy loss in a static lattice.

In mechanism (b) the collision sequence loses energy by passing through a defective region of the lattice. For instance, in the neighbourhood of a dislocation line, the atomic rows are distorted as shown in Fig. (5.9b). If a row actually passes through the stacking fault region, they are sheared discontinuously. A collision sequence passing along one of these rows which endsabruptly will have some of its energy refocused into new sequences starting from the opposite side of the fault and a large proportion will be lost. If enough energy is available, an atom may be displayed.

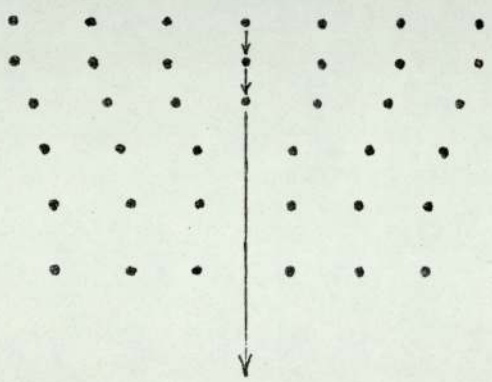

Fig. (5.9b). Interaction of a focused collision sequence with a dislocation.

On the other hand, measurements of the probability of entrapment of energetic inert gas ionsincident on polycrystalline material has been discussed by several workers (Brown and Davies 1963, Kornelsen 1964, Corkhill and Carter 1965, Close and Yarwood 1966, 1967, and Erents and Carter 1967). Significant quantitative differences between the data of various investigators have been found although all measurements have generally exhibited qualitatively similar behaviour. The study of Kornelsen and Sinha (1966) throws light on a possible

explanation for the discrepancies. They found that the trapping probability of 100 eV K+ ions incident upon single crystal tungsten specimens varies from $2 \times 10^{-2}$ to $5 \times 10^{-5}$ when irradiated parallel to the <110> and <100> directions respectively. For many years it was assumed that ion penetration into crystalline material would not differ substantially from that in amorphous media, despite the fact that as early as 1912 Stark had predicted that interatomic fields would play a major part in determining the motion of charged particles through crystals. He described explicitly an experiment for observing channelled transmitted ions photographically. The present ellipsometric measurements suggest three points of interpretation based on the results of sections 5.2.1, 5.2.2 and 5.2.3:

1. At energies lower than $E_d$ the change in the value of $\Delta$ is in the direction characteristic of contamination of the bombarded surface by the incident ions.
2. For energies higher than $E_d$, the values of $\Delta$ show the formation of a disturbed layer which increases in thickness with increasing bombarding ion energy. This is clear from the combined electrical and optical measurements.
3. The amount of damage produced depends on the ease of penetration of the incident ion which in turn depends on the arrangement (structure) of the bombarded surface. The polycrystalline films suffer the highest disturbances as it is considered to be composed of several different crystallites randomly oriented. This result agrees with Kornelsen and Sinha's observations.

The effect produced by argon is found to be higher than that due to neon, due to the fact that the atomic weight of argon is nearly twice as much as that for neon (39.946 and 20.183 respectively) also as shown from table 5.8b, the amount of energy transferred to the target

atom is much higher for argon than that for neon, together with a smaller diameter for neon atom than argon (argon = 2.8 Å, neon = 2.3 Å).

Irradiation at high temperature may suggest the type of defects present. When irradiation is at high enough temperature for one defect to be mobile, for example, interstitials, the concentration of trapped interstitials will increase as the irradiation proceeds and the number of free trapping sites will decrease. The presence of unsaturable traps will not produce saturation in the defect concentration but simply a curvature of the damage curve because as the concentration of vacancies increases, there is an increasing tendency for interstitials to annihilate vacancies rather than to become trapped. Results of the present optical and electrical measurements agree with this model as the change of $\delta\Psi$ and $\delta\Delta$ and the electrical resistance upon irradiation do not follow a linear relationship with bombarding ion energy.

A more realistic model must take account of other sinks for interstitials. If the interstitials can condense on the network of dislocations causing them to climb, to a first approximation the number of such trapping sites remains constant. Thus the unsaturable traps may be regarded as unaffected by the concentration of interstitials that have passed to them. Alternatively the escape of interstitials to crystal boundaries can be represented by a constant concentration of sinks which are again unsaturable. Mobile interstitials are produced in gold at 50°C as observed by Merkle (1966). The interstitials on the unsaturable traps can probably be assumed to contribute very little to electrical resistivity. The increase in resistance can be analysed into two terms, one of which saturates as the saturable traps become filled, the

other increasing steadily. If $a_{sti}$ is considered as the resistivity increase due to unit concentration of interstitials on saturable traps and $a_v$ as the corresponsing resistivity for vacancies, then the total resistivity may be written as:

$$\Delta\rho = (a_{sti} + a_v)C_{sti} + a_v C_{uti}$$

where $C_{sti}$ and $C_{uti}$ are the concentrations of saturable and unsaturable trapped interstitials respectively. The optical and electrical measurements are consistent with this explanation since the change of both $\Psi$ and $\Delta$ and consequently the values of n and k for the surface, and electrical resistance follow a non-linear relationship with the ion energy.

X-rays diffraction patterns show that a polycrystalline film developed preferred orientation in the 100 direction after argon ion bombbardment, ions of energy 400 eV resulting in a change in the intensities of the diffraction pattern lines given by the film as shown in Table(5.9a).

| Line | Intensity | |
|---|---|---|
| | Before | After |
| 111 | 5 | 5 |
| 200 | 83 | 130 |
| 220 | 65 | 58 |
| 311 | 21 | 18 |

Table (5.9a) The integrated intensity of diffraction lines from a polycrystalline film before and after ion bombardment..

The properties of the material are likely to be dominated by the

many defects that each ion will produce in coming to rest. Only when this damage has been minimized do the properties of the embedded ions themselves become observable. In the present work, the gas atoms embedded in the gold film after bombardment were detected but not identified since measurements at different wavelengths for the two gases resulted in the same changes in $\Delta$ and $\Psi$ values, unlike the measurements made on adsorbed gas and shown in Section 4.3.1.

# CHAPTER SIX

# SUMMARY AND CONCLUSION

## SUMMARY AND CONCLUSIONS

The tedious nature of the calculations of refractive index from ellipsometric parameters has to some extent impeded the exploitation of ellipsometric techniques in scientific investigations. The availability of computers has removed these computational difficulties.

Preliminary investigations of thin films, in this laboratory using ellipsometry, have indicated the usefulness of the technique in surface studies.

The aim of the present investigation was to extend this earlier work and to assess the applicability to gas adsorption/desorption measurements and the determination of the depth of damage resulting from low energy ion bombardment. By correlation of the optical and electrical properties of a surface, it was hoped to detect surface damage resulting from low energy ion bombardment.

In order to achieve these aims it was necessary to develop the basic instrument originally used in two main directions:

(i) An extension of the working wavelength range

(ii) Improvement in the sensitivity.

To make measurements over a continuous wavelength range from 0.39 μ to 1 μ, it was found necessary to modify the existing instrument in several ways:

(i) Replacement of simple polarizers by quartz prisms

(ii) Removal of the quarter wave plate necessitating the use of the Beattie & Conn technique

(iii) Improvement in the detection system to improve the sensitivity and avoid the necessity for "bracketing".

The following components were incorporated to achieve the above aims:

(i) A constant deviation spectrometer with exit slit as the light source

(ii) Nicol prisms mounted on suitably modified divided circles enabling readings to be made to $0.02^{o}$ as opposed to $0.05^{o}$ previously

(iii) A light chopper used in conjunction with a phase sensitive detector and digital voltmeter to measure the output of a photomultiplier detector. In order to achieve stable readings it was found necessary to eliminate mechanical vibrations from the pumping system and to utilize low leakage cables for connections between the photomultiplier and detector.

The performance of the system was checked by measuring the optical constants of annealed, freshly evaporated gold films, both by the Beattie & Conn technique and by using the compensator technique over the appropriate wavelength range. Complete agreement between the present work and previously published results of Abeles & Jonson & Christy proved that the requirements for the present investigation had been met.

Physical adsorption at the gas-solid interface occupies a special place in surface science because it plays a most important part in many theoretical and practical problems, and also because any process of gas-solid interaction (chemisorption, catalysis, heterogeneous chemical reaction) includes, as one of its stages, physical adsorption of a gas on the solid surface. The ellipsometric

parameters $\psi$ and $\Delta$ used for the determination of the optical constants of a surface are characteristic of the surface and are modified by the presence of a film as thin as few angstroms. For example, the presence of a thin film of argon (6 $\overset{o}{A}$ thick) adsorbed on polycrystalline golf film, held at liquid nitrogen temperature, changed the ellipsometric parameters $\psi$ and $\Delta$ by 0.1 degrees in the value of $\psi$ and 0.16 degrees in the value of $\Delta$. The complex refractive index of the freshly evaporated gold film, at liquid nitrogen temperature, and pressure of $6 \times 10^{-9}$ torr was (0.216 - 3.38i) measured at a wavelength of 6500 $\overset{o}{A}$. The composite surface refractive index (film + gas) after introducing the gas (argon) to a pressure of $5 \times 10^{-5}$ torr was (0.212 - 3.36i). This is a pseudoconstant calculated from $\psi$ and $\Delta$ modified by the presence of the gas. The error in determining the value of n ignoring the surface film is 1.9% and that in the value of k is 0.59%. Preparation of the film in a poorer vacuum (in a pressure of $10^{-6}$ torr of argon) produced corresponding changes of 3.8% in the value of n and 1.95% in the value of k. Thus the presence of a small amount of adsorbed gas would lead to an error in the measurement of the optical constants of a metal surface. The ability of the present ellipsometer arrangement to detect such differences has been exploited in the present adsorption studies.

Calculations show that an additional improvement would result from selecting an appropriate angle of incidence, in the present case the optimum value was $72^{o}$ as indicated in Table (4.7a). With the vacuum chamber available, measurements were restricted at an angle of incidence of $64^{o}$.

The sensitivity of the measurements were further improved by an order of magnitude in the value of $\psi$, and by a factor of two in the value of $\Delta$ by selecting wavelengths near strong absorption lines for the gas. For examination of unknown surface film, a number of different wavelengths should be tried.

For the interpretation of the results of the present investigation, it was necessary to consider a two layer system where the gas film is assumed to be a separate layer of refractive index (n-ik) on the gold surface rather than a compound surface with a pseudoconstant. Following the computational techniques as outlined in section (4.6) the refractive indices for argon layer were found to be

$$(1.18 - 0.13i) \text{ at } 3900 \text{ Å}$$
$$(1.14 - 0.73i) \text{ at } 4700 \text{ Å}$$
$$(1.08 - 0.25i) \text{ at } 6150 \text{ Å}$$

previously published values are

$$n = 1.27 \quad \text{at } 4750 \text{ Å}$$
$$n = 1.275 \quad \text{at } 3650 \text{ Å}$$

where absorption was assumed to be zero, i.e. $k = 0$.

The use of concepts concerning surface layers of finite thickness opens the possibility for the construction and use of models which entail various postulations about the structure of the surface layer. The adsorption properties of any adsorbent with respect to a particular adsorbate depend on two basic factors.

(i) The nature of the solid surface. Both the chemical composition of the surface layer and its structure in the crystallographic sense are important.

(ii) The specific surface area of the solid.

These two aspects were examined by ellipsometry in the present work. Adsorption of gases on different crystallographic surfaces were examined and revealed the dependence on the surface orientation of the amount of gas adsorbed. The amount adsorbed on single crystal $<110>$ was found to be twice as much as for adsorption on $<100>$. For a polycrystalline surface the adsorption is close to the average of those on the two orientations. This can be explained by the fact that the amount of gas adsorbed depends on the number of sites available on the surface to accommodate an adatom (see sections 4.3.2, 4.3.3 and 4.3.4).

The second aspect was shown from the annealing experiments after adsorption. The adsorption was made with the surface held at liquid nitrogen temperature. Annealing to room temperature and even to $100^{o}C$ did not return the values of the ellipsometric parameters $\psi$ and $\Delta$ to those for the surface before adsorption.

The combined ellipsometric and electrical measurement of low energy ion bombardment revealed several important features.

1. Very low ion energy results in contamination of the bombarded surface.
2. Adsorption is restricted to about two monolayers.
3. A threshold energy above which the bombardment produces permanent damage.
4. The threshold energy depends on both, the type of ions and the structure of the bombarded surface.
5. The damage produced depends on surface structure.
6. The nature of the defects produced.

The bombardment of a surface held at room temperature with ions of energies less than the threshold energy, which is the energy required to produce permanent damage, gave the same effect as for physical adsorption on a surface held at liquid nitrogen temperature. This was shown from ellipsometric measurements in which changes in the values of $\psi$ and $\Delta$ were in the same direction indicating contamination of the surface. Measurements of the surface layer thickness, after bombardment, showed that for polycrystalline gold films, for ion energies less than 130 eV argon ions were adsorbed or embeded into the surface layer to thickness of 6 $\overset{o}{A}$. This same value was observed when a polycrystalline gold film was held at liquid nitrogen temperature and argon atoms were introduced into the system and the pressure rose from $6 \times 10^{-9}$ torr to $5 \times 10^{-5}$ torr. No effect was observed on the electrical resistance of either the bombarded surface or the surface with an adsorbed gas layer. The value of the surface layer thickness resulting from low energy ion bombardment and adsorption of gas on a surface determine the limit of the layer thickness which can be adsorbed on a surface when the gas pressure in the system is raised from $6 \times 10^{-9}$ torr to $5 \times 10^{-5}$ torr. This limit was calculated to be approximately two atomic layers of the gas used (argon) corresponding to film of thickness of 6 $\overset{o}{A}$.

Bombardment with ions of energies higher than the threshold caused $\delta\Delta$ to be changed in the direction opposite to that characterising the contaminated surface. The threshold energy is observed from bombarding and annealing experiments. The fact that the electrical measurements did not show appreciable change after ion bombardment with energies up to 200 eV may be explained by the low concentration of the damage produced, and the small damaged thickness

compared with the overall film thickness. The values of the threshold energy depend on the gas used. In the present investigations the value for neon ions was found to be higher than for argon ions. This can be understood by comparison of the values of energy transferred from both ions on impact (see section 5.8).

It can be seen from sections 5.2 and 5.3 that the damage produced depends on the surface structure of the bombarded samples. Both the ion type and the surface orientation determine the amount of damage produced and this is measured optically by ellipsometric parameters $\psi$ and $\Delta$. Table (5.2.3a) shows the threshold energies for argon and neon on different orientations of the gold films used. Also Tables (5.5a, b, c) show the dependence of the amount of damage on surface structure. From damaged thickness calculations and the ellipsometric values $\delta\psi$ and $\delta\Delta$ ,it is clear that the damage produced in polycrystalline films is higher than that produced in single crystals.

The defects produced by ions of energy as low as 300 eV are not simple Frenkel pairs but could be more complex due to embeded gas atoms which would disturb the periodicity of the lattice or due to displaced target atoms which may result in dislocation lines. This is shown from annealing experiments and results in section 5.7.

The results of the present investigation clearly show that the ellipsometer is capable of determining thicknesses of damaged layers resulting from low energy ion bombardment. Thicknesses thus determined lie within the limits of the thicknesses estimated from changes in resistivity. The thicknesses measured in this work are in reasonable agreement with values calculated on the basis of the Lindhard theory

over the energy range 200 - 300 eV but show departure from the model in the rest of the energy region. The discrepancy between the calculated and measured value of the damage thickness may be due to the fact that the Lindhard theory takes no account of the crystalline nature of the surface and also due to the difference in definition with respect to the depth of damage or penetration.

These results may be compared with those of Walls (Ph.D.thesis, University of Aston, 1973) who found from experiments made in this department using a field ion microscope, that low energy inert gas ion bombardment of tungsten gave the same order of magnitude of damage thickness. For example, argon ions of energy 400 eV tend to penetrate and remain in tungsten to a depth of 7 - 8 atomic layers. This was shown by sputtering off layer by layer of the surface. In the case of neon, the depth at which neon atoms were found was between 13 - 14 atomic layers. The present results also show that neon ions cause damage to a greater depth than argon ions. In the case of argon the damage in gold was 38 $\mathring{A}$ for 400 eV bombardment energy which corresponds to between 9 - 10 atomic layers. Bearing in mind that the structures of tungsten and gold are different. The results obtained from the two techniques are in reasonable agreement. Also, Ibrahim and Bashara (1972), using an ellipsometric technique, reported an estimated damage thicmness of 45 $\mathring{A}$ for 400 eV argon ions bombarding silicon surfaces. As far as can be ascertained, no other investigations have been made in the low and very low bombarding energy region with which to make comparisons.

Several different techniques for studying surfaces are limited by the kind of information they provide. X-ray spectroscopy, atomic absorption, optical emission spectroscopy, mass spectroscopy and neutron activation analysis provide a range of methods for measuring elemental impurities. Auger spectroscopy provides information about the chemical composition of a surface to a depth of about 12 $\mathring{A}$. For some elements present as impurities or contaminants on the surfaces it has been found possible to derive information about the chemical form of the element. LEED and RHEED are used mainly in the study of the internal and surface structure of metallic or non-metallic solids using electron energies in the range of about $10^2$ eV to $10^6$ eV. The penetration of electrons into solids is very small and therefore only thin specimens or surface layers can be studied. The field ion microscope gives information about the electronic structure of material surfaces and the way this is modified by adsorption. In most of these methods, and particularly in the case of neutron activation analysis, one disadvantage is the fact that the technique depends on an initial bombardment which may in itself cause damage.

The ellipsometer is thus seen as a complementary instrument in that it is non-destructive and provides information on layer thicknesses and damage, in the case of metals to a depth of a few hundred angstroms depending on the wavelength of light used.

One useful extension to these studies would be a further investigation into damage produced in tungsten films by ion bombardment using an ellipsometer in order to make a direct comparison with the field ion microscope results of Walls. Problems arise in the execution of such studies in that the production of films of tungsten involve the

use of electron gun evaporation to produce the temperatures and in ultra high vacuum to prevent volume oxidation.

Further experiments using silicon would also be of interest and enable comparisons to be made with other reported work. Shallow ion implantation in semiconductors could be measured ellipsometrically and taken in conjunction with the well known properties of such doped layers.

A combination of LEED or Auger techniques with ellipsometry would facilitate the identification of surface or buried species and this permit a better understanding of the mechanicms involved in adsorption and the production of damage.

## APPENDIX I

Description of Fortran computer programmes:

a) For the calculation of the ellipsometric parameters $\psi$ and $\Delta$ from experimental measurements:

The programme is made to calculate the values of the ellipsometric parameters $\psi$ and $\Delta$ from a set of absolute intensities of the light beam transmitted by the system polarizer-specimen-analyzer measured experimentally. All values of intensities were measured when the polarizer azimuth was set at $\psi_p = 45^o$ and analyzer azimuth $\psi_A$ at

$$I_1 = I(45^o, 90^o)$$

$$I_2 = I(45^o, 0^o)$$

$$I_3 = I(45^o, +45^o)$$

$$I_4 = I(45^o, -45^o)$$

Four equivalent values were measured for which $\psi_p$ was at $-45^o$.

The values of $\psi$ and $\Delta$ were calculated from the relations:

$$\rho = \tan\psi = (I_2/I_1)^{\frac{1}{2}}$$

$$\cos\Delta = \tfrac{1}{2}\left(\frac{1}{\rho} + \rho\right)\left(\frac{I_3 - I_4}{I_3 + I_4}\right)$$

The measured values of $I_1$ to $I_4$ are fed to the programme and then $\psi$ and $\Delta$ values are calculated.

The test of the programme is attached.

```
0001                LIST (LP)
0002                PROGRAM (FXXX)
0003                INPUT  1 = CR0
0004                INPUT  3 = TR0
0005                INPUT  5 = CR1
0006                OUTPUT 2 = LP0
0007                OUTPUT 6 = LP1
0008                COMPRESS INTEGER AND LOGICAL
0009                COMPACT
0010                TRACE 2
0011                END



0012                TRACE 1
0013                READ FROM (CR)
0001                MASTER
0002                WRITE(2,4)
0003              4 FORMAT(1H1,5X,4H ROW,9X,4H PSY,6X,6H DELTA,5X,4H AI1,5X,4H AI2,5X,
0004               14H AI3,5X,4H AI4)
0005              3 READ(1,5)AI1,AI2,AI3,AI4
0006              5 FORMAT(4F5.2)
0007                IF(AI1)10,0,0
0008                X1=SQRT(AI2/AI1)
0009                ROW=X1
0010                PSY=(ATAN(X1))*57.29578
0011                X2=1.0/X1
0012                X=X1+X2
0013                Y1=AI3-AI4
0014                Y2=AI3+AI4
0015                Y=Y1/Y2
0016                Z=0.5*X*Y
0017                DELTA=180.0-((ACOS(Z))*57.29578)
0018                WRITE(2,8)ROW,PSY,DELTA,AI1,AI2,AI3,AI4
0019              8 FORMAT(1H0,4X,F8.5,4X,F7.3,4X,F8.3,4X,F5.2,4X,F5.2,4X,F5.2,4X,F5.2
0020               1)
0021                GO TO 3
0022             10 STOP
0023                END
```

b) For the calculation of the optional constants of freshly evaporated metal films:

The values of the optional constants n and k for freshly evaporated metal films can be calculated using the equations:

$$n^2 - k^2 = \sin^2\phi_o \left[ 1 + \frac{\tan^2\phi_o (\cos^2 2\bar{\psi} - \sin^2 2\bar{\psi} \sin^2 2\bar{\Delta})}{(1 + \sin 2\bar{\psi} \cos\bar{\Delta})^2} \right]$$

$$2nk = \frac{\sin^2\phi_o \tan^2\phi_o \sin 4\bar{\psi} \sin\bar{\Delta}}{(1 + \sin 2\bar{\psi} \cos\bar{\Delta})^2}$$

where $\phi_o$ is the angle of incidence and $\bar{\psi}$ and $\bar{\Delta}$ are the ellipsometric parameters for freshly evaporated metal film.

The programme calculates the values of n and k for a given range of values of $\psi$ and $\Delta$, within which the experimental values lie, and the values of $\psi$ and n and $\psi$ and k are plotted at constant values of $\Delta$. From the experimentally determined $\psi$ and $\Delta$ values, the optical constant of the metal surface can be determined from the graphs as explained in section 4.5. Two separate programmes with graph plotter, one to determine n and the other to determine k, were written. The test of the two programmes are attached.

```
0001                LIST (LP)
0002                PROGRAM (FXXX)
0003                INPUT  1 = CR0
0004                INPUT  3 = TR0
0005                INPUT  5 = CR1
0006                OUTPUT 2 = LP0
0007                OUTPUT 6 = LP1
0008                COMPRESS INTEGER AND LOGICAL
0009                COMPACT
0010                TRACE 2
0011                END


0012                TRACE 1
0013                READ FROM (CR)
0001                 MASTER
0002          C     CALCULATIONS OF N AND K FOR FILM FREE SURFACE
0003                REAL K
0004                REAL N
0005                DIMENSION C1(200),C2(200),B1(400),B2(400),D(400)
0006                DIMENSION F(200),G(200),N(200),K(200),X1(200),Y1(200)
0007                CALL OPENPLOT
0008                CALL HGPLOT(-3.0,28.0,0,4)
0009                READ(1,10)THETA
0010              10 FORMAT(F6.2)
0011                Z=(THETA/57.29578)
0012                A1=(SIN(Z))**2.0
0013                A2=(TAN(Z))**2.0
0014                A=A1*A2
0015              44 READ(1,50)DELTA,DELTAINT,X,PSY,PSYINT,Y
0016              50 FORMAT(F8.3,F6.3,F8.3,F7.3,F6.3,F7.3)
0017                PSYS=PSY
0018                CALL HGPAXIS(0.0,0.0,2H N,-2,43.1,0.0,0.98,0.02)
0019                CALL HGPAXIS(0.0,0.0,4H PSY,4,27.0,90.0,20.0,0.5)
```

```
0020                DO 100 I=1,200
0021                CALL HGPLOT(0.0,0.9,3,0)
0022                Z1=(DELTA/57.29578)
0023                C1(I)=SIN(Z1)
0024                C2(I)=COS(Z1)
0025                WRITE(2,12)DELTA
0026             12 FORMAT(1H1,8X,7H DELTA=,F8.3)
0027                WRITE(2,14)
0028             14 FORMAT(1H0,10X,4H PSY,13X,2H N,13X,2H K)
0029                NPTS=0
0030                DO 200 J=1,200
0031                B1(J)=SIN(2.0*PSY/57.29578)
0032                B2(J)=SIN(4.0*PSY/57.29578)
0033                D(J)=(1.0+(B1(J)*C2(I)))**2
0034                F(J)=A1*(1.0+(A2*((1.0-B1(J)*B1(J))-((B1(J)*C1(I))**2))/D(J)))
0035                G(J)=(A*B2(J)*C1(I))/D(J)
0036                N(J)=SQRT((F(J)+SQRT(F(J)*F(J)+G(J)*G(J)))/2.0)
0037                X1(J)=PSY
0038                K(J)=G(J)/(2.0*N(J))
0039                NPTS=NPTS+1
0040                WRITE(2,15)PSY,N(J),K(J)
0041             15 FORMAT(1H ,8X,F7.3,8X,F7.3,8X,F7.3)
0042                PSY=PSY+PSYINT
0043                IF(PSY-Y)200,200,40
0044            200 CONTINUE
0045             40 DO 888 J=1,200
0046                N(J)=(N(J)-1.0)*50.0
0047                X1(J)=(X1(J)-20.0)*2.0
0048                IF(X1(J)-(Y-20.0)*2.0)888,888,8
0049            888 CONTINUE
0050              8 CALL HGPSCURVE(N,X1,NPTS,0,0,0,0,0)
0051                PSY=PSYS
0052                DELTA=DELTA+DELTAINT
0053                IF(DELTA-X)100,100,13
0054            100 CONTINUE
0055             13 CALL CLOSEPLOT
0056                STOP
0057                END
```

```
0001                    LIST (LP)
0002                    PROGRAM (FXXX)
0003                    INPUT  1 = CR0
0004                    INPUT  3 = TR0
0005                    INPUT  5 = CR1
0006                    OUTPUT 2 = LP0
0007                    OUTPUT 6 = LP1
0008                    COMPRESS INTEGER AND LOGICAL
0009                    COMPACT
0010                    TRACE 2
0011                    END



0012                    TRACE 1
0013                    READ FROM (CR)
0001                    TRACE 2,500
0002                     MASTER
0003          C         CALCULATIONS OF N AND K FOR FILM FREE SURFACE
0004                    REAL K
0005                    REAL N
0006                    DIMENSION C1(200),C2(200),B1(400),B2(400),D(400)
0007                    DIMENSION F(200),G(200),N(200),K(200),X1(200),Y1(200)
0008                    CALL OPENPLOT
0009                    CALL HGPLOT(-3.0,28.0,0.4)
0010                    READ(1,10)THETA
0011                 10 FORMAT(F6.2)
0012                    Z=(THETA/57.29578)
0013                    A1=(SIN(Z))**2
0014                    A2=(TAN(Z))**2
0015                    A=A1*A2
0016                 44 READ(1,50)DELTA,DELTAINT,X,PSY,PSYINT,Y
0017                 50 FORMAT(F8.3,F6.3,F8.3,F7.3,F6.3,F7.3)
0018                    PSYS=PSY
0019                    CALL HGPAXIS(0.0,0.0,2H K,-2,41.0,0.0,1.18,0.02)
0020                    CALL HGPAXIS(0.0,0.0,4H PSY,4,27.0,90.0,20.0,0.5)
```

```
0021                DO 100 I=1,200
0022                CALL HGPLOT(0.0,0.0,5,0)
0023                Z1=(DELTA/57.29578)
0024                C1(I)=SIN(Z1)
0025                C2(I)=COS(Z1)
0026                WRITE(2,12)DELTA
0027             12 FORMAT(1H1,8X,7H DELTA=,F8.3)
0028                WRITE(2,14)
0029             14 FORMAT(1H0,10X,4H PSY,13X,2H N,13X,2H K)
0030                NPTS=0
0031                DO 200 J=1,200
0032                B1(J)=SIN(2.0*PSY/57.29578)
0033                B2(J)=SIN(4.0*PSY/57.29578)
0034                D(J)=(1.0+(B1(J)*C2(I)))**2
0035                F(J)=A1*(1.0+(A2*((1.0-B1(J)*B1(J))-((B1(J)*C1(I))**2))/D(J)))
0036                G(J)=(A*B2(J)*C1(I))/D(J)
0037                N(J)=SQRT((F(J)+SQRT(F(J)*F(J)+G(J)*G(J)))/2.0)
0038                X1(J)=PSY
0039                K(J)=G(J)/(2.0*N(J))
0040                NPTS=NPTS+1
0041                WRITE(2,15)PSY,N(J),K(J)
0042             15 FORMAT(1H ,8X,F7.3,8X,F7.3,8X,F7.3)
0043                PSY=PSY+PSYINT
0044                IF(PSY-Y)200,200,40
0045            200 CONTINUE
0046             40 DO 888 J=1,200
0047                K(J)=(K(J)-1.18)*50.0
0048                X1(J)=(X1(J)-20.0)*2.0
0049                IF(X1(J)-(Y-20.0)*2.0)888,888,8
0050            888 CONTINUE
0051              8 CALL HGPSCURVE(K,X1,NPTS,0,0,0,0,0)
0052                PSY=PSYS
0053                DELTA=DELTA+DELTAINT
0054                IF(DELTA-X)100,100,13
0055            100 CONTINUE
0056             13 CALL CLOSEPLOT
0057                STOP
0058                END
```

## REFERENCES


1. ABELES, F. and THEYE, M.L. — Report of European Research Office, United States Army, Contract No. DAJA37 - 67 - C - 0945 (1969).

2. ABRAHAMSON, A.A. — Phys. Rev. 178 No.1 (1969) 76

3. AIRY, G.B. — Trans.Cambridge Phil. Soc. 4 (1833) 279.

4. ALMEN, O.E. and BRUCE, G. — Nuclear Instruments and Methods, North Holland Publishing Co. 11 (1961) 257.

5. ALMEN, O.E. and BRUCE, G. — Nuclear Instruments and Methods, North Holland Publishing Co. 11 (1961) 279.

6. ARCHER, R.J. — J. Electrochem. Soc. 104 (1957) 619.

7. ARCHER, R.J. — J. Opt. Soc. Am. 52 (1962) 970.

8. ARCHER, R.J. — Ellipsometry in the measurements of surfaces and thin films. E.Passaglia, R.R.Stromberg, J.Kruger, eds. Natl. Bur. Stds. Misc. 256, U.S. Govert. Printing off. Washington, (1964).

9. ARCHER, R.J. and GOBELI, G.W. — J. Phys. Chem. Solids 26 (1965) 343.

10. ARMSTRONG, T.W. and CHANDLER, K.C. — Report of ORNL-4869, UC-32-Mathematics and Computer, Contract No.W-7405-eng-26 Neutron Physics Division.

10a. BARDEEN, J. Phys. Rev. 58 (1940) 727

11. BARTELL, L.S. and BETTS, J.F. J. Phys. Chem. 64 (1960) 1075

12. BEATTIE, J.R. Phil. Mag. 46 (1955) 235.

13. BLODGETT, K. J. Am. Chem. Soc. 56 (1934) 495

14. BOOTSMA, G.A. and MEYER, F. Surface Sci. 13 (1969) 110

15. BOOTSMA, G.A. and MEYER, F. Surface Sci. 14 (1969) 52

16. BOOTSMA, G.A. and MEYER, F. Surface.Sci. 18 (1969) 123

17. BOWDEN, P.B. and BRANDON, D.G. Phil. Mag. 8 (1963) 935

18. BOWDEN, P.B. and BRANDON, D.G. J. Nucl. Mat. 9 (1963) 348

19. BREWSTER, D. Phil. Trans. 105 (1815) 125

20. BRINKMAN, J.A. J.Appl.Phys. 25 (1954) 961

21. BROWN, F. and DAVIES, J.A. Canad. J. Phys. 41 (1963) 844

22. BROWN, R.E. and LECK, J.H. — Brit. J. Appl. Phys. 6 (1955) 161

23. BRUNAUER, S., EMMETT, P.H. and TELLER, E. — J.Am. Chem. Soc. 60 (1938) 309

24. BURGE, D.K. and BENNETT, H.E. — J. Opt. Soc. Am. 54 (1964) 1428

25. CARMICHAEL, J.H. and TRENDELENBURG, J.H. — J.Appl. Phys. 29 (1958) 1570

26. CARROLL, J.J. and MELMED, A.J. — Surface Sci. 16 (1969) 251

27. CLAUSEN, B.H. — J. Electrochem. Soc. 111 (1964) 646

28. CLOSE, K.J. and YARWOOD, J. — Brit. J. Appl. Phys. 17 (1966) 1165

29. CLOSE, K.J. and YARWOOD, J. — Brit. J. Appl. Phys. 18 (1967) 1593

30. CORKHILL, D.P. and CARTER, G. — Nucl. Instrum. Methods 38 (1965) 192

31. CUNNINGHAM, R.E. and GWATHMEY, A.T. — J.Am. Chem. Soc. 76 (1954) 391

32. CUSSINS, W.D. Proc.Phys. Soc. B 68 (1955) 213

33. De BOER, J.H. and CUSTERS, J.F. Z.Phys. Chem. B 25 (1934) 238

34. DEBYE, P. Phys. Z. 21 (1920) 178

35. DIGNAM, M.J. MOSKOVITS, M. and STOBIE, R.W. Trans. Faraday Soc. 67 (1971) 3306

36. DIGNAM, M.J. MOSKOVITS, M. and STOBIE, R.W. J. Opt. Soc. Am. 61 (1971) 1460

37. DRUDE, P. Ann. Physik. Chemie. 39 (1890) 481

38. EHRLICH, G. and HUDDA, F.G. J. Chem. Phys. 33 (1960) 4

39. EHRLICH, G. Brit. J. Appl. Phys. 15 (1964) 349

40. ERENTS, K. and CARTER, G. Vacuum 17 (1967) 215

41. EVERHART, E. CARBONE, R.J. and STONE, G. Phys. Rev. 99 No.4 (1955) 1287

42. FANE, R.W. and NEAL, W.E.J. — J.Opt. Soc. Am. 60 No.6 (1970) 790

43. FARNSWORTH, H.E. SCHLIER, R.E. GEORGE, T.H. and BUGER, R.M. — J. Appl. Phys. 26 (1955) 252

44. FARNSWORTH, H.E. and HAYEK, K. — Surface Sci. 8 (1967) 35

45. FIRSOV, O.B. — Soviet. Physics. JETP, 6 (33) (1958) 535

46. FRY, T.C. — J. Opt. Soc. Am. 15 (1927) 137

47. GOMER, R. — Discussions Faraday Soc. 28 (1959) 23

48. GUNTHERSCHULZE, A. and TOLLMIER, W. — Z.Physik 119 (1942) 685

49. HALL, A.C. — J. Phys. Chem. 70 No.6 (1966) 1702

50. HART, R.R. and MARSH, O.J. — Appl. Phys. Letters 14 (1969) 225

51. HAYFIELD, P.C.S. and WHITE, G.W.T. — Ellipsometry in the measurements of surfaces and thin films, Symposium procedings, Washington 1963, Natl. Bur. Std. Misc. Publ. (1964) p.157

52. HAUSCHILD, H. Ann. Physik, Chemie. 63 (1920) 816

53. HEAVENS, O.S. Optical properties of thin solid films, Dover publications, New York (1955).

54. HENZLER, M. Surface Sci. 22 (1970) 12

55. HOBSON, J.P. Can. J. Phys. 37 (1959) 300

56. HOBSON, J.P. and ARMSTRONG, R.A. J. Phys. Chem. 67 (1963) 2000

57. HOLMES, D.K. Cours International d'ete sur la physique des solides, Mol, Belgique, 1963.

58. IBRAHIM, M.M. and BASHARA, N.M. Surface Sci. 30 (1972) 632

59. IVES, H.E. and JOHNSRUD, J. Opt. Soc. Am. 15 (1927) 374

60. JACKSON, L.C. and BURGE, E.J. Nature, 164 (1949) 660

61. JACKOBSON, R.L. and WEHNER, G.K. J. Appl. Phys. 36 (1965) 2674

62. JAMIN, J. Compt. Rend. (Paris) 31 (1850) 696

63. JAMIN, J. Ann. Chem. 31 (1851) 165

64. JOHNSON, P.B. and CHRISTY, R.W. Phys. Rev. B 6 No.12 (1972) 4370

65. KEESOM, W.H. Physik. Z. 22 (1921) 129

66. KEESOM, W.H. Physik. Z. 22 (1921) 643

67. KEESOM, W.H. Physil. Z. 23 (1922) 225

68. KELLY, R. and NAGUIB, H.M. Atomic collision phenomena in solids, North Holland publications 1970 p.172.

69. KINCHIN, G.H. and PEASE, R.S. Rep. Prog. Phys. 18 (1955) 1

70. KORNELSEN, E.V. Can. J. Phys. 42 (1964) 364

71. KORNELSEN, E.V. and SINHA, M.K. Appl. Phys. Letters 9 (1966) 112

72. LANDER, J.J. and MORRISON, J. Surface Sci. 6 (1967) 1

73. LANGMUIR, I. Phys. Rev. 8 (1916) 149

74. LANGMUIR, I. J. Am. Chem. Soc. 40 (1918) 1361

75. LANGMUIR, I. Phys. Rev. 33 (1929) 954

76. LEHMANN, C. and LEIBFRIED, G. — J. Appl. Phys. 34 (1963) 2821

77. LEIBFRIED, G. — J. Appl. Phys. 30 (1959) 1388

78. LENEL, F.V. — Z. Physik. Chem. B 23 (1933) 379

79. LENNARD-JONES, J.E. — Trans. Faraday Soc. 28(1932) 333

80. LINDHARD, J., SCHARFF, M. and SCHIOTT, H.E. — Mat. Fys. Medd. Dan. Vid. Selsk. 33 No. 14 (1963)

80a. LONDON, F. — Z. Physik. B 11 (1930) 222

81. LONDON, F. — Z. Physik. 63 (1930) 245

82. LORENZ, L. — Ann. Physik. 3 (1860) 460

83. MacDONALD,R.J. and HANEMAN, D. — J. Appl. Phys. 37(1966) 3048

84. MALUS, E.L. — Nouvel Bull. Soc. Philomath 1 (1808) 266

85. MAYER, J.W. ERIKSSON, L.and DAVIES, J.A. — Ion implantation in semiconductors Academic Press, 1970

86. MAXWELL, J.C. — Scientific papers, Vol.1, J.Hermann, Paris 1927.

87. McCRACKIN, F.L. ELIO PASSAGLIA, STROMBERG, R.R. and STEINBERG, H.L. — J. Rsc. Natl. Bur, Std. 67A, No.4. (1963) 363

88. MERKLE, K. — Symposium on defects clusters UKAEA unclassified report AERE-R-5269 (325) (1966 ).

89. MERKLE, K.L. — Atomic collision Phenomena in solids, North Holland publication 1970, p.192

90. MESSIER, J., Le COROLLER Y. and MERLO FLORES, J. — I.E.E.E. Trans Nucl. Sci. NS-11, No.3 (1964) 276

91. MILLER, J.R. and BERGER, J.E. — J. Phys. Chem. 70 (1966) 3070

92. MORGAN, A.E. — Surface Sci. 43 (1974) 150

93. MOTT, N.F. and JONES, H. — Theory of the properties of metals and alloys, (Clarendon Press, Oxford) 1936, 2nd. edn. (Dover, New York) 1958

94. MURMANN, H. — Z. Physik. 80 (1933) 161

95. MURMANN, H. — Z. Physik. 101 (1936) 643

96. NEAL, W.E.J., FANE, R.W. and GRIMES, N.W. — Phil. Mag. 21 N 169 (1970) 167

97. NOMURA, A. KANAYAMA, M. and KIYONO S. — J. Appl. Phys. 45 No.6 (1974) 2394

98. OGILVIE, G.L. and RIDGE, M.J. — J. Physik. Chem. Solids 10 (1959) 222

99. OVERHAUSER, A.W. — Phys. Rev. 90 (1953) 393

100. POLANYI, M. — Verh. Dent. Phys. Ges. 18 (1916) 55

101. POLANYI, M. — Trans. Faraday Soc. 28 (1932) 316

102. POLANYI, M. — Science 141 (1963) 1010

103. RAYLEIGH, L. — Phil. Mag. 33 (1892) 1

104. ROTHEN, A. — Rev. Sci. Instrum. 16 (1945) 26

105. ROTHEN, A. and HANSON, M. — Rev. Sci. Instrum. 19 (1948) 839

106. ROUGHAN, P. and MANCHESTER, K.E. — Bull. Am. Phys. Soc. 12 (1967) 140

107. SAXENA, A.N. — J. Opt. Soc. Am. 55 (1965) 1061.

108. SCHEELE, C.W. — Collected papers of Carl Wilhelm Scheele, (L. Dobbin, ed.), p.173

109. SCHULZ, L.G. — Adv. Phys. 6(1957) 102

110. SEITZ. F. — Discussions Faraday Soc. 5 (1949) 271.

111. SILSBEE, R.H. — J. Appl. Phys. 28 (1957) 1246

112. SKINNER, C. — J. Opt. Soc. Am. 10(1925) 491

113. SLATER, J.C. and KIRKWOOD,J.G. — Phys. Rev. 37 (1931) 682.

114. SMITH, T. — Surface Sci. 32 (1972) 527

115. SMITH, T. — J. Electrochem. Soc. 119 (1972) 1398

116. STARK, K. and WENDT, G. — Ann. Phys. 38 (1912) 921

117. STEBBINS, J.P. and HALSEY, G.D. — J. Phys. Chem. 68 (1964) 3863

118. STEIGER, R.F. MORABITO, J.M. Jr., SOMORJAI, G.A. and MULLER, R.H. — Surface Sci. 14 (1969) 279

119. STROMBERG, R.R. GRANT, W.G. and PASSAGLIA, E. — J. Res. Natl. Bur. Std. 68A (1964) 391

120. TAYLOR, H.S. Frontiers of Chemistry (R.E.Burk & O.Grummit, Eds.) P 1-28 Interscience, New York.

121. THOMPSON, M.W. and NELSON, R.S. Proc. Roy. Soc. A 259 (1961) 458

122. THOMPSON, M.W. Phys. Letters 6 (1963) 24

123. TRILLAT, J.J. Applications J. Chim. Physique 53 (1956) 570

124. TRONSTAD, L. and FEASHEM, C.G.P. Proc. Roy. Soc. 145A (1934) 115

125. TRONSTAD, L. Trans. Faraday Soc. 31 (1935) 1151

126. VAN RYN ALKEMADE, A.C. Ann. Physik 20 (1883) 22

127. VARNERIN, L.J. and CARMICHAEL, J.H. J. Appl. Phys. 28 (1957) 913

128. VASICEK, A. Optics of thin film (North Holland, Amsterdam, 1960).

129. VEDAM, K., KNAUSENBERG, W. and LUKES, F. J. Opt. Soc. Am. 59 (1969) 64

130. VENABLES, J.A. Atomic collision phenomena in solids, North Holland Publications 1970, P 132.

131. VOIGT, W. — Ann. Physik. 35 (1888) 76

132. VOLMER, M. — Trans. Faraday Soc. 28 (1932) 363

133. WAGNER, J.B. and GWATHMEY, A.T. — J..Am. Chem. Soc. 76 (1954) 390

134. WEISLER, G.L. and WILSON, T.N. — J. Appl. Phys. 24 (1953) 472

135. WIGNER, E.P. and FREENBERG, E. — Rep. Phys. Soc. Progr. Phys. 8 (1942) 274

136. YOUNG, D.M. and CROWELL, A.D. — Physical adsorption of gases, (Butterworth, London, 1962).